Buoyancy Driven Three-Phase Flow in Porous Media

Panters Rodríguez Bermúdez

panters@impa.br

Adviser: Dan Marchesin

June 2010

To my parents and to my wife.

Acknowledgments

I first express my gratitude towards IMPA and Brazil. During these four years of Ph.D study I felt right at home. I also want to thank my advisor, Professor Dr. Dan Marchesin. His teaching, leadership, support, attention to details, and hard work have set an example I hope to match some day. I thank to CNPq-TWAS who provided me with a full four-years Ph.D fellowship.

I would like to thank to all my colleges in the Fluids Dynamics group at IMPA. Interchanging ideas with them and discussing about the different research problems; as part of the seminar sections of the group, it has certainly contributed to the progress of my work. I want to thank specially Prof. Frederico Furtado (University of Wyoming), and Dr. Vitor Matos (Porto University) for their suggestions along my research.

I thank to professor Dr. Baldomero Valiño Alonso (Havana University). He is my mentor; first, during my years of undergraduate studies and then during my Master degree studies. I thank him for his advices, his teachings and his friendship. This thesis is a tribute to his work.

I thank all my friends who helped make my stay in Brazil delightful. In particular I thanks to Cristina Onofri and her family, and to my best friend Yoisell.

Finally I thank to my family and specially to the most important persons in my life, my parents Juan and Irene, and my wife Silvia. Without their love, affection, encouragement and support I would not have been able to complete my studies.

Abstract

We study the buoyancy-driven flow for a system of two nonlinear conservation laws that models three-phase flow in a porous medium. We solve a class of Riemann problems for a simplified case where two of the fluids have equal density. We also perform a hyperbolic analysis for the system of conservation laws finding a new type of coincidence point on the boundary of the saturation triangle. The investigation combines the theory of conservation laws with computational experiments.

Resumo

Estudamos o escoamento trifásico de fluidos em meios porosos resultante exclusivamente da força de gravidade. O problema é modelado por um sistema de duas leis não-lineares de conservação. Resolvemos uma classe de problemas de Riemann para o caso em que dois fluidos têm densidades iguais. Também apresentamos uma análise geral de hiperbolicidade para o sistema de leis de conservação, e caracterizamos um novo tipo de ponto de coincidência, que se encontra na fronteira do triângulo de saturações. A pesquisa combina análise teórica com experimentos numéricos.

Contents

Chapter 1

Introduction

We study the flow in a porous medium of three fluids under the effect of gravity force. We assume that the fluids do not mix when put into a container and that they have different densities and viscosities, in general. The flow occurs along a very long vertical thin cylinder of porous rock surrounded by an impermeable material. We assume that the rock cylinder is totally saturated by the three fluids and that initially there is an impermeable interface separating a homogeneous mixture of two of the fluids on top from the third fluid at the bottom, see Fig. 1.1. We pretend that until time zero the gravity force is inactive, so the fluids do not move. We study the longitudinal motion of the fluids from the instant when the gravity is activated and the interface disappears. This study is done near the location of the initial interface as if the cylinder were infinitely long. For example, one can think that the cylinder initially was in the horizontal position and at time zero it is quickly rotated to the vertical position. Of course, we assume that there are no phenomena such as fingering that cause irregularities in the flow transversely to the cylinder axis. In mathematical language, this is equivalent to solve Riemann problems for certain 2×2 systems of conservation laws in one-dimensional space measured along the cylinder axis, for a special class of initial data. This system reflects the conservation of mass of each incompressible fluid, as well as a generalization to immiscible fluids of Darcy's law of force relating pressure gradient to fluid flow rate in porous media.

The main applications of this work are petroleum recovery, geological carbon dioxide storage to mitigate global warming, and clean up of hydrocarbon polluted aquifers.

It is well known that there exist two different convective transport phenomena that take part in the motion of fluids within a porous medium: convection due to pressure gradients and buoyancy due to density differences between the fluids. Until now, all mathematical work on immiscible three-phase flow in porous media has focused on convection-driven flow, when there are no gravitational effects. In this work we focus onto buoyancy-driven flow, and we solve a class of Riemann problems for the "pure gravitational" case (*i.e.*, neglecting convection effects due to longitudinal pressure gradients rather than due to buoyancy).
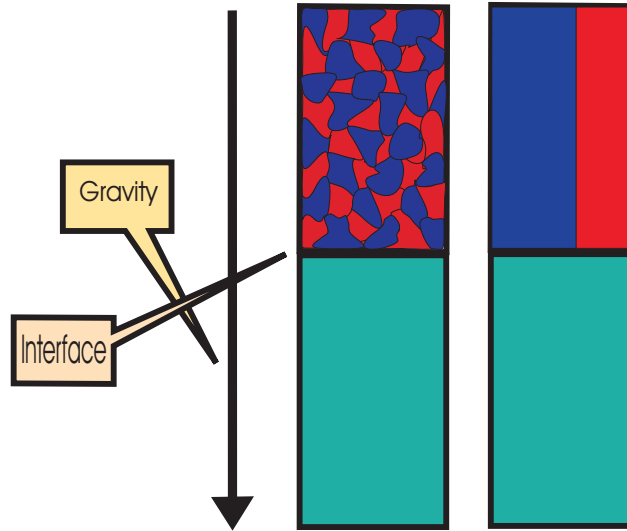
Figure 1.1: *Initial condition in the reservoir. Left figure: initial distribution of the three fluids in the porous medium. Each fluid is represented by a color (or a shade of gray). Right figure: schematic representation for the saturation of the fluids at the initial time.*

The solution of this problem depends on the physical properties of the three fluids. In other words, the evolution from the initial situation reflects the disparity in densities and viscosities of the fluids. Because of this fact this solution should be studied for all physically meaningful values of the density and viscosity parameters. Nevertheless, as a first step toward understanding the influence of gravity in three-phase flow in porous media, we will consider the simplified case in which two of the fluids have equal densities. We call this case the *simplified pure gravitational problem*, or SPGP.

We obtain interesting results, *e.g.*, for the following initial situation: one of the fluids above the interface has the same density as the fluid below the interface, while the other fluid located above the interface is the heaviest. For certain initial proportions of the fluids on top, the solution consists of two wave groups separated by a region with a constant state, see Fig. 1.2. The first wave group moves upwards. It contains a shock embedded into two spreading or rarefaction waves; sometimes the upper rarefaction is preceded by an additional shock. Within this upward wave group, the waves faster than the embedded shock involve only two fluids, precisely the fluids that were on top initially; the fluid initially at the bottom is only present below the embedded shock. The second wave group moves downwards and involves two fluids only. This wave group consists of a rarefaction wave adjacent to a faster shock; in the downward waves the lower-density fluid that was initially located on top is absent, *i.e.*, the lower-density fluid never moves downwards, as one could expect. As we said, there is a homogeneous region, *i.e.*, a constant state, separating the two wave groups. The span of this region grows linearly with time.

We observe a curious feature of this Riemann solution: while the proportion in the mixture initially on top keeps within a certain range away from a critical value, the mixture slows down the upward motion of the bottom fluid. This blocking property perhaps could
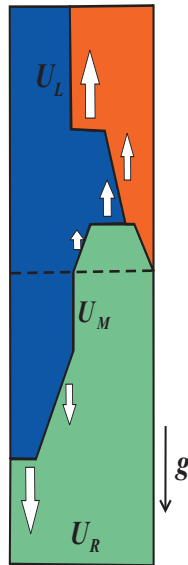
Figure 1.2: *Schematic representation for saturations in a non trivial Riemann solution for the "pure gravitational problem", where the green and red fluids have equal densities, while the blue fluid is heavier. The white arrows indicate the motion of the waves. Larger arrows correspond to higher speeds of the waves.*

be important in applications.

Riemann problem theory dates from 1860, when he solved the shock tube problem employing the method of characteristics, see [39]. That problem reduces to solving a piecewise constant initial value problem for a system of non-linear conservation laws that describes gas motion, Euler's equations. Riemann obtained the scale-invariant solution and explained why rarefaction waves and shock waves are generated when the membrane separating regions with gases at different pressures is broken.

Non-linear conservation laws govern flows in porous media. The simplest nonlinear problem in porous media, the two-phase flow injection problem, was solved by Buckley and Leverett [5] in 1942. Their resolution method can be interpreted geometrically by means of the graph of the standard S-shaped flux function, giving rise to the fractional flow method, of common usage in petroleum enginering. This method is a powerful and simple tool to solve flow problems involving no more than two phases, but many chemical components, see [13], [14], [49].

The Riemann problem for immiscible three-phase flow is more difficult than for two-phase flow. The fractional flow method cannot be extended to three-phase flow problems such as those arising for the rock permeability models of Corey et al. [6] and Stone [48]. The resolution of such problems requires a more general solution method, the *wave curve method*, developed by Liu [29], which generalizes the Lax's theorem [28]. This method constructs the solution by means of a sequence of rarefaction waves, shock waves, and constant states, by following a sequence of curves in state space.

The wave curve method developed by Liu assumes that the system of conservation laws is strictly hyperbolic. Nevertheless, systems of conservation laws modelling immiscible three-phase flow in porous media fail to be hyperbolic. Isaacson, Marchesin, Plohr and Temple [20] showed that for Corey model for immiscible three-phase flow in porous media, there exist a sole isolated point interior to the saturation triangle where strict hyperbolicity fails (nowdays known as umbilic point). They also solved by the wave curve method the Riemann problem, neglecting gravitational effects. Their method is more general than Liu's, because it allows for loss of hyperbolicity and for other difficulties that typically occur in three-phase flow. In [20] the solution was obtained under the simplifying assumption that the three fluids have equal viscosities. De Souza [8] extended the study to the case in which one of the viscosity parameters is slightly different from the other two.

Recently Azevedo, De Souza, Furtado, Marchesin and Plohr [1] showed applications of the wave curve method to solve the injection problem for immiscible three-phase flow in which a mixture of water and gas is injected into a horizontal one-dimensional porous medium containing oil. See the "Extended bibliography review" in Appendix D.

On the other hand, buoyancy effects in the flow of two immiscible fluids in porous media are quite well understood, as they are modelled by a scalar conservation law, which is easily solved through Oleinik's construction [34]. For instance Proskurowski in [35] solved the Buckley-Leverett equation for two-phase flow in the presence of gravity. There are other works on two-phase flow with gravity and their applications, see *e.g.* [37], [38], [51], [24], [12].

The state of the art for three-phase flow with gravity is quite different. Up to now, there are few works on three-phase flow with gravity taken in to account. Medeiros [33] performed an analysis of hyperbolic singularities for certain models including gravity.

Here we study in detail the simplified pure gravitational problem (SPGP), *i.e.*, neglecting convection effects unrelated to buoyancy and assuming that two of the fluids have equal densities. We expect that Riemann solutions for the simplified cases will help in solving the more general problems of three different-density fluids, as such problems can be interpreted as "perturbations" of the simplified cases. The Riemann solutions obtained in this work together with the new theoretical results presented can be considered a first step toward the study of the general three-phase flow in porous media driven by both buoyancy and pressure gradients.

We explain briefly how this work is organized. In Chapter 2 we derive the system of conservation laws that models three-phase flow in porous media with gravity, under a few physical simplifications. We non-dimensionalize the equations, giving rise to the "convection-to-gravity ratio" parameter α, which measures the dominant effect. We also introduce the Corey model with quadratic permeabilities for the fluids used in this work.

In Chapter 3 we recall some basic aspects of the general theory for systems of conservation laws, of the theory of bifurcation of Riemann solution and of the wave curve

method in order to provide the non-specialist reader with a brief background on these subjects. Specialists should skip it. We warn the non-specialist that this review is neither complete nor perfectly accurate, to keep it short. However, it is too new to be found in books.

In Chapter 4 we calculate the characteristic speeds for the system of conservation laws corresponding to the Corey model with quadratic permeabilities. We determine completely where strict hyperbolicity fails. The analysis is made for generic convection-to-gravity ratio. We obtain a new type of points where characteristic speeds coincide, which we call *quasi-umbilic* points. They are located at the boundary of the physical saturation triangle, in the case when the gravitational effects are dominant. Understanding these quasi-umbilic points and their influence on the Riemann solution are some of the main theoretical results of this work.

In Chapter 5 we study two-phase flows occurring in the pure gravitational problem, in which the convection-to-gravity ratio α is zero. The results of this chapter are necessary for the Riemann solution studied in the present work since generically two-phase waves can be part of a three-phase Riemann solution. This fact was observed by Azevedo et al. in [1] too.

In Chapter 6 we perform the analysis of possible shocks separating two states, one of which consists of a pure fluid, and the other is a mixture of the three fluids. This is done by studying the Hugoniot loci for the vertices of the saturation triangle. The analysis is done for a generic α, rather than for $\alpha = 0$. These Hugoniot loci play an important role in the resolution of the Riemann problem where the initial bottom state represents a pure fluid.

In Chapter 7 we perform the analysis of shocks separating two states, one of which is a mixture of two fluids, and the other is a genuine mixture of the three fluids. This is done by studying the Hugoniot loci for states on the edges of the saturation triangle. This analysis is necessary for the resolution of the Riemann problem where the initial top state is a mixture of two fluids, while the third fluid is absent. In this chapter we present a simple geometrical construction, the "wedge construction", which allows the determination of admissible shocks joining states on distinct two-phase regimes appearing in three-phase flow, such as the ones represented by points on the edges of the saturation triangle. The wedge construction is independent of the form of the two-phase flux functions, of the permeability functions and of the presence of gravity; it depends only on the fact that along the edges of the saturation triangle a phase is missing, so we have two-phase flow of the existing fluids; therefore this construction can be extended for very general models. It is one of the main results of this work. The wedge construction has the same mathematical nature as the "banana construction" in [1].

In Chapter 8 we prove a "reversal symmetry" theorem, which holds for the simplified pure gravitational problem. We also prove additional theoretical results for bifurcation manifolds in SPGP. These results give support for the Riemann solution obtained partially via numerical calculations of the waves curves.

In Chapter 9 we solve the Riemann problem for the SPGP when the equal-density fluids are heavier than the third fluid. We consider all the combinations of edge-opposite vertex Riemann data. We construct the solution to satisfy generalized Lax conditions and then we verify that this solution is admissible according to the viscous profile criterion. Although we do not prove rigorously that the solution for each problem is unique, we perform an analysis utilizing analytical and numerical arguments that support uniqueness of the solution presented.

In Chapter 10 we solve the Riemann problem for the SPGP when the equal-density fluids are lighter than the third fluid. Again we consider all the combinations of edge-opposite vertex Riemann data. In most cases we analyzed, the slow-family wave curves have disconnected branches that turn out to be crucial for the solution. The existence of shocks between pairs of states that belong to a certain one-dimensional manifold, the slow-family double contact manifold, is a new feature crucial for the existence of the Riemann solutions. In this case the Lax entropy criterion alone does not guarantee uniqueness of the solution, so we are led to use the full viscous profile criterion to select the sole physically correct solution.

In Appendix A we perform additional calculations which complete the proof of Theorem 5.1. In Appendix B we present the proof of Lemma 8.2. In Appendix C we show numerical and analytical arguments for uniqueness of the Riemann solution for one of the cases studied (RP1). In Appendix D we present an extended bibliographic review, in order to summarize the main mathematical works relevant for three-phase flow in porous media.

Along this work, we performed numerical experiments using the computer code RP written by Marchesin, Isaacson and Plohr. This code allowed us to obtain the integral curves, Hugoniot curves, the main bifurcation loci, the phase portraits for dynamical systems and the wave curves, which are fundamental for the construction of the solution. Numerical calculations in MATLAB were also performed.

Chapter 2

The model

In the first section of this chapter we derive the system of conservation laws that models three-phase flow with gravity in porous media, under some physical assumptions listed at the beginning of the section. In the second section we obtain the dimensionless equations and the parameter groups relevant for the study of the buoyancy effects for three-phase flow. In the third section we introduce the quadratic Corey model that we will use in the entire work in order to highlight the phenomena of interest while avoiding complicated analysis. In the last section of the chapter we define the triangle where the three fluid saturations are defined, and some important lines and points inside the triangle that we will use frequently along the work.

2.1 Derivation of the system of conservation laws

We will study a simplified model for three-phase flow in porous media assuming that the porosity ϕ and the absolute permeability of the rock K are constant. The temperature is constant and there is no mass interchange between phases. In this section we derive the equations for an arbitrary spatial dimension, nevertheless in this work we restrict our study to one spatial dimension assuming that the flow occurs uniformly in the vertical direction filling the entire porous medium. We also neglect compressibility effects and assume that there are no sources or sinks.

Let consider the conservation of mass for each phase

$$\frac{\partial}{\partial t}\phi u_i + \nabla \cdot \mathbf{v}_i = 0 \qquad i = 1, 2, 3, \tag{2.1}$$

where u_i denotes saturation and $\mathbf{v}_i$ is the seepage velocity of each phase. We assume that Darcy's Law is satisfied for each phase i:

$$\mathbf{v}_i = -K\frac{k_i}{\mu_i}\big(\nabla p_i - \rho_i g\boldsymbol{e_z}\big) \quad i = 1, 2, 3, \tag{2.2}$$

where k_i is the relative permeability, p_i is the pressure, μ_i is the viscosity and ρ_i is the density for each phase i. We denoted by $\boldsymbol{e_z}$ the unit vector in the vertical direction pointing downwards, g is the gravitational constant. We assume that the permeabilities k_i are functions of the saturations. We assume also that the fluids are incompressible, and that the porous medium is totally saturated, meaning that $\sum_{i=1}^{3} u_i = 1$. The viscosities μ_i, $i = 1, 2, 3$ are constant. In this section and in most of the work, we neglect capillary pressure effects, so that the phase pressures are equal. In Chapters 9 and 10, we will take into account such effects. They will be important in selecting physically admissible shocks.

Now we define

$$\Lambda_i = k_i/\mu_i \quad i = 1, 2, 3; \quad \Lambda = \sum_{i=1,2,3} \Lambda_i, \tag{2.3}$$

$$f_i = \Lambda_i/\Lambda \quad i = 1, 2, 3; \quad \mathbf{v} = \sum_{i=1,2,3} \mathbf{v}_i; \tag{2.4}$$

the functions Λ_i and f_i are the mobility and the fractional flow function corresponding to each phase i, Λ is the total mobility and $\mathbf{v}$ is the total seepage velocity.

We first note that $\sum_{i=1,2,3} f_i = 1$. Let us assume that $p_i = p_j$ (*i.e.*, we are neglecting the capillary pressures), so substituting Darcy' s Law (2.2) in (2.4) and performing some calculations we obtain

$$\mathbf{v}_i = \mathbf{v}f_i + K\Lambda_i \sum_{j\neq i} f_j\rho_{ij}g\boldsymbol{e_z}, \quad i = 1, 2, 3, \tag{2.5}$$

where we are denoting by ρ_{ij} the density difference $\rho_i - \rho_j$ between the phases i and j. Finally, we substitute (2.5) into the system (2.1) to obtain the system of conservation laws for the saturations u_1, u_2 and u_3

$$\frac{\partial}{\partial t}\phi u_i + \nabla \cdot F_i = 0, \quad i = 1, 2, 3, \tag{2.6}$$

where

$$F_i = \mathbf{v}f_i + G_i, \quad i = 1, 2, 3, \tag{2.7}$$

are the components of the vector flow function $(F_1, F_2, F_3)^T$ containing the gravitational terms

$$G_1 = K\Lambda_1\big((1 - f_1)\rho_{13} + f_2\rho_{32}\big)g\boldsymbol{e_z}, \tag{2.8}$$

$$G_2 = K\Lambda_2\big((1 - f_2)\rho_{21} + f_3\rho_{13}\big)g\boldsymbol{e_z}, \tag{2.9}$$

$$G_3 = K\Lambda_3\big((1 - f_3)\rho_{32} + f_1\rho_{21}\big)g\boldsymbol{e_z}. \tag{2.10}$$

Remark 2.1. *Notice that $G_1 + G_2 + G_3 = 0$, therefore $F_1 + F_2 + F_3 = \mathbf{v}$ (the total velocity).*

By adding the equations in (2.5) and using the relations (2.3)-(2.4), we obtain that $\nabla \cdot \mathbf{v} = 0$; this equality reflects the incompressibility of the fluids. Another important fact to take into account is that the conservation of mass system (2.1) has a redundant equation, *i.e.*, any of these equations can be derived from the other two if we use the incompressibility property of the fluids and the fact that the medium is totally saturated. Because of this redundance we can drop any equation in (2.6) obtaining a 2×2 system of conservation law to be studied. The equation to be dropped will be chosen conveniently for each case.

2.2 Dimensionless equations

In this section we rewrite the system of conservation law (2.6) in non-dimensional form, in order to identify the most important non-dimensional parameter groups for the evolution problem, and we reduce to the minimal the number of parameters appearing in the system of conservation law.

We denote as K_{ref} $[m^2]$ the reference absolute permeability, $\mathrm{v}_{\mathrm{ref}}$ $[m/s]$ the reference velocity of the problem, ρ_{ref} $[kg/m^3]$ the reference density, L $[m]$ the reference length of the system and μ_{ref} $[kg \cdot m^{-1} \cdot s^{-1}]$ the reference viscosity. Now we define the dimensionless variables as follows

$$
\begin{aligned}
\widetilde{t} = t\mathrm{v}_{\mathrm{ref}}/L\phi, \quad \widetilde{\mathbf{x}} = \mathbf{x}/L, \quad \widetilde{\mathbf{v}} = \mathbf{v}/\mathrm{v}_{\mathrm{ref}}, \quad \widetilde{K} = K/K_{\mathrm{ref}}, \\
\widetilde{\Lambda}_i = \Lambda_i \mu_{\mathrm{ref}}, \quad \widetilde{\rho}_i = \rho_i/\rho_{\mathrm{ref}}, \quad \widetilde{\mu}_i = \mu_i/\mu_{\mathrm{ref}}, \quad i = 1, 2, 3.
\end{aligned}
\tag{2.11}
$$

As a consequence of above definitions we obtain other useful relations:

$$
\widetilde{\nabla} = L\nabla, \quad \widetilde{\Lambda} = \sum_{i=1,2,3} \widetilde{\Lambda}_i, \quad \widetilde{f}_i = \widetilde{\Lambda}_i/\widetilde{\Lambda}, \quad i = 1, 2, 3.
\tag{2.12}
$$

If we substitute the dimensionless variables and the relations above into the system (2.6), we obtain

$$
\frac{\partial u_i}{\partial \widetilde{t}} + \widetilde{\nabla} \cdot \left(\widetilde{\mathbf{v}} \widetilde{f}_i + C_g \widetilde{G}_i \right) = 0, \quad i = 1, 2, 3,
\tag{2.13}
$$

where

$$
\widetilde{G}_1 = \widetilde{K} \widetilde{\Lambda}_1 \left((1 - \widetilde{f}_1) \widetilde{\rho}_{13} + \widetilde{f}_2 \widetilde{\rho}_{32} \right) \boldsymbol{e_z},
\tag{2.14}
$$

$$
\widetilde{G}_2 = \widetilde{K} \widetilde{\Lambda}_2 \left((1 - \widetilde{f}_2) \widetilde{\rho}_{21} + \widetilde{f}_3 \widetilde{\rho}_{13} \right) \boldsymbol{e_z},
\tag{2.15}
$$

$$
\widetilde{G}_3 = \widetilde{K} \widetilde{\Lambda}_3 \left((1 - \widetilde{f}_3) \widetilde{\rho}_{32} + \widetilde{f}_1 \widetilde{\rho}_{21} \right) \boldsymbol{e_z},
\tag{2.16}
$$

and $C_g = \frac{K_{\text{ref}} \cdot \rho_{\text{ref}} \cdot g}{v_{\text{ref}} \cdot \mu_{\text{ref}}}$ is the dimensionless parameter reflecting the gravitational effects.

We can choose reference values in different ways. As we are interested in cases in which the total velocity is small (possibly equal to zero) but with non-negligible gravitational effects, we set the reference velocity as $v_{\text{ref}} = \frac{K_{\text{ref}} \cdot \rho_{\text{ref}} \cdot g}{\mu_{\text{ref}}}$, so we obtain that $C_g = 1$ in (2.13). We denote by

$$\alpha = \widetilde{\mathbf{v}} = \frac{\mathbf{v}}{v_{\text{ref}}} = \frac{\mathbf{v} \cdot \mu_{\text{ref}}}{K_{\text{ref}} \cdot \rho_{\text{ref}} \cdot g}. \qquad (2.17)$$

Omitting the "$\sim$" and dropping the equation corresponding to phase 3 in (2.13) we obtain the following 2×2 system of conservation law

$$\frac{\partial u_i}{\partial t} + \nabla \cdot \big(\alpha f_i(u_1, u_2) + G_i(u_1, u_2)\big) = 0, \quad i = 1, 2, \qquad (2.18)$$

where now G_1 and G_2 denote the dimensionless gravitational terms given by (2.14) and (2.15).

The parameter α defined in (2.17) is called in this work the "convection/gravity ratio" (cgr). Nevertheless, from Eq. (2.18) with gravitational terms given in (2.14)-(2.15) notice that for equal-density fluids the gravitational terms vanish independently of the value of α.

2.3   The Corey model

We will restrict our analysis to the Corey model with quadratic permeabilities. With this choice we can highlight the phenomena of interest while avoiding complicated analysis. (We expect that solutions for more realistic models are qualitatively similar to those of quadratic models). Explicitly, the mobility of each phase depends only of the saturation of the phase and is quadratic, *i.e.*,

$$\Lambda_i(u_i) = u_i^2/\mu_i, \quad i = 1, 2, 3; \quad \Lambda = \sum_{i=1,2,3} u_i^2/\mu_i, \qquad (2.19)$$

Notice that for simplicity we are setting to zero irreducible saturation values, so we are neglecting the fact that the fluids become immobile at non-zero saturation.

From now on we restrict our study to one spatial dimension flows, by assuming that the flow occurs uniformly in the vertical direction x, filling the entire porous medium. In our convention, the gravitational force points to the positive x-direction.

The flux functions (including gravity) for the quadratic Corey model with permeabil-

ities in (2.19) are

$$F_1(u_1, u_2, u_3) = \frac{u_1^2}{\mu_1}\left(\alpha + \frac{u_3^2}{\mu_3}\rho_{13} + \frac{u_2^2}{\mu_2}\rho_{12}\right)/\Lambda(u_1, u_2, u_3), \qquad (2.20)$$

$$F_2(u_1, u_2, u_3) = \frac{u_2^2}{\mu_2}\left(\alpha + \frac{u_3^2}{\mu_3}\rho_{23} + \frac{u_1^2}{\mu_1}\rho_{21}\right)/\Lambda(u_1, u_2, u_3), \qquad (2.21)$$

$$F_3(u_1, u_2, u_3) = \frac{u_3^2}{\mu_3}\left(\alpha + \frac{u_1^2}{\mu_1}\rho_{31} + \frac{u_2^2}{\mu_2}\rho_{32}\right)/\Lambda(u_1, u_2, u_3). \qquad (2.22)$$

As $u_3 = 1 - u_1 - u_2$, we drop the equation corresponding to phase 3 and rewrite the 2×2 system (2.18) for this model (in one dimension denoted by x):

$$\begin{cases} \frac{\partial u_1}{\partial t} + \frac{\partial}{\partial x}F_1(u_1, u_2) = 0 \\ \frac{\partial u_2}{\partial t} + \frac{\partial}{\partial x}F_2(u_1, u_2) = 0, \end{cases} \qquad (2.23)$$

with flux functions F_1, F_2 given by (2.20)-(2.21), which have α as a parameter.

2.4 The saturation triangle

In order to study the Riemann solution for three-phase flow with gravity for the Corey model, we need to perform all the calculations in the space of saturations. We define the saturation triangle as follow

$$T = \left\{(u_1, u_2) \in \mathbb{R}^2 : \ 0 \le u_1 \le 1, \ 0 \le u_2 \le 1, u_1 + u_2 \le 1\right\}; \qquad (2.24)$$

a useful alternative definition would be

$$T = \left\{(u_1, u_2, u_3) \in \mathbb{R}^3 : \ 0 \le u_i \le 1, \ i = 1, 2, 3, \ \text{and } u_3 = 1 - u_1 - u_2\right\}. \qquad (2.25)$$

We will use any one of the above expressions for the saturation triangle according to the situation.

The interior of the saturation triangle in the context of (2.25) is

$$\tilde{T} = \{U \in T : u_i \ne 0 \ \ i = 1, 2, 3\}. \qquad (2.26)$$

The point of maximum saturation for phase i is the vertex of the triangle denoted by

$$V_i = \{U \in T : u_i = 1\}. \qquad (2.27)$$

The two-phase edge opposite to V_i, which does not include the phase i, will be denoted by

$$\partial_i = \{U \in T : u_i = 0\}. \qquad (2.28)$$

For each phase i, let $j, k \in \{1, 2, 3\}$ be the indices of the other two phases; we define

$$R_i = \left\{ U \in T : \frac{u_j}{\mu_j} = \frac{u_k}{\mu_k}, j \neq k \right\}, \tag{2.29}$$

where μ_j, μ_k are the viscosities of the phases j, k.

Notice that R_i defined by (2.29) represents a segment starting from the vertex V_i and ending on the edge ∂_i at the point B_i. The coordinates of the points B_i, $i = 1, 2, 3$, are given by

$$B_1 = (0, \tfrac{\mu_2}{\mu_2+\mu_3}, \tfrac{\mu_3}{\mu_2+\mu_3}), \quad B_2 = (\tfrac{\mu_1}{\mu_1+\mu_3}, 0, \tfrac{\mu_3}{\mu_1+\mu_3}), \quad B_3 = (\tfrac{\mu_1}{\mu_1+\mu_2}, \tfrac{\mu_2}{\mu_1+\mu_2}, 0). \tag{2.30}$$

Remark 2.2. *For the case $\mu_j = \mu_k$ we have that B_i is the middle point of the edge ∂_i.*

All segments and points defined above are displayed in Fig. 2.1
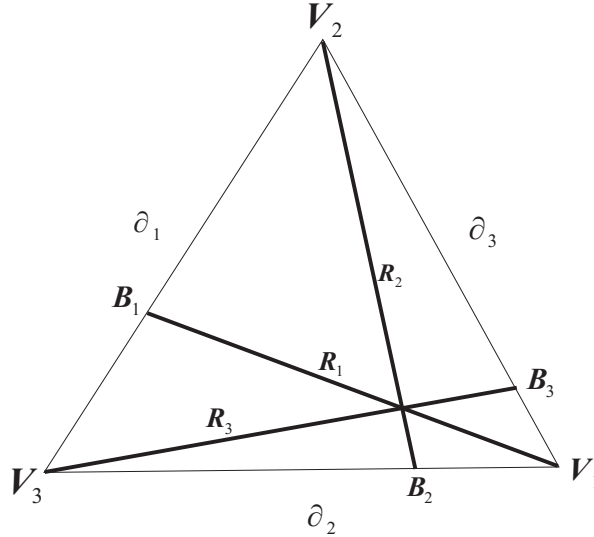
Figure 2.1: *Saturation triangle for a case where all viscosities are distinct. Segments R_i, vertices V_i and points B_i*

Chapter 3

General bifurcation theory for Riemann problems

In this chapter we recall some basic aspects of general theory for systems of conservation laws and the theory of bifurcation of Riemann solutions, in order to provide the non-specialist reader with a brief background on these subjects. Specialists should skip it. Essentially we collect information from [21], [9], [20], [40], [45].

3.1 Riemann solutions for a system of conservation laws. Lax conditions.

Consider the system of conservation laws

$$U_t + F(U)_x = 0 \tag{3.1}$$

governing the evolution, in one space dimension, of a 2-dimensional state vector $U(x,t)$, *i.e.*, for each (x,t), $U(x,t) \in \mathbb{R}^2$. The function $F : \Omega \subset \mathbb{R}^2 \to \mathbb{R}^2$ is called the flux. The characteristic speeds for Eq. (3.1), *i.e.*, the eigenvalues λ^-, λ^+ of the Jacobian matrix $dF(U)$, are given by the formula

$$\lambda^{\pm}(U) = (1/2)\Big(tr(dF(U)) \pm \sqrt{[tr(dF(U))]^2 - 4\det(dF(U))}\Big) \tag{3.2}$$

Definition 3.1. *The system* (3.1) *is hyperbolic if* $\lambda^{\pm}(U) \in \mathbb{R}$, $\forall U \in \Omega \subset \mathbb{R}^2$.

In the hyperbolic region, where the characteristic speeds are real, we have the natural ordering

$$\lambda^-(U) \leq \lambda^+(U), \tag{3.3}$$

so we call λ^- the slow-family characteristic speed and λ^+ the fast-family characteristic speed. The nonlinearity of F implies the dependence of the characteristic speeds on U;

which leads, in general, to focusing of waves and the formation of discontinuous solutions, so that Eq. (3.1) must be interpreted in the sense of distributions.

Remark 3.1. *Sometimes we will denote by s and f (instead of $-$ and $+$) the slow and fast families, respectively.*

Definition 3.2. *Riemann Problem**. A Riemann problem for the conservation law (3.1) is a special Cauchy problem with initial data*

$$U(0, x) = \begin{cases} U_L & \text{if } x < 0 \\ U_R & \text{if } x > 0, \end{cases} \tag{3.4}$$

where U_L and U_R are constant.

The general solutions of Eq. (3.1) consist of weak solutions that respect the invariance of the equation under the scaling transformation $(t, x) \to (ct, cx)$ with $c > 0$. Such scale-invariant solutions satisfy the initial conditions of the Riemann problem as well as the PDE (3.1).

Conversely, solutions of a Riemann problem are expected to be scale-invariant, *i.e.*, they depend on t and x only through the combination $\xi = x/t$. Although Riemann problems are only special initial value problems, the solutions of the general Cauchy initial value problem may be viewed as a nonlinear superposition of scale invariant solutions [11].

A scale-invariant solution can be partitioned into several groups of waves; the waves in each group move together as a single entity. More precisely, we define a wave group to be a scale-invariant solution that contains no intermediate constant states. Thus a solution of a Riemann problem comprises a sequence of wave groups moving apart from each other, as in Fig. 3.1(a). Wave groups are composed of two basic ingredients: centered rarefaction waves and centered discontinuous waves, see Fig. 3.1(b).
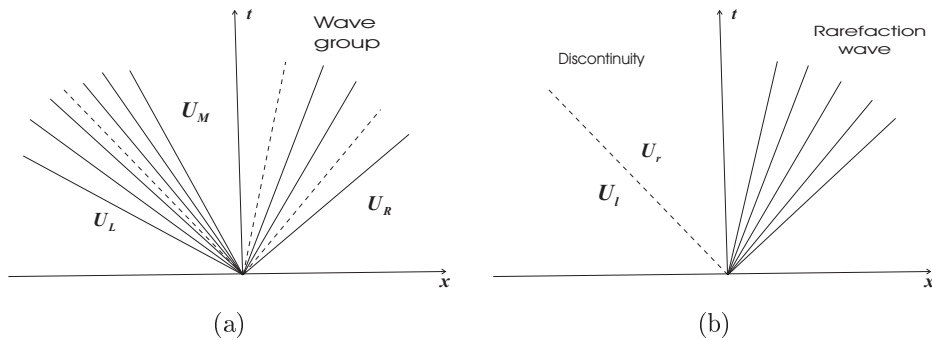
Figure 3.1: Scale-invariant solutions. (a) Example of solution for a Riemann problem, comprising a sequence of two wave groups. (b) A centered rarefaction wave and a centered discontinuous wave.

A centered rarefaction wave associated with a characteristic family i ("$-$" or "$+$") is constructed using integral curves of the "differential equation"

$$\dot{U} = r^i(U), \tag{3.5}$$

where $r^i(U)$ is a right eigenvector of $dF(U)$ corresponding to $\lambda^i(U)$ in (3.2). We notice that (3.5) is an ordinary differential equation only locally in regions where strict hyperbolicity is satisfied, the sign and amplitude of r^i are arbitrary. A rarefaction wave corresponds to a segment of an integral curve along which λ^i is nondecreasing; it is defined by inverting the relation $\lambda^i(U) = \xi$.

A centered discontinuous wave is a jump discontinuity that propagates at speed σ and separates two states U_l and U_r, where U_l, U_r and σ satisfy the system of two equations

$$-\sigma[U_r - U_l] + F(U_r) - F(U_l) = 0, \tag{3.6}$$

called the Rankine-Hugoniot jump condition. By convention, U_l is on the left side of the discontinuity and U_r is on the right side. In general, these states are different from the states U_L and U_R of the Riemann problem initial data. For a fixed U_l, the set of states U such that the pair U_l, U satisfy (3.6) for some σ comprises the Hugoniot locus, $\mathcal{H}(U_l)$. The Hugoniot locus $\mathcal{H}(U_l)$ through U_l can be constructed by finding the zero-set $H_{U_l}(U, \sigma) = 0$ of the Hugoniot function $H_{U_l} : \mathbb{R}^2 \times \mathbb{R} \to \mathbb{R}^2$ defined by

$$H_{U_l}(U, \sigma) = -\sigma(U - U_l) + F(U) - F(U_l). \tag{3.7}$$

The projection of this zero-set onto state space gives $\mathcal{H}(U_l)$.

A very useful tool employed in this work is the Triple Shock Rule [22]. Next we state two distinct version of this result.

Triple Shock Rule (first version). *For system (3.1), assume that the states U_1, U_2 and U_3 satisfy $U_1 \in \mathcal{H}(U_2)$, $U_2 \in \mathcal{H}(U_3)$ and $U_3 \in \mathcal{H}(U_1)$. Then either U_1, U_2, U_3 are collinear or else $\sigma(U_2, U_1) = \sigma(U_3, U_2) = \sigma(U_1, U_3)$.*

Triple Shock Rule (second version). *For system (3.1), assume that the states U_1, U_2 and U_3 satisfy $U_2 \in \mathcal{H}(U_1)$, $U_3 \in \mathcal{H}(U_2)$ and $\sigma(U_1, U_2) = \sigma(U_2, U_3)$ then $U_3 \in \mathcal{H}(U_1)$ and $\sigma(U_1, U_3) = \sigma(U_1, U_2) = \sigma(U_2, U_3)$.*

To avoid non-uniqueness of solutions of Riemann problems, the class of allowable discontinuous waves must be restricted. For systems of n conservation laws that are genuinely nonlinear, Lax [28] introduced the admissibility requirement that the characteristics of one family impinge on both sides of the discontinuity, while the characteristics of the other families cross the discontinuity undergoing deflection. For more general conservation laws, characteristics must be permitted to become tangent to the discontinuity, so we have the following definitions for admissible shocks.

Definition 3.3. *Slow-family and fast-family shock wave.* *We define a centered discontinuous wave to be a (generalized) Lax discontinuity of the slow-family (slow shock) provided that the characteristic speeds are related to the propagation speed as follow:*

$$\lambda^-(U_r) \leq \sigma \leq \lambda^-(U_l), \quad and \quad \sigma \leq \lambda^+(U_r). \tag{3.8}$$

where only one of the inequalities in (3.8)–(a) is allowed to become an equality. Similarly, we define a centered discontinuous wave to be a (generalized) Lax discontinuity of the fast-family (fast shock) provided that the characteristic speeds are related to the propagation speed as follow:

$$\lambda^+(U_r) \leq \sigma \leq \lambda^+(U_l), \quad and \quad \lambda^-(U_l) \leq \sigma. \tag{3.9}$$

where only one of the inequalities in (3.9)–(a) is allowed to become an equality.

In certain cases we allow equalities in (3.8) or (3.9) to occur. They will be discussed latter. Lax used the nomenclature 1-and 2-shock for slow and fast shocks.

If we adopt the admissibility criterion based on characteristics and assume that both characteristic speeds are distinct, then any wave, *i.e.*, rarefaction wave or discontinuity, has an associated family. In this work we only consider solutions satisfying: (1) no slow wave is preceded by a wave of the fast family; and (2) two waves of the same family must belong to the same wave group. Therefore a solution of a Riemann problem can contain at most 2 wave groups, a slow wave group followed by a fast wave group. These facts [30] generalize the classical picture [11] in which a solution of a Riemann problem consists of at most 2 shock or rarefaction waves, separated by constant states, where each wave is associated with a distinct family.

In order to describe the Riemann solution we will use the notation found in Furtado [9]. Thus we will denote $U_l \xrightarrow{w} U_r$ to express the fact that U_l is connected to U_r (on the right) by an elementary wave of type w. The elementary waves types are denoted as follows.

Wave nomenclature

(a) R^- if the wave is a rarefaction of the slow family.

(b) R^+ if the wave is a rarefaction of the fast family.

(c) S^- if $\lambda^-(U_r) < \sigma < \lambda^-(U_l)$ and $\sigma < \lambda^+(U_r)$

(d) S^+ if $\lambda^+(U_r) < \sigma < \lambda^+(U_l)$ and $\lambda^-(U_l) < \sigma$

(e) CS^- if $\lambda^-(U_r) < \sigma = \lambda^-(U_l)$ and $\sigma < \lambda^+(U_r)$

(f) CS^+ if $\lambda^+(U_r) < \sigma = \lambda^+(U_l)$.

(g) SC^- if $\lambda^-(U_r) = \sigma < \lambda^-(U_l)$.

(h) SC^+ if $\lambda^+(U_r) = \sigma < \lambda^+(U_l)$ and $\lambda^-(U_l) < \sigma$

(i) C^- if $\lambda^-(U_l) = \sigma = \lambda^-(U_r)$.

(j) C^+ if $\lambda^+(U_l) = \sigma = \lambda^+(U_r)$.

(k) C^+_- if $\lambda^-(U_l) = \sigma = \lambda^+(U_r)$.

(l) C_+^- if $\lambda^+(U_l) = \sigma = \lambda^-(U_r)$.

(m) $(GC)^i$ if the wave is a genuine contact for the family i, *i.e.*, a wave on which $\nabla\lambda^i \cdot r^i \equiv 0$.

Remark 3.2. *Notice that discontinuities* $(c), (d)$ *denote classical Lax shock of slow and fast families respectively. The discontinuities* $(e), (f)$ *denote shocks that are characteristic at the left* (i.e., *with speed equal to a characteristic speed on the left), for both families, and discontinuities* $(g), (h)$ *denote shocks that are characteristic on the right. Finally the discontinuities* $(i), (j)$ *denote double contact discontinuities of slow and fast family respectively, while* (k) *and* (l) *denote a double-contact discontinuity involving the two families. Finally* (m) *denotes a genuine contact, this is a discontinuity travelling with constant characteristic speed, see [47], [49].*

Remark 3.3. *For two-phase solutions we will use the same notation for the elementary wave without using superscripts.*

Lax original or generalized criteria, however, are sometimes overly restrictive and other times too lax: a Riemann problem might have no solution or it might have many. We are led to impose the admissibility criterion to require discontinuous waves to possess viscous profiles, as described in the next section. This is the viscosity admissibility criterion. In general, it is distinct from the characteristic criterion, since there exist Lax discontinuities that do not have viscous profiles, while some discontinuities with viscous profiles are not of Lax type, see [25]. The viscosity criterion, too, can fail to guarantee existence and uniqueness of solutions of Riemann problems. In this work we construct solutions to satisfy Lax criterion and after we verify that such solutions also satisfy the viscosity admissibility criterion.

3.2   Viscosity admissibility criterion

Typically, Eq. (3.1) is an approximation to a system of the form

$$U_t + F(u)_x = \epsilon[D(U)U_x]_x \tag{3.10}$$

in the (singular) limit as $\epsilon \to 0^+$. Here D is the viscosity matrix, which models certain physical effects (such as capillarity effects in multiphase flow in porous media) that are neglected in the model. We usually require that the eigenvalues of $D(U)$ have positive real part; this guarantees that short wavelength perturbations of constant solutions decay exponentially in time. For more details, see Majda-Pego [31] and Azevedo et al. [3].

Physically realizable solutions of Eq. (3.1) are expected to be limits of solutions of the parabolic equation (3.10). In particular, certain centered discontinuous waves arise as limits of travelling wave solutions as follows. A travelling wave depends on t and x only

through the combination $\xi = (x - \sigma t)/\epsilon$, and it approaches limits U_r and U_l as $\xi \to \pm\infty$. Therefore Eq. (3.10) can be integrated once to obtain the associated ODE system

$$-\sigma[U(\xi) - U_l] + F(U(\xi)) - F(U_l) = D(U(\xi))\dot{U}(\xi), \qquad (3.11)$$

where the dot denotes differentiation with respect to ξ. Taking the limits of Eq. (3.11) as $\xi \to \pm\infty$ shows that U_r, U_l and σ must be related by the Rankine-Hugoniot condition (3.6), so that U_r and U_l are critical points for the ODE system. As $\epsilon \to 0^+$, the spatial region over which the solution makes the transition from U_l to U_r shrinks to a point at $x = \sigma t$. Consequently, the travelling wave solution approaches a centered discontinuous wave. Thus a discontinuity is said to have a viscous profile when the system of ordinary differential equation (3.11) has a connecting orbit flowing from U_l to U_r. It is natural to regard a discontinuity as admissible only if it has a viscous profile; this is the viscosity criterion for shock admissibility [7], [18], [10].

The critical points of a system of ordinary differential equations are crucial to its study. For Eq. (3.11), a critical point is a state U_c that satisfies the Rankine-Hugoniot condition for the given state U_l and the speed σ. For ODE's, in the hyperbolic case the behavior of solutions in the neighborhood of a critical point U_c is reflected in qualitative features of solutions of the linearization of Eq. (3.11) about U_c:

$$[-\sigma + F'(U_c)](U - U_c) = D(U_c)\dot{U} . \qquad (3.12)$$

Such solutions are determined by the eigenvalues β and corresponding eigenvectors $\hat{U}_\beta$ that satisfy

$$[-\sigma + F'(U_c)]\hat{U}_\beta = \beta D(U_c)\hat{U}_\beta . \qquad (3.13)$$

For example, $U = U_c + \sum_\beta c_\beta \exp(\beta\xi)\hat{U}_\beta$ when the eigenvalues are distinct. Thus the character of the critical point is determined by the eigenvalues β.

As we are restricted to system of two conservation laws, (3.11) is a system of ODE's in the plane. A critical point is classified as an anti-saddle point (*i.e.*, a node, focus or center) or as a saddle point. Generically an orbit for the system of ODE's connects either two saddle points, two anti-saddle points or a saddle and an anti-saddle. In studies of viscous profiles for shock waves the first step is to choose D as the identity matrix. For this choice the eigenvalues at a critical point U_c are $\beta_i = \lambda^i(U_c) - \sigma$, $i = -, +$. A Lax shock of the slow family has $\sigma < \lambda^-(U_l) < \lambda^+(U_l)$ and $\lambda^-(U_r) < \sigma < \lambda^+(U_r)$, so that the critical points U_l and U_r of Eq. (3.11) are, respectively, a repelling node and a saddle point. Similarly, U_l and U_r are, respectively, a saddle point and an attracting node in the case of a Lax shock wave of the fast family. In summary, an admissible discontinuity of Lax type corresponds to a saddle-node connection.

3.3   The Bethe-Wendroff theorem

Away from primary and secondary bifurcation points, the Hugoniot locus is a curve and it may be parameterized by a single variable. We use a superimposed dot to denote the derivative with respect to this variable and let $\sigma(U)$ be the speed of the shock as U moves along the Hugoniot locus. The following theorem gives an analytic description of the qualitative behavior of $\sigma(U)$.

Theorem 3.1. *(Bethe-Wendroff, see [52]) Consider the Hugoniot locus through a state U_0. Let U be a point on the locus and assume that (3.14) does not hold at U. Then the following are equivalent: (a) $\dot{\sigma} = 0$, (b) $\lambda^i(U) = \sigma(U)$ for some i. In this case, $\lambda^i(U) - \sigma(U)$ and $\dot{\sigma}(U)$ vanish to the same order. Also, the characteristic vector of the i-th family is tangent with the same order to the Hugoniot locus.*

Remark 3.4. *The Bethe-Wendroof theorem can be stated for the composite locus too.*

The Bethe-Wendroff theorem relates the monotonicity of the propagation speed along the Hugoniot and composite curves to the admissibility of the shock waves, at points where equality in the Lax entropy relations (3.8)-(3.9) holds with respect to one of the characteristic speeds for U_r. This fact makes Bethe-Wendroff theorem an important tool in the construction of waves curves.

3.4   Bifurcation manifolds

Now we define certain 1-dimensional "manifolds" which play a fundamental role in the wave curve construction in our problem in two unknowns. They are not genuine manifolds since they may have self intersections or other singularities.

The secondary bifurcation manifold consists of the states which do not satisfy the hypothesis of the implicit function theorem; generically, the Hugoniot locus changes topology at such locus. In general we know that locally through each state U_L there exist two Hugoniot branches, each branch transversal to the other, so each U_L is a primary bifurcation.

Definition 3.4. *A state U belongs to the **secondary bifurcation manifold** for the family i (denoted by Bif_i $i = -, +$) if there exist a state $U' \neq U$ such that*

$$U' \in \mathcal{H}(U) \quad with \quad \lambda^i(U') = \sigma(U, U') \quad and \quad l^i(U')(U' - U) = 0 \qquad (3.14)$$

where we have denoted by $l^i(U')$ a left eigenvector of the Jacobian matrix $dF(U')$.

Now we will define the inflection manifold; it is named by analogy with scalar conservation laws. It is the manifold where genuine nonlinearity is lost, *i.e.*, the eigenvalue does not vary monotonically along a rarefaction curve near an inflection point.

Definition 3.5. *The state U belongs to the **inflection manifold** for the family i (denoted by Inf_i $i = -, +$) if and only if*

$$\nabla \lambda^i(U) \cdot r^i(U) = 0 \tag{3.15}$$

where we have denoted by $r^i(U)$ a right eigenvector of the Jacobian matrix $dF(U)$.

Remark 3.5. *Rarefaction curves stop at inflection manifold.*

The following definition corresponds to the hysteresis manifold, which contains states of a composite segment joined to the end of a rarefaction segment by a nonlocal shock wave.

Definition 3.6. *The state U lies on the **Hysteresis manifold** for the family i, if there exist a state $U' \neq U$ such that*

$$U \in \mathcal{H}(U') \quad with \quad \lambda^i(U') = \sigma(U, U') \quad and \quad \nabla \lambda^i(U') \cdot r^i(U') = 0 \tag{3.16}$$

where we have denoted by $r^i(U')$ a right eigenvector of the Jacobian matrix at the point U'.

Remark 3.6. *Notice that such U' in the definition of the Hysteresis must be on the inflection manifold.*

Definition 3.7. *The state U belongs to the (i,j)-**Double Contact manifold** if there exist a state U' such that*

$$U' \in \mathcal{H}(U) \quad with \quad \lambda^i(U) = \sigma(U, U') = \lambda^j(U'), \tag{3.17}$$

where the families i and j may be the same or different.

Remark 3.7. *A shock joining such U and U' is called a double-contact shock.*

Remark 3.8. *States on the Double Contact manifold can be junctions of composite and rarefaction segments in wave curves. This is analogous with the scalar case, where a shock happen to be embedded between two rarefaction waves, see Oleinik [34].*

Definition 3.8. *(Extension of a point) Consider a state A in the saturation triangle. We say that P_A^i is the **extension** of the point A corresponding to the family i, if $P_A^i \in \mathcal{H}(A)$ and $\sigma(A, P_A^i) = \lambda^i(P_A^i)$; in other words, the shock joining the state A with the state P_A^i is characteristic at P_A^i for the family i.*

Remark 3.9. *One can define another extension, in which the shock is characteristic at A.*

Because of the presence of the boundary of the physical region, another manifold plays a role in the model problem, which we call an interior boundary contact and is defined as the internal extension of the physical boundary.

Definition 3.9. *The state U belongs to the **boundary contact manifold** for the family i (or **extension** of the boundary), denoted by E_∂^i if there exist a state U' such that*

$$U \in \mathcal{H}(U') \quad \text{with } U' \text{ on the boundary and} \quad \lambda^i(U) = \sigma(U, U'). \qquad (3.18)$$

Remark 3.10. *A boundary contact wave occurs when a junction between wave segments coincides with the boundary.*

Remark 3.11. *Notice that hysteresis manifold is the (suitable) extension of the inflection manifold.*

3.5   Wave curves

In this section, we describe briefly the concept of wave curve. A wave curve of the family i, starting at the state U_L is a parametrization of the states U in state space that can be connected on the right hand side of U_L by an i-wave group, in other words a wave curve is a parametrization of certain coherent sequences of invariant waves as points in the space of possible states.

As we already said, in physical space, Riemann solutions consist of sequences of rarefaction fans, discontinuities and constant states. In the cases studied in this work, these elementary waves are grouped into waves that belong either to the slow-family or the fast-family. These solutions obey the geometrical constraint that speeds in physical space increase from left to right.

Wave curves in this type of problems (in which strict hyperbolic and genuine nonlinearity fail) differ from classical wave curves in several respects, see [30] and [34]. First, they are represented in state space by three types of elementary segments, consisting not only of shock curves and rarefaction curves as in the classical case, but also of composite curves, which represent shock waves adjacent to rarefaction waves. The final state U of a composite curve satisfies

$$U \in \mathcal{H}(U') \quad \text{with} \quad \lambda^i(U') = \sigma(U, U'),$$

where U' traverses a rarefaction segment. Second, in each wave curve there are many such elementary segments. Each elementary segment must stop whenever its wave speed attains an extremum, and the type of elementary segment that follows is determined by simple rules. Third, since Hugoniot curves possess nonlocal (*i.e.*, detached) branches, wave curves also have complicated shapes; *e.g.*, they may have disconnected parts or branching points, see [20].

The continuation rules for wave curves are justified by the Bethe-Wendroff theorem, as applied to determine the qualitative behavior of the wave speed along a wave curve. This analysis is conveniently performed using wave speed diagrams, which generalize to systems Oleinik's convex envelope construction for scalar conservation laws [34]. Using

these techniques, the stability of waves curves with respect to perturbations of the left state can be established [9].

A typical wave speed diagram is shown in Fig. 3.2(b). The horizontal axis corresponds to a parametrization of the wave curve, and the vertical axis is speed. The solid lines are the two characteristic speeds, while the dashed (resp. crossed) curves are the propagation speeds of shocks waves (resp. composite waves). The particular example shows the speeds for the fast-family wave curve starting at a state U_L in the interior of the saturation triangle, for the simplified pure gravitational problem ($\alpha = 0$, $\rho_1 = \rho_2 > \rho_3$). Near this state the curve consists of rarefaction and shock waves, as usual. The rarefaction segment ends when the characteristic speed reaches a maximum, where the wave curve continues through a segment of composite waves. Points on the composite correspond to points on the rarefaction at the same speed; these points which work back along the rarefaction segment, are indicated by dots. The composite segment ends when its speed coincides with the faster characteristic speed on the right, and is followed by another rarefaction segment, whose speed eventually maximizes, leading to another composite segment. This composite segment ends when the corresponding rarefaction points have reached the beginning of the segment; then the wave curve continues with a new composite segment based on the previous rarefaction segment. Finally this last composite wave ends when the speed coincides with the fast-family characteristic speed on the left, where the wave curve becomes a shock segment.

The wave curve corresponding to the wave speed diagram is shown in Fig. 3.2(a). Again, solid, dashed, and crossed curves represent rarefaction, shock, and composite segments respectively.
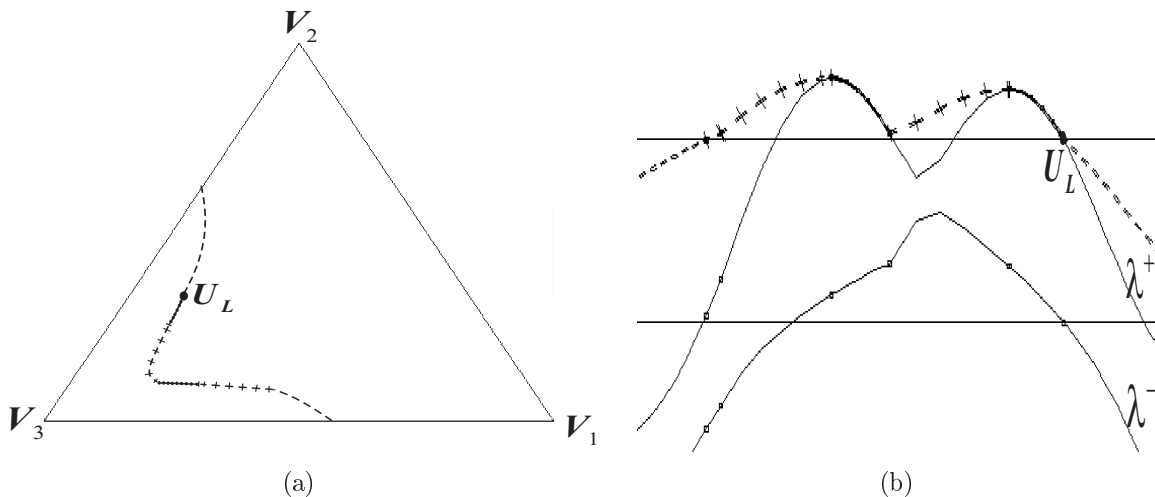
Figure 3.2: Example of wave curve for the case $\alpha = 0$, $\rho_1 = \rho_2 > \rho_3$. (a) Fast-family wave curve through U_L. (b) Wave speed diagram.

3.6 Hyperbolicity, umbilic and quasi-umbilic points

3.6.1 Loss of strict hyperbolicity

The system of conservation law (3.1) is strictly hyperbolic if the Jacobian matrix $dF(U)$ has real and distinct eigenvalues for all U in state space.

The hyperbolic character of the system of conservation law can be lost in different ways, so we define:

Definition 3.10. *A point $U = (u_1, u_2)$ is called a **coincidence point** for the flux F if the eigenvalues of the Jacobian matrix dF coincide at this point, i.e., if $\lambda^-(U) = \lambda^+(U)$.*

Definition 3.11. *We say that a coincidence point $U^* = (u_1^*, u_2^*)$ is an **umbilic point** of the PDE system (with flow function given by F), if it satisfies the following conditions*

(H1) $dF(U^*)$ is diagonalizable.

(H2) There is a neighborhood $\mathcal{V}$ of U^* such that $dF(U)$ has distinct eigenvalues for all $U \in \mathcal{V} - U^*$.

Remark 3.12. *If there exist Ω region where the eigenvalues are complex conjugate, this region is called "elliptic region".*

Definition 3.12. *We have the following definitions:*

  *(i) We say that a coincidence point U is a **quasi-umbilic point** if the condition $(H2)$ holds but $(H1)$ fails.*

  *(ii) We say that a coincidence point U belongs to a **diagonalization curve** if there exists a curve through U along which condition $(H2)$ fails but condition $(H1)$ holds. If such curve is a line, we call it as **diagonalization line**.*

Remark 3.13. *Quasi-umbilic points and diagonalization lines seem to have been characterized for the first time in this work.*

3.6.2 Hyperbolicity analysis.

Schaeffer and Shearer [40] classified umbilic points for the general 2×2 system of conservation laws, by means of a local analysis of the quadratic form arising from the Taylor expansion of the flux function in a neighborhood of the umbilic point. This analysis is possible only if hypotheses $H1$ and $H2$ hold. They also presented in [40] some ideas that will help us in performing an hyperbolicity analysis and determine the umbilic and quasi-umbilic points of the system of conservation laws. In the following we summarize the main ideas.

For a real 2×2 matrix M let us define

$$devM = M - \frac{1}{2}(trM)I \tag{3.19}$$

as the projection of M into the space of trace-free matrices. In (3.19), dev is known as the *deviator operator*. The deviator of a matrix M retains all information about multiple eigenvalues. We Introduce coordinates on the (three dimensional) space of trace-free matrices by the formula

$$devM = \begin{pmatrix} X & Y + Z \\ Y - Z & -X \end{pmatrix}. \tag{3.20}$$

In other words, X, Y, Z are the coordinates associated with the basis of 2×2 matrices

$$\begin{pmatrix} 1 & 0 \\ 0 & -1 \end{pmatrix}, \begin{pmatrix} 0 & 1 \\ 1 & 0 \end{pmatrix}, \begin{pmatrix} 0 & 1 \\ -1 & 0 \end{pmatrix}.$$

Now we have an important result for the deviator of a matrix M proven in [40]:

Proposition 3.1.

(i) *M has equal eigenvalues and is diagonalizable if and only if $devM = 0$.*

(ii) *M has distinct real eigenvalues, coincident real eigenvalues, or complex conjugate eigenvalues according to whether (X, Y, Z) lies outside, on the surface of, or inside the cone $X^2 + Y^2 = Z^2$, respectively.*

Remark 3.14. *This proposition follows from the fact that the characteristic polynomial for (3.20) is $\lambda^2 - X^2 - Y^2 + Z^2 = 0$.*

Application of the deviator operator to the Jacobian matrix

We can consider the mapping $dev\, dF$ (deviator of the Jacobian Matrix of the system of conservation laws (3.1)) from the U-plane into the space of trace-free matrices given by $U \mapsto (X, Y, Z)$; geometrically, this mapping defines a surface in $\mathbb{R}^3$. Condition $(H1)$ implies that all the umbilic points are mapped into the origin, the vertex of the cone $X^2 + Y^2 = Z^2$. Let be U^* an umbilic point; since F is strictly hyperbolic on a punctured neighborhood of the umbilic point $\mathcal{V} - U^*$, the image of $\mathcal{V} - U^*$ must lie outside this cone, *i.e.*, in the open region $\{X^2 + Y^2 > Z^2\}$. Assuming that this surface is nonsingular at U^*, It follows that the tangent plane lies in the region $X^2 + Y^2 \geq Z^2$.

The following result was also proved by Schaeffer and Shearer [40].

Theorem 3.2. *Let U^* be a coincidence point, condition $(H2)$ is satisfied if and only if the surface that is the image of $\mathbb{R}^2$ by $dev\, dF$ is nonsingular at U^* and, the punctured tangent plane at U^* lies in the open region $\{X^2 + Y^2 > Z^2\}$.*

Chapter 4

Characteristic analysis

In this chapter we calculate the Jacobian matrix of the 2×2 conservation law system (2.23), with flux functions given by (2.20)-(2.21). We calculate a formula for the characteristic speeds. We present an exhaustive analysis of the conservation law in order to determine where strict hyperbolicity fails; the analysis includes the cases in which two of the phases have equal densities, for which the solutions have special structures.

4.1 Characteristic speed analysis

We will denote by dF or J the Jacobian matrix of the vector flux function $(F_1, F_2)^T$ corresponding to the 2×2 system given in (2.23). We write

$$J \equiv dF = \frac{\partial(F_1, F_2)}{\partial(u_1, u_2)} = \begin{pmatrix} J_{11} & J_{12} \\ J_{21} & J_{22} \end{pmatrix} = \alpha A + B. \tag{4.1}$$

We recall the definition of Λ_i and Λ in Eq. (2.19). We will denote by $\Lambda_i^{'}$ the derivative $d\Lambda_i/du_i$ for $i = 1, 2, 3$. The matrix A in (4.1) is given by

$$A = \begin{pmatrix} \Lambda_1^{'}\Lambda - \Lambda_1(\partial\Lambda/\partial u_1) & -\Lambda_1(\partial\Lambda/\partial u_2) \\ -\Lambda_2(\partial\Lambda/\partial u_1) & \Lambda_2^{'}\Lambda - \Lambda_2(\partial\Lambda/\partial u_2) \end{pmatrix} /\Lambda^2; \tag{4.2}$$

it is the part of the Jacobian matrix that represents the motion without gravity, and the matrix

$$B = \begin{pmatrix} b_{11} & b_{12} \\ b_{21} & b_{22} \end{pmatrix} \tag{4.3}$$

is the part of the Jacobian matrix that represents buoyancy effects (which depend of the densities difference between the fluids), with elements

$$b_{11} = \Lambda_1' \Big[(1 - \frac{\Lambda_1}{\Lambda})\rho_{13} + \frac{\Lambda_2}{\Lambda}\rho_{32} \Big] - \Lambda_1 \Big[\Big(\frac{\Lambda_1'\Lambda - \Lambda_1(\partial\Lambda/\partial u_1)}{\Lambda^2} \Big)\rho_{13} + \frac{\Lambda_2(\partial\Lambda/\partial u_1)}{\Lambda^2}\rho_{32} \Big],$$

$$b_{12} = \Lambda_1 \Big[\frac{\Lambda_1(\partial\Lambda/\partial u_2)}{\Lambda^2}\rho_{13} + \frac{\Lambda_2'\Lambda - \Lambda_2(\partial\Lambda/\partial u_2)}{\Lambda^2}\rho_{32} \Big],$$

$$b_{21} = \Lambda_2 \Big[\frac{\Lambda_2(\partial\Lambda/\partial u_1)}{\Lambda^2}\rho_{23} + \frac{\Lambda_1'\Lambda - \Lambda_1(\partial\Lambda/\partial u_1)}{\Lambda^2}\rho_{31} \Big],$$

$$b_{22} = \Lambda_2' \Big[(1 - \frac{\Lambda_2}{\Lambda})\rho_{23} + \frac{\Lambda_1}{\Lambda}\rho_{31} \Big] - \Lambda_2 \Big[\Big(\frac{\Lambda_2'\Lambda - \Lambda_2(\partial\Lambda/\partial u_2)}{\Lambda^2} \Big)\rho_{23} + \frac{\Lambda_1(\partial\Lambda/\partial u_2)}{\Lambda^2}\rho_{31} \Big].$$

Thus we have for J in (4.1)

$$
\begin{aligned}
J_{11} = 2\Big(& \frac{\alpha u_1 u_2^2}{\mu_1\mu_2} + \frac{\alpha u_1^2 u_3}{\mu_1\mu_3} + \frac{\alpha u_1 u_3^2}{\mu_1\mu_3} + \frac{u_1 u_2^4}{\mu_1\mu_2^2}\rho_{12} + \frac{u_1 u_2^2 u_3^2}{\mu_1\mu_2\mu_3}\rho_{12} + \\
& + \frac{u_1 u_2^2 u_3^2}{\mu_1\mu_2\mu_3}\rho_{13} + \frac{u_1 u_3^4}{\mu_1\mu_3^2}\rho_{13} - \frac{u_1^4 u_3}{\mu_1^2\mu_3}\rho_{13} + \frac{u_1^2 u_2^2 u_3}{\mu_1\mu_2\mu_3}\rho_{32} \Big)/\Lambda^2,
\end{aligned}
\tag{4.4}
$$

$$
\begin{aligned}
J_{12} = 2\Big(& -\frac{\alpha u_1^2 u_2}{\mu_1\mu_2} + \frac{\alpha u_1^2 u_3}{\mu_1\mu_3} + \frac{u_1^4 u_2}{\mu_1^2\mu_2}\rho_{12} + \frac{u_1^2 u_2 u_3^2}{\mu_1\mu_2\mu_3}\rho_{32} + \\
& + \frac{u_1^2 u_2^2 u_3}{\mu_1\mu_2\mu_3}\rho_{32} - \frac{u_1^4 u_3}{\mu_1^2\mu_3}\rho_{13} \Big)/\Lambda^2,
\end{aligned}
\tag{4.5}
$$

$$
\begin{aligned}
J_{21} = 2\Big(& -\frac{\alpha u_1 u_2^2}{\mu_1\mu_2} + \frac{\alpha u_2^2 u_3}{\mu_2\mu_3} + \frac{u_1 u_2^4}{\mu_1\mu_2^2}\rho_{21} + \frac{u_1 u_2^2 u_3^2}{\mu_1\mu_2\mu_3}\rho_{31} + \\
& + \frac{u_1^2 u_2^2 u_3}{\mu_1\mu_2\mu_3}\rho_{31} - \frac{u_2^4 u_3}{\mu_2^2\mu_3}\rho_{23} \Big)/\Lambda^2,
\end{aligned}
\tag{4.6}
$$

$$
\begin{aligned}
J_{22} = 2\Big(& \frac{\alpha u_1^2 u_2}{\mu_1\mu_2} + \frac{\alpha u_2^2 u_3}{\mu_2\mu_3} + \frac{\alpha u_2 u_3^2}{\mu_2\mu_3} + \frac{u_1^4 u_2}{\mu_1^2\mu_2}\rho_{21} + \frac{u_1^2 u_2 u_3^2}{\mu_1\mu_2\mu_3}\rho_{21} + \\
& + \frac{u_1^2 u_2 u_3^2}{\mu_1\mu_2\mu_3}\rho_{23} + \frac{u_2 u_3^4}{\mu_2\mu_3^2}\rho_{23} - \frac{u_2^4 u_3}{\mu_2^2\mu_3}\rho_{23} + \frac{u_1^2 u_2^2 u_3}{\mu_1\mu_2\mu_3}\rho_{31} \Big)/\Lambda^2,
\end{aligned}
\tag{4.7}
$$

The formula for the characteristic speeds of equation (2.23) in terms of J in (4.1) is

$$\lambda^{\pm} = \frac{(J_{11} + J_{22}) \pm \sqrt{\big(J_{11} + J_{22}\big)^2 - 4\big(J_{11}J_{22} - J_{12}J_{21}\big)}}{2}.
\tag{4.8}$$

4.2   Hyperbolicity analysis

For Corey three-phase flow model without gravity effects, Marchesin et al. [20] showed the existence of four umbilic points. Three of them are the vertices of the saturation

triangle; there is also an additional umbilic point inside the saturation triangle. In the rest of the triangle the system is strictly hyperbolic.

In this work (in the presence of gravity effects) we will split our analysis in two different cases. In the first one the parameter α (the convection/gravity ratio) is equal to zero: we call this case "the pure gravitational problem", because the motion of the flow occurs only as a consequence of gravitational buoyancy effects due to fluid density differences.

In the second case α is non zero. This problem presents different levels of complexity depending of the value of α. For high values of α the behavior of this problem would be similar to the case without gravity studied by Marchesin et al. in [20], while for small values of α (i.e, for predominant gravitational effects) the problem could acquire high levels of complexity presenting features from both the pure gravitational problem and the problem without gravity.

Applying the deviator operator (see definition in Eq. (3.19)) to the Jacobian matrix dF, we obtain from (4.4)-(4.7) a parametrization for the surface $dev(dF)$ in the three-dimensional space of trace-free matrices with coordinates (X, Y, Z) given by (3.20). So we obtain

$$dev(dF) = \big(X(u_1, u_2), Y(u_1, u_2), Z(u_1, u_2)\big), \tag{4.9}$$

where X, Y, Z are given below, remembering that $u_3 = 1 - u_1 - u_2$:

$$
\begin{aligned}
X = \Big(& \frac{\alpha u_1 u_2^2}{\mu_1 \mu_2} + \frac{\alpha u_1^2 u_3}{\mu_1 \mu_3} - \frac{\alpha u_2^2 u_3}{\mu_2 \mu_3} - \frac{\alpha u_1^2 u_2}{\mu_1 \mu_2} - \frac{\alpha u_2 u_3^2}{\mu_2 \mu_3} + \frac{\alpha u_1 u_3^2}{\mu_1 \mu_3} + \\
& + \frac{u_1 u_2^4 \rho_{12}}{\mu_1 \mu_2^2} + \frac{u_1 u_2^2 u_3^2 \rho_{12}}{\mu_1 \mu_2 \mu_3} + \frac{u_1 u_2^2 u_3^2 \rho_{13}}{\mu_1 \mu_2 \mu_3} + \frac{u_1 u_3^4 \rho_{13}}{\mu_1 \mu_3^2} - \\
& - \frac{u_1^4 u_3 \rho_{13}}{\mu_1^2 \mu_3} + \frac{u_1^2 u_2^2 u_3 \rho_{12}}{\mu_1 \mu_2 \mu_3} + \frac{u_1^4 u_2 \rho_{12}}{\mu_1^2 \mu_2} + \frac{u_1^2 u_2 u_3^2 \rho_{12}}{\mu_1 \mu_2 \mu_3} - \\
& - \frac{u_1^2 u_2 u_3^2 \rho_{23}}{\mu_1 \mu_2 \mu_3} - \frac{u_2 u_3^4 \rho_{23}}{\mu_2 \mu_3^2} + \frac{u_2^4 u_3 \rho_{23}}{\mu_2^2 \mu_3} \Big) / \Lambda^2,
\end{aligned}
\tag{4.10}
$$

$$
\begin{aligned}
Y = \Big(& \frac{\alpha u_1^2 u_3}{\mu_1 \mu_3} - \frac{\alpha u_1 u_2^2}{\mu_1 \mu_2} + \frac{\alpha u_2^2 u_3}{\mu_2 \mu_3} - \frac{\alpha u_1^2 u_2}{\mu_1 \mu_2} + \\
& + \frac{u_1^4 u_2 \rho_{12}}{\mu_1^2 \mu_2} - \frac{u_1^2 u_2 u_3^2 \rho_{23}}{\mu_1 \mu_2 \mu_3} - \frac{u_1^2 u_2^2 u_3 \rho_{23}}{\mu_1 \mu_2 \mu_3} - \frac{u_1^4 u_3 \rho_{13}}{\mu_1^2 \mu_3} - \\
& - \frac{u_1 u_2^4 \rho_{12}}{\mu_1 \mu_2^2} - \frac{u_1 u_2^2 u_3^2 \rho_{13}}{\mu_1 \mu_2 \mu_3} - \frac{u_1^2 u_2^2 u_3 \rho_{13}}{\mu_1 \mu_2 \mu_3} - \frac{u_2^4 u_3 \rho_{23}}{\mu_2^2 \mu_3} \Big) / \Lambda^2,
\end{aligned}
\tag{4.11}
$$

$$
\begin{aligned}
Z = \Big(& \frac{\alpha u_1^2 u_3}{\mu_1 \mu_3} - \frac{\alpha u_1^2 u_2}{\mu_1 \mu_2} + \frac{\alpha u_1 u_2^2}{\mu_1 \mu_2} - \frac{\alpha u_2^2 u_3}{\mu_2 \mu_3} + \\
& + \frac{u_1^4 u_2 \rho_{12}}{\mu_1^2 \mu_2} - \frac{u_1^2 u_2 u_3^2 \rho_{23}}{\mu_1 \mu_2 \mu_3} + \frac{u_1^2 u_2^2 u_3 \rho_{12}}{\mu_1 \mu_2 \mu_3} - \frac{u_1^4 u_3 \rho_{13}}{\mu_1^2 \mu_3} + \\
& + \frac{u_1 u_2^4 \rho_{12}}{\mu_1 \mu_2^2} + \frac{u_1 u_2^2 u_3^2 \rho_{13}}{\mu_1 \mu_2 \mu_3} + \frac{u_2^4 u_3 \rho_{23}}{\mu_2^2 \mu_3} \Big) / \Lambda^2.
\end{aligned}
\tag{4.12}
$$

4.2.1 Hyperbolicity analysis for the "pure gravitational problem"

Consider the "pure gravitational problem" ($\alpha = 0$). First we analyze a simplified model in which two fluids have equal densities while the third fluid has a different density. We call this problem the "simplified pure gravitational problem". In this section we take phases 1 and 2 as having equal densities while phase 3 has a different density; see Fig. 2.1 for notation.

Proposition 4.1. *Consider the "pure gravitational problem" where $\alpha = 0$, $\rho_1 = \rho_2 \neq \rho_3$, and denote $\rho = \rho_{13} = \rho_{23}$. Then the system* (2.23) *is hyperbolic on the saturation triangle and all the coincidence points lie on its boundary. The vertex V_3 is an umbilic point. The entire edge ∂_3 is a diagonalization line; also there exist two quasi-umbilic points $Q_1 \in \partial_1$, $Q_2 \in \partial_2$. The system is strictly hyperbolic in the rest of the closed saturation triangle.*

Proof. Substituting $\alpha = 0$ and $\rho = \rho_{13} = \rho_{23}$ in equations (4.10)-(4.12) we obtain

$$
X = \rho\Big(\frac{u_1 u_2^2 u_3^2}{\mu_1 \mu_2 \mu_3} + \frac{u_1 u_3^4}{\mu_1 \mu_3^2} + \frac{u_2^4 u_3}{\mu_3 \mu_2^2} - \frac{u_1^4 u_3}{\mu_1^2 \mu_3} - \frac{u_1^2 u_2 u_3^2}{\mu_1 \mu_2 \mu_3} - \frac{u_2 u_3^4}{\mu_2 \mu_3^2}\Big)/\Lambda^2,
$$

$$
Y = \rho\Big(-\frac{u_2^4 u_3}{\mu_2^2 \mu_3} - \frac{u_1 u_2^2 u_3^2}{\mu_1 \mu_2 \mu_3} - \frac{u_1^4 u_3}{\mu_1^2 \mu_3} - \frac{u_1^2 u_2 u_3^2}{\mu_1 \mu_2 \mu_3} - 2\frac{u_1^2 u_2^2 u_3}{\mu_1 \mu_2 \mu_3}\Big)/\Lambda^2, \qquad (4.13)
$$

$$
Z = \rho\Big(\frac{u_2^4 u_3}{\mu_2^2 \mu_3} + \frac{u_1 u_2^2 u_3^2}{\mu_1 \mu_2 \mu_3} - \frac{u_1^4 u_3}{\mu_1^2 \mu_3} - \frac{u_1^2 u_2 u_3^2}{\mu_1 \mu_2 \mu_3}\Big)/\Lambda^2.
$$

From (4.13) we have

$$
Y + Z = \rho\frac{u_1^2 u_3}{\mu_1 \mu_3 \Lambda^2}\Big(-2\frac{u_1^2}{\mu_1} - 2\frac{u_2^2}{\mu_2} - 2\frac{u_2 u_3}{\mu_2}\Big),
$$

$$
Y - Z = \rho\frac{u_2^2 u_3}{\mu_2 \mu_3 \Lambda^2}\Big(-2\frac{u_2^2}{\mu_2} - 2\frac{u_1^2}{\mu_1} - 2\frac{u_1 u_3}{\mu_1}\Big). \qquad (4.14)
$$

We notice that $(Y + Z)/\rho \leq 0$ and $(Y - Z)/\rho \leq 0$, therefore

$$
Y^2 - Z^2 \geq 0 \quad \forall U \in T. \qquad (4.15)
$$

Thus $X^2 + Y^2 \geq Z^2$ in T showing that there does not exist an "elliptic region", in other words, that the system (2.23) is hyperbolic in the saturation triangle.

In general it is known that U_0 is a coincidence point for the characteristic speeds (see Sec. 3.6.2) if and only if

$$
X^2(U_0) + Y^2(U_0) - Z^2(U_0) = 0. \qquad (4.16)
$$

From (4.15)-(4.16) we obtain the following necessary and sufficient conditions for U_0 to be a coincidence point:

(i) $X(U_0) = 0$, together with

(ii) $Y(U_0) = Z(U_0)$ or $Y(U_0) = -Z(U_0)$.

Now for $U_0 = (u_1^0, u_2^0, u_3^0)$, using (4.14) we see that

$$
\begin{aligned}
Y(u_1^0, u_2^0, u_3^0) &= \quad Z(u_1^0, u_2^0, u_3^0) \quad \Leftrightarrow u_2^0 = 0 \ \text{ or } \ u_3^0 = 0, \\
Y(u_1^0, u_2^0, u_3^0) &= - Z(u_1^0, u_2^0, u_3^0) \quad \Leftrightarrow u_1^0 = 0 \ \text{ or } \ u_3^0 = 0.
\end{aligned}
\tag{4.17}
$$

We note that the edge ∂_3 is mapped by $dev(dF)$ into the vertex of the cone $X^2 + Y^2 = Z^2$, therefore the entire edge ∂_3, including the vertices V_1 and V_2 of the saturation triangle, is a diagonalization line according to Proposition 3.1 and Eqs (4.13).

For U_0 out of the edge ∂_3 we have two cases. If $u_3^0 > 0$, $u_1^0 = 0$ we obtain two other coincidence points on the edge ∂_1 by requiring that $X(u_1^0, u_2^0, u_3^0) = 0$. One of them is the vertex $V_3 = (0, 0, 1)$, which is an umbilic point (notice that $X(0, 0, 1) = Y(0, 0, 1) = Z(0, 0, 1) = 0$). Define

$$
a(\mu_i, \mu_j) = \frac{\sqrt[3]{\mu_i / \mu_j}}{1 + \sqrt[3]{\mu_i / \mu_j}}, \quad \forall i \neq j.
\tag{4.18}
$$

The other coincidence point

$$
Q_1 = \Big(0, a(\mu_2, \mu_3), 1 - a(\mu_2, \mu_3) \Big)
\tag{4.19}
$$

is mapped by $dev(dF)$ into the cone surface out of the vertex of the cone, so according to Proposition 3.1, the Jacobian matrix $dF(Q_1)$ is non diagonalizable. We know from the above calculations that Q_1 is a boundary coincidence point, which is isolated if we restrict our analysis to the saturation triangle. Nevertheless, in order to classify Q_1 as a quasi-umbilic point, we prove that Q_1 is an isolated coincidence point in a whole neighborhood of Q_1, so we extend our hyperbolicity analysis for points with a negative first component, *i.e.*, to allow infinitesimal "negative saturations" for phase 1. From (4.14), we see that if a point $U_\varepsilon \neq Q_1$ belongs to a sufficiently small neighborhood of Q_1 (and therefore its first component u_1^ε could be negative but it is close to zero) we have that $(Y(U_\varepsilon) + Z(U_\varepsilon))/\rho < 0$ and $(Y(U_\varepsilon) - Z(U_\varepsilon))/\rho < 0$. Thus we obtain that $X^2(U_\varepsilon) + Y^2(U_\varepsilon) + Z^2(U_\varepsilon) > 0$, concluding that Q_1 is an isolated coincidence point. Thus Q_1 is a quasi-umbilic point.

For the case $u_3^0 > 0$, $u_2^0 = 0$ and $u_1^0 > 0$ we obtain in a similar way the point on the edge ∂_2

$$
Q_2 = \Big(a(\mu_1, \mu_3), 0, 1 - a(\mu_1, \mu_3) \Big),
\tag{4.20}
$$

which is quasi-umbilic point. $\square$

Now we have the following Proposition for the case in which the three phases have distinct densities.

Proposition 4.2. *Assume* $\alpha = 0$, $\rho_1 \neq \rho_2 \neq \rho_3 \neq \rho_1$. *Then the system* (2.23) *is hyperbolic on the saturation triangle; all the coincidence points are isolated and lie on its boundary. The vertices* V_1, V_2 *and* V_3 *are umbilic points. There exist three quasi-umbilic points* $Q_i \in \partial_i$, $i = 1, 2, 3$. *The system is strictly hyperbolic in the rest of the closed saturation triangle.*

Proof. Medeiros [33] proved that for the Corey model including gravitational effects with zero total flow speed, the system is strictly hyperbolic in the interior of the saturation triangle. Now we will analyze hyperbolicity at the boundary of the triangle.

Setting $\alpha = 0$ in equations (4.10)-(4.12) we obtain the following relations

$$Y + Z = 2\Big(\frac{u_1^4 u_2 \rho_{12}}{\mu_1^2 \mu_2} - \frac{u_1^2 u_2 u_3^2 \rho_{23}}{\mu_1 \mu_2 \mu_3} - \frac{u_1^2 u_2^2 u_3 \rho_{23}}{\mu_1 \mu_2 \mu_3} - \frac{u_1^4 u_3 \rho_{13}}{\mu_1^2 \mu_3}\Big)/\Lambda^2, \tag{4.21}$$

$$Y - Z = -2\Big(\frac{u_1^2 u_2^2 u_3 \rho_{13}}{\mu_1 \mu_2 \mu_3} + \frac{u_1 u_2^4 \rho_{12}}{\mu_1 \mu_2^2} + \frac{u_1 u_2^2 u_3^2 \rho_{13}}{\mu_1 \mu_2 \mu_3} + \frac{u_2^4 u_3 \rho_{23}}{\mu_2^2 \mu_3}\Big)/\Lambda^2, \tag{4.22}$$

$$X - Z = \Big(\frac{u_1 u_2^2 u_3^2 \rho_{12}}{\mu_1 \mu_2 \mu_3} + \frac{u_1 u_3^4 \rho_{13}}{\mu_1 \mu_3^2} + \frac{u_1^2 u_2 u_3^2 \rho_{12}}{\mu_1 \mu_2 \mu_3} - \frac{u_2 u_3^4 \rho_{23}}{\mu_2 \mu_3^2}\Big)/\Lambda^2. \tag{4.23}$$

If $\hat{U} = (0, \hat{u}_2, 1 - \hat{u}_2) \in \partial_1$, from (4.21) we have $Y(\hat{U}) + Z(\hat{U}) = 0$. Thus $Y^2(\hat{U}) = Z^2(\hat{U})$ and from (4.16) $\hat{U}$ is a coincidence point if and only if $X(\hat{U}) = 0$. From (4.10) we have

$$X(\hat{U}) = -\frac{\hat{u}_2(1 - \hat{u}_2)\rho_{23}}{\mu_2 \mu_3 (\Lambda(\hat{U}))^2}\Big(\frac{(1 - \hat{u}_2)^3}{\mu_3} - \frac{\hat{u}_2^3}{\mu_2}\Big); \tag{4.24}$$

setting $X(\hat{U}) = 0$ we obtain three coincidence points on the edge ∂_1, which are V_2, V_3 and Q_1 given in (4.19). According to Proposition 3.1, the points V_2, V_3 are umbilic because for V_2 we have $X(0, 1, 0) = Y(0, 1, 0) = Z(0, 1, 0) = 0$ and for V_3 we have $X(0, 0, 1) = Y(0, 0, 1) = Z(0, 0, 1) = 0$. The point Q_1 is again quasi-umbilic because it is mapped by $dev(dF)$ onto the cone surface out of the vertex. The fact that Q_1 is an isolated coincidence point follows from (4.21)-(4.22), since $(Y(U_\varepsilon) + Z(U_\varepsilon))/(u_1^\varepsilon)^2 \rho_{23} < 0$ and $(Y(U_\varepsilon) - Z(U_\varepsilon))/\rho_{23} < 0$ for all point U_ε in a neighborhood of Q_1 which imply that $X^2(U_\varepsilon) + Y^2(U_\varepsilon) + Z^2(U_\varepsilon) > 0$.

For $\hat{U} = (\hat{u}_1, 0, 1 - \hat{u}_1) \in \partial_2$, from (4.22) we have $Y(\hat{U}) - Z(\hat{U}) = 0$ and therefore $\hat{U}$ is again a coincidence point if and only if $X(\hat{U}) = 0$, where

$$X(\hat{U}) = \frac{\hat{u}_1(1 - \hat{u}_1)\rho_{13}}{\mu_1 \mu_3 (\Lambda(\hat{U}))^2}\Big(\frac{(1 - \hat{u}_1)^3}{\mu_3} - \frac{\hat{u}_1^3}{\mu_1}\Big); \tag{4.25}$$

as in the previous case three coincidence points are obtained: the umbilic points V_1, V_3 and a quasi-umbilic point Q_2 in (4.20) on the edge ∂_2.

If $\hat{U} = (\hat{u}_1, 1 - \hat{u}_1, 0) \in \partial_3$, from (4.23) we have $X(\hat{U}) - Z(\hat{U}) = 0$, and $X^2(\hat{U}) = Z^2(\hat{U})$. Therefore $\hat{U}$ is a coincidence point if and only if $Y(\hat{U}) = 0$. From (4.11) we have

$$Y(\hat{U}) = -\frac{\hat{u}_1(1 - \hat{u}_1)\rho_{12}}{\mu_1 \mu_2 (\Lambda(\hat{U}))^2}\Big(\frac{(1 - \hat{u}_1)^3}{\mu_2} - \frac{\hat{u}_1^3}{\mu_1}\Big); \tag{4.26}$$

in this case, we obtain the umbilic points V_1, V_2. We obtain also a quasi-umbilic point Q_3 on the edge ∂_3:

$$Q_3 = (a(\mu_1, \mu_2), 1 - a(\mu_1, \mu_2), 0), \tag{4.27}$$

where $a(\mu_1, \mu_2)$ is given in (4.18).

$\square$

4.2.2   Hyperbolicity analysis for the general gravitational problem

We analyze hyperbolicity when the convection/gravity ratio α is non-zero; even though we will not use these results in the rest of the work. As we said earlier, the complexity of this analysis depends on the value of α. For values of $|\alpha|$ so high that the convection effects are dominant with respect to the gravitational effects, the three vertices are umbilic points and there exist an additional umbilic point U_α^* in the interior of the saturation triangle (Medeiros [33]). For small non-zero values of $|\alpha|$ (*i.e.*, for predominant gravitational effects) the problem, besides the four umbilic points will also possess quasi-umbilic points at the boundary of the triangle. The following proposition summarizes these results.

Proposition 4.3. *Consider the system (2.23) with $\alpha \neq 0$, in the saturation triangle. Then the following assertions are true:*

  (i) *The vertices of the saturation triangle are umbilic points. In the interior of the triangle the system is strictly hyperbolic except at the umbilic point U_α^*.*

 (ii) *Without loss of generality, consider the two-phase edge ∂_1 where phases 2 and 3 coexist. Assume also $\rho_2 > \rho_3$, then there exists a quasi-umbilic point $Q_1 \in \partial_1$ if and only if α lies in the interval $(-\frac{\rho_{23}}{\mu_3} < \alpha < \frac{\rho_{23}}{\mu_2})$. The system is strictly hyperbolic in the rest of the edge ∂_1.*

(iii) *In the case $\rho_2 = \rho_3$ all points on the edge ∂_1 are strictly hyperbolic, except for the vertices V_2, V_3.*

Remark 4.1. *As phases $1, 2, 3$ are arbitrary we can write items $(ii), (iii)$ of Prop. 4.3 using any permutation of indices $\{1, 2, 3\}$ obtaining analogous results for the other edges ∂_2 and ∂_3.*

Remark 4.2. *Notice that in the case $\alpha \neq 0$, when $\rho_2 = \rho_3$ we have strict hyperbolicity on the edge ∂_1 except for the vertices V_2, V_3. This behavior differs from the simplified pure gravitational case, where ∂_1 is a diagonalization line (see Prop. 4.1 with the indices 1 and 3 interchanged).*

Proof. (i)- It is obvious that the vertices V_1, V_2 and V_3 are umbilic points since

$$X(V_i) = Y(V_i) = Z(V_i) = 0, \quad i = 1, 2, 3.$$

The existence of the interior umbilic point U^*_α and the strict hyperbolicity of the remaining interior points for the case $\alpha \neq 0$ was proved by Medeiros [33].

(ii)- From equations (4.4)-(4.7) we obtain that the characteristic values at a point $U \in \partial_1$ are

$$\lambda(U) = 0, \tag{4.28}$$

$$\lambda^*(U) = 2\frac{u_2(1-u_2)}{\mu_2\mu_3\Lambda^2}\Big(\big(-\frac{u_2^3}{\mu_2}+\frac{(1-u_2)^3}{\mu_3}\big)\rho_{23}+\alpha\Big). \tag{4.29}$$

Here the eigenvalues λ and λ^* are not associated to specific families since λ^* could be positive or negative. The important fact is that $U \in \partial_1$ will be a coincidence point if and only if $\lambda^*(U) = 0$; this occurs on this edge at the vertices V_2, V_3 and at the intermediate point Q_1^α

$$Q_1^\alpha = (0, q_\alpha, 1-q_\alpha), \quad \text{where } q_\alpha \text{ solves } \ (q_\alpha^3/\mu_2 - (1-q_\alpha)^3/\mu_3)\rho_{23} = \alpha. \tag{4.30}$$

From (4.30) we have that $Q_1^\alpha \in T$ if and only if

$$-\frac{\rho_{23}}{\mu_3} < \alpha < \frac{\rho_{23}}{\mu_2}. \tag{4.31}$$

Now we will prove under condition (4.31) that Q_1^α is a quasi-umbilic point. As in Proposition 4.2 using Eqs. (4.10), it is possible to show that $Q_1^\alpha \in \partial_1$ is an isolated coincidence point. Next we will prove that it is not an umbilic point, by contradiction. Assume that Q_1^α is an umbilic point, then necessarily $X(Q_1^\alpha) = Y(Q_1^\alpha) = Z(Q_1^\alpha) = 0$.
From (4.11) we have that

$$Y(Q_1^\alpha) = \frac{q_\alpha^2(1-q_\alpha)}{\mu_2\mu_3}(\alpha - \frac{q_\alpha^2\rho_{23}}{\mu_2})/\Lambda^2, \tag{4.32}$$

where Λ is evaluated at Q_1^α.

Equations (4.30) and (4.31) imply $0 < q_\alpha < 1$, so we have from (4.32) that $\alpha = q_\alpha^2\rho_{23}/\mu_2$. Substituting this value into the definition (4.30) for q_α, we obtain

$$\frac{q_\alpha^2}{\mu_2}(1-q_\alpha) = -\frac{(1-q_\alpha)^3}{\mu_3}. \tag{4.33}$$

The fact $0 < q_\alpha < 1$ contradicts (4.33). We conclude that Q_1^α is a quasi-umbilic point because Q_1^α is an isolated coincidence point that is not mapped to the vertex of the cone $X^2 + Y^2 = Z^2$.

(iii)- For the case $\rho_2 = \rho_3$ we can see from (4.10)-(4.12) that for U in ∂_1

$$X(U) = -\frac{\alpha u_2 u_3}{\mu_2\mu_3}/\Lambda^2, \quad Y(U) = \frac{\alpha u_2^2 u_3}{\mu_2\mu_3}/\Lambda^2, \quad Z(U) = -\frac{\alpha u_2^2 u_3}{\mu_2\mu_3}/\Lambda^2, \quad \text{where } \Lambda = \Lambda(U). \tag{4.34}$$

If U is not a vertex we have from (4.34) that $X(U)$ is non-zero. We also have $Y(U) + Z(U) = 0$, therefore $X^2(U) + (Y^2(U) - Z^2(U)) > 0$. We have obtained the strict hyperbolicity of the system on the edge ∂_1 except at the vertices V_2 and V_3. $\square$

The following theorem describes the edges as integral curves that change family when crossing the quasi-umbilic points.

Theorem 4.1. *Consider the system* (2.23) *for any value of* α, *in the saturation triangle. Assume that* $\rho_2 \neq \rho_3$ *and that* (4.31) *holds, i.e., the quasi-umbilic point* $Q_1^\alpha \in \partial_1$ *exists. We have the following facts along the edge* ∂_1. *Analogous facts are true along* ∂_2 *and* ∂_3.

(a) *The single right eigenvector at* Q_1^α *has the direction of the edge* ∂_1.

(b) *Away from the vertices* V_2, V_3 *and the quasi-umbilic point* Q_1^α *on* ∂_1, *the right eigenvector corresponding to one of the families is parallel to* ∂_1, *while the eigenvector for the other family is transversal to* ∂_1.

(c) *Consider a point* U *in the edge* ∂_1. *Let us move the point* U *along the integral curve that coincides with the edge. There is a change of family when* U *crosses the quasi-umbilic point* Q_1^α.

(d) *For* U *out of the coincidence points on* ∂_1, *one of the characteristic speeds is equal to zero while the other one is non-zero. The family of the zero-characteristic speed (resp. non-zero characteristic speed) changes according to the position of* U *with respect to the quasi-umbilic point* Q_1^α.

All this facts are illustrated in *e.g.*, Fig. 9.1.

Proof. Without loss of generality we assume that $\rho_2 > \rho_3$. If (4.31) holds we guarantee the existence of the quasi-umbilic point $Q_1^\alpha \in \partial_1$.

Consider a point $U \in \partial_1$. From (4.4)-(4.7) we obtain $J_{11}(U) = 0, J_{12}(U) = 0$ and the eigenvalues of the Jacobian matrix at this point are given by (4.28) and (4.29).

(a)-Let us denote by $r^*(U)$ the right eigenvector associated to the eigenvalue $\lambda^*(U)$. We have

$$\big(J(U) - \lambda^*(U)I\big)r^*(U) = \begin{pmatrix} -\lambda^*(U) & 0 \\ J_{21}(U) & 0 \end{pmatrix} \begin{pmatrix} r_1^*(U) \\ r_2^*(U) \end{pmatrix} = 0.$$

Since $\lambda^*(U)$ and $J_{21}(U)$ do not vanish simultaneously along ∂_1, we obtain $r_1^*(U) = 0$ for all $U \in \partial_1$ and therefore the eigenvector $r^*(U)$ has the direction of the edge ∂_1. For the particular case $U = Q_1^\alpha$ we conclude the result of item (a).

(b)- We already proved that for $U \in \partial_1$ the eigenvector associated to the eigenvalue λ^* is parallel to the edge ∂_1. If $U \neq Q_1^\alpha$ we denote by $r^0(U)$ the right eigenvector corresponding

to the zero eigenvalue. We have

$$J(U)r^0(U) = \begin{pmatrix} 0 & 0 \\ J_{21}(U) & \lambda^*(U) \end{pmatrix} \begin{pmatrix} r_1^0(U) \\ r_2^0(U) \end{pmatrix} = 0.$$

Out of the quasi-umbilic point $\lambda^* \neq 0$ so we obtain that r_1^0 must be different from zero and $r_2^0(U) = J_{21}(U)r_1^0(U)/\lambda^*$, concluding that the eigenvector $r^0(U)$ is transversal to the edge ∂_1.

(c)- From the calculations above we have that the right eigenvector r^* associated to the non-zero eigenvalue λ^* has the direction of the edge ∂_1. But notice that for the eigenvalue zero we have

$$0 = \lambda(U) = \begin{cases} \lambda^+(U) & \text{if } U \in [V_2, Q_1^\alpha] \\ \lambda^-(U) & \text{if } U \in [V_3, Q_1^\alpha] \end{cases}, \tag{4.35}$$

while for the non-zero eigenvalue

$$\lambda^*(U) = \begin{cases} \lambda^-(U) < 0 & \text{if } U \in (V_2, Q_1^\alpha) \\ \lambda^+(U) > 0 & \text{if } U \in (V_3, Q_1^\alpha) \end{cases}, \tag{4.36}$$

so we have

$$r^*(U) = \begin{cases} r^-(U) & \text{if } U \in (V_2, Q_1^\alpha) \\ r^+(U) & \text{if } U \in (V_3, Q_1^\alpha) \end{cases}, \tag{4.37}$$

reflecting change of family along the edge ∂_1 when crossing Q_1^α.

(d)-The proof of this item is a consequence of Eqs. (4.35)-(4.36). □

Now we give an implicit formula for the umbilic point U_α^* given in Prop 4.3, item (i). Requiring that $X(U_\alpha^*) = Y(U_\alpha^*) = Z(U_\alpha^*) = 0$ at U_α^*, the following relations hold

$$\alpha(\Lambda_2' - \Lambda_3') + [\Lambda_1\Lambda_2'\rho_{21} + (\Lambda_2\Lambda_3' + \Lambda_2'\Lambda_3)\rho_{23} + \Lambda_1\Lambda_3'\rho_{13}] = 0, \tag{4.38}$$

$$\alpha(\Lambda_1' - \Lambda_3') + [\Lambda_2\Lambda_1'\rho_{12} + (\Lambda_1\Lambda_3' + \Lambda_1'\Lambda_3)\rho_{13} + \Lambda_2\Lambda_3'\rho_{23}] = 0, \tag{4.39}$$

$$\alpha(\Lambda_1' - \Lambda_2') + [\Lambda_1'\Lambda_3\rho_{13} + (\Lambda_2\Lambda_1' + \Lambda_2'\Lambda_1)\rho_{12} + \Lambda_2'\Lambda_3\rho_{32}] = 0. \tag{4.40}$$

Remark 4.3. *Equations (4.38)-(4.40) represent curves crossing the umbilic point U_α^*; only two of these equations are independent; any one of them can be obtained from the other two by a simple addition or subtraction. The umbilic point U_α^* is the intersection point of any pair of curves given implicitly by (4.38)-(4.40) inside the saturation triangle.*

Chapter 5

Two-phase behavior in the pure gravitational problem.

In this chapter we study two-phase flows occurring in the pure gravitational problem, in which $\alpha = 0$. We recall the well known features of the two-phase flows restricted to the edges ∂_i. It is known that the Riemann solution for two-phase regime is obtained by the Oleinik construction. A new result of interest is obtained for the pure gravitational problem simplified so that two fluids j and k have equal densities; we show that within the triangle there is a straight line segment R_i through the vertex V_i (see definition in (2.29)), where the three-phase problem behaves like a two-phase flow.

The results presented in this chapter will be very useful for the analysis of Hugoniot loci in the chapters that follow and for the construction of Riemann solutions for three-phase flow.

5.1   Two-phase flow on edges of the saturation triangle

Without loss of generality we will study the two-phase flow on the edge ∂_3. To fix ideas, let us assume $\rho_1 \neq \rho_2$. We notice that on ∂_3 the system (2.23) reduces to the scalar equation

$$\frac{\partial u_1}{\partial t} + \frac{\partial}{\partial x} F_1^{\partial_3}(u_1) = 0, \text{ where } F_1^{\partial_3}(u_1) = \frac{u_1^2(1-u_1)^2}{\mu_1\mu_2\left(\frac{u_1^2}{\mu_1} + \frac{(1-u_1)^2}{\mu_2}\right)}\rho_{12} \tag{5.1}$$

is a scalar flux function.

Remark 5.1. *Because of Remark 2.1, since $\alpha = 0$ (and consequently $\mathbf{v} = 0$), we see that $F_2^{\partial_3}(u_2) = -F_1^{\partial_3}(u_1)$, so the choice $F_1^{\partial_3}(u_1)$ and u_1 or $F_2^{\partial_3}(u_2)$ and u_2 as the two-phase flux function and conserved quantity along the ∂_3 edge makes no difference. In other words, we can use any one of the PDE's: $(u_1)_t + \left(F_1^{\partial_3}(u_1)\right)_x = 0$ or $(u_2)_t + \left(F_2^{\partial_3}(u_2)\right)_x = 0$.*

We can calculate the derivative of this flux function,

$$\frac{dF_1^{\partial_3}(u_1)}{du_1} = \frac{-2\rho_{12}u_1(1-u_1)P(u_1)}{\mu_1\mu_2\left(\frac{u_1^2}{\mu_1} + \frac{(1-u_1)^2}{\mu_2}\right)^2}, \tag{5.2}$$

where

$$P(u_1) = (1 + \frac{\mu_1}{\mu_2})u_1^3 - 3\frac{\mu_1}{\mu_2}u_1^2 + 3\frac{\mu_1}{\mu_2}u_1 - \frac{\mu_1}{\mu_2} \tag{5.3}$$

is a cubic polynomial. We will show this polynomial has only one real root. Indeed with the change of variable $\zeta = u_1 - \mu_1/(\mu_1 + \mu_2)$ we eliminate the quadratic term for polynomial P, obtaining a new cubic polynomial in ζ of the form

$$\zeta^3 + p\zeta + q, \tag{5.4}$$

with

$$p = \frac{3\frac{\mu_1}{\mu_2}}{(1 + \frac{\mu_1}{\mu_2})^2}, \quad q = -2\left(\frac{\frac{\mu_1}{\mu_2}}{(1 + \frac{\mu_1}{\mu_2})}\right)^3 + 3\left(\frac{\frac{\mu_1}{\mu_2}}{1 + \frac{\mu_1}{\mu_2}}\right)^2 - \frac{\frac{\mu_1}{\mu_2}}{1 + \frac{\mu_1}{\mu_2}}. \tag{5.5}$$

If we consider the discriminant $\Delta = \left(4p^3 + 27q^2\right)$, it is known from elementary algebra that if $\Delta > 0$, the polynomial (5.4) in ζ has only one real root. In our case we see that $\Delta > 0$ since all the quantities involved in the expression for p in (5.5) are positive. Is easy to see that $\hat{u}_1 = \sqrt[3]{\frac{\mu_1}{\mu_2}}/\left(1 + \sqrt[3]{\frac{\mu_1}{\mu_2}}\right)$ is the unique root of the cubic polynomial P, so we can rewrite the derivative of the flux function on the edge ∂_3 as follows

$$\frac{dF_1^{\partial_3}(u_1)}{du_1} = \frac{-2\rho_{12}u_1(1-u_1)(u_1 - \hat{u}_1)\tilde{P}(u_1)}{\mu_1\mu_2\left(\frac{u_1^2}{\mu_1} + \frac{(1-u_1)^2}{\mu_2}\right)^2}, \tag{5.6}$$

where $\tilde{P}(u_1)$ has no real roots.

Assume that $\rho_1 > \rho_2$. We notice that the flux function $F_1^{\partial_3}(u_1)$ has only three local extrema in the interval $(0,1)$, one of them a local maximum at $\hat{u}_1$ (minimum if $\rho_1 < \rho_2$) depending on the viscosities μ_1 and μ_2, and two local minima (maxima if $\rho_1 < \rho_2$) at the end points $u_1 = 0, u_1 = 1$, therefore the flux function has only two inflection points in this interval. The plot of $F_1^{\partial_3}(u_1)$ for a non-symmetrical case is shown in Fig. 5.1(a).

Remark 5.2. *Notice that the point of local maximum (minimum if $\rho_1 < \rho_2$) for the two-phase flux $F_1^{\partial_3}(u_1)$ coincides in the saturation triangle with the quasi-umbilic point called Q_3. For the symmetrical case where $\mu_1 = \mu_2$ we have $\hat{u}_1 = 1/2$.*

Because of Remark 5.1 we have that the plot of $F_2^{\partial_3}(u_2)$ is like the Fig. 5.1(b).

Remark 5.3. *We must regard this two-phase problem as a particular case of the general three-phase flow, in this sense, we can say that local extrema for the scalar function $F_1^{\partial_3}(u_1)$ correspond to all coincidence points on the ∂_3 edge; because of item (c) of Theorem (4.1) the two sides of the edge ∂_3 relative to the coincidence point Q_3 are identical to integral curves for different families. Similarly the derivative of the two-phase flux function $F_1^{\partial_3}$ coincides with the characteristic speed of the fast (slow if $\rho_1 < \rho_2$) family in the interval (V_2, Q_3) and with the characteristic speed of the slow (fast if $\rho_1 < \rho_2$) family in the interval (Q_3, V_1).*
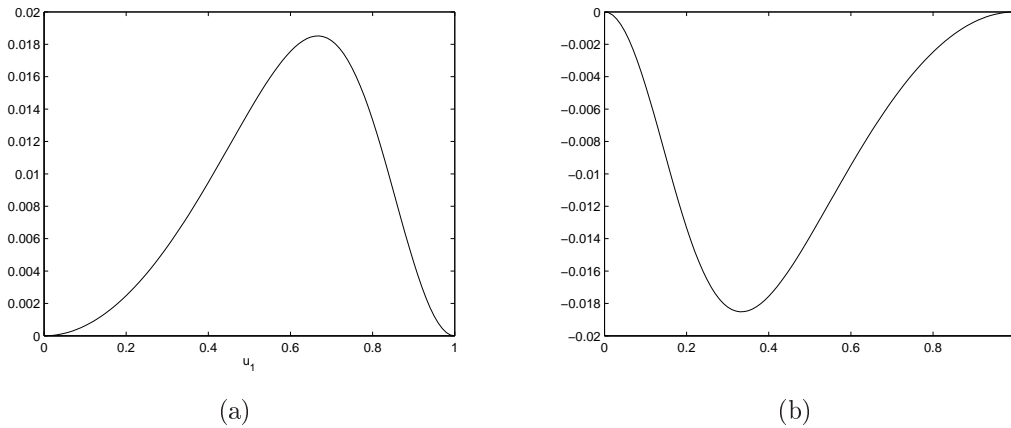
Figure 5.1: For both cases $\mu_1 = 1$, $\mu_2 = 0.5$, $\rho_{12} = 0.7$. (a) Two-phase scalar flux $F_1^{\partial_3}(u_1)$. (b) Two-phase scalar flux $F_2^{\partial_3}(u_2)$.

If both left and right states of the Rieman problem lie on the ∂_3 edge, the solution of the Riemann problem is the well known Oleinik solution [34] for the Buckley-Leverett equation (5.1) with flux function shown in Fig. 5.1(a).

5.2   Two-phase flow for the simplified pure gravitational problem.

Now, assume $\rho_1 = \rho_2 \neq \rho_3$. If we restrict the system (2.23) to the ∂_3 edge, with $\alpha = 0$, all components of the flow function are identically equal to zero, and the system reduces to

$$\frac{\partial u_i}{\partial t} = 0, \quad i = 1, 2. \tag{5.7}$$

The wave joining any pair of states on the edge ∂_3 for this case is an immobile "genuine" contact discontinuity (the speed σ is equal to zero). Along the other edges the solution is the Buckley-Leverett solution as described in the previous section.

Two-phase flow along the critical line

Now we will show that when $\rho_1 = \rho_2$ the system (2.23) restricted to the segment R_3 (see Fig.(2.1)) behaves like a two-phase flow problem too. We call the segment R_3 for this simplified problem the "critical line". We have the following theorem

Theorem 5.1. *Assume $\alpha = 0$, $\rho_1 = \rho_2 \neq \rho_3$ and denote $\rho = \rho_{13} = \rho_{23}$. Let U_L and U_R be states on the critical line R_3. The Riemann solution $U(x,t)$ satisfies $u_1(x,t)/\mu_1 = u_2(x,t)/\mu_2$ for all t,x (i.e., the solution remains on R_3 for all times). The Riemann solution consists of waves solely from the slow family if $\rho > 0$, and solely from the fast family if $\rho < 0$.*

Proof. Following Azevedo et al. [1], we can parameterize the line segment R_3 in terms of the saturation of phase 3

$$R_3 = \left\{ (u_1, u_2) : u_1 = \frac{\mu_1(1 - u_3)}{\mu_1 + \mu_2}, u_2 = \frac{\mu_2(1 - u_3)}{\mu_1 + \mu_2}, 0 \leq u_3 \leq 1 \right\}. \qquad (5.8)$$

Using this parametrization of R_3 and the expressions for the flow components (2.20)-(2.21) we obtain that along segment R_3

$$\frac{F_1}{\mu_1} = \frac{\frac{u^2}{(\mu_1 + \mu_2)^2} \frac{(1-u)^2}{\mu_3} \rho}{\frac{(1-u)^2}{\mu_3} + \frac{u^2}{\mu_1 + \mu_2}} = \frac{F_2}{\mu_2}, \quad \text{where} \quad u = 1 - u_3. \qquad (5.9)$$

Now we define the following function of the variable u along R_3

$$F_{12}(u) \equiv (\mu_1 + \mu_2) \frac{F_1}{\mu_1} = (\mu_1 + \mu_2) \frac{F_2}{\mu_2} = \frac{\frac{u^2}{(\mu_1 + \mu_2)} \frac{(1-u)^2}{\mu_3} \rho}{\frac{(1-u)^2}{\mu_3} + \frac{u^2}{\mu_1 + \mu_2}}. \qquad (5.10)$$

If we substitute the parametrization (5.8) of the segment R_3 into the system (2.23) we obtain that on R_3 both equations of the system reduce to the scalar gravitational Buckley-Leverett equation

$$\frac{\partial u}{\partial t} + \frac{\partial}{\partial x} F_{12}(u) = 0, \qquad (5.11)$$

with the flux F_{12} given by (5.10). We conclude that along the critical line R_3 the quantity u (remembering that $u = 1 - u_3 = u_1 + u_2$) is conserved according to (5.11). So the critical line R_3 is invariant under the evolution governed by system (2.23). In this sense, we can say that along R_3 the behavior of the fluid is like two-phase flow, with phases: (phase 1 "+" phase 2) and (phase 3). Compare the scalar conservation law (5.11) and the "flux" function F_{12} defined in (5.10) with the conservation law and the corresponding flux function $F_1^{\partial_3}$ in (5.1) . Notice that the function F_{12} has exactly the same expression as $F_1^{\partial_3}$ but with viscosities μ_3 instead of μ_2 and $\mu_1 + \mu_2$ instead of μ_1.

In order to prove the second part of the theorem we will assume that $\rho > 0$ (then the case $\rho < 0$ can be regarded as a direct consequence of Theorem 8.1).

Assuming that $\rho > 0$ we will show that the entire segment R_3 is an integral curve of the slow family. From (4.8), we have that in each arbitrary point U the characteristic speed of the slow family is given by $\lambda^-(U)$. We denote by $r^-(U) = (r_1^-(U), r_2^-(U))^T$ the right eigenvector associated to $\lambda^-(U)$. We have that

$$\big(DF(U) - \lambda^-(U)I\big) r^-(U) = 0, \qquad (5.12)$$

more specifically

$$\big[J_{11}(U) - \lambda^-(U)\big] r_1^-(U) + J_{12}(U) r_2^-(U) = 0, \qquad (5.13)$$

$$J_{21}(U) r_1^-(U) + \big[J_{22}(U) - \lambda^-(U)\big] r_2^-(U) = 0. \qquad (5.14)$$

We will assume that U is an interior point of the saturation triangle, then from (4.5)-(4.6) we have $J_{12}(U) < 0, J_{21}(U) < 0$, so we obtain from (5.14) that

$$r_1^-(U) = \frac{\left[\lambda^-(U) - J_{22}(U)\right]r_2^-(U)}{J_{21}(U)}. \tag{5.15}$$

If we substitute (5.15) into (5.13) we see that (5.13) is satisfied trivially.

Since $r^-(U)$ is an eigenvector, from (5.15) we have $r_2^-(U) \neq 0$. Thus we can assume without loss of generality $r_2^-(U) = 1$ and $r_1^-(U) = \frac{J_{22}(U) - \lambda^-(U)}{-J_{21}(U)}$. Let us calculate $r_1^-(U)$, more details appear in Appendix A.

We can write

$$J_{22}(U) - \lambda^-(U) = \frac{J_{22} - J_{11} + \sqrt{\left(J_{22} - J_{11}\right)^2 + 4J_{12}J_{21}}}{2}. \tag{5.16}$$

Assume now that $U \in R_3$. From (4.4)-(4.7) we obtain after some calculation the following relations

$$J_{21}(U) = -2\frac{(\mu_2/\mu_1)u_1^3 u_3 \rho}{\mu_1^2 \mu_3 \Lambda^2}, \tag{5.17}$$

$$J_{22}(U) - J_{11}(U) = 2\frac{u_1^3 u_3 \rho}{\mu_1^2 \mu_3 \Lambda^2}(1 - \mu_2/\mu_1), \tag{5.18}$$

$$J_{12}(U)J_{21}(U) = 4\frac{(\mu_2/\mu_1)u_1^6 u_3^2 \rho^2}{\mu_1^4 \mu_3^2 \Lambda^4}, \tag{5.19}$$

then

$$J_{22}(U) - \lambda^-(U) = -\frac{\mu_1}{\mu_2}J_{21}(U) \Rightarrow r_1^-(U) = \frac{\mu_1}{\mu_2}. \tag{5.20}$$

So we have proved that the eigenvector $r^-(U)$ has the direction of the segment R_3 for any $U \in R_3$.

$\square$

Remark 5.4. *For a more general case in which $\alpha \neq 0$, $\rho_1 = \rho_2 \neq \rho_3$, we can apply the same procedure to obtain that on R_3 the flow has again a two-phase behavior, but in such a case the Riemann solution on R_3 consists of waves of both families. This is a consequence of the presence of the umbilic point U_α^* on R_3 (see Lemma 6.4).*

Remark 5.5. *The fact that the solution behaves like a two-phase flow along segment R_3 was already observed in the problem without gravity (see [1]), therefore we can regard the theorem above as a generalization of that result for the gravitational case in which two fluids have equal densities.*

Remark 5.6. *Notice that in the case without gravity the presence of the umbilic point in the interior of the triangle again implies a change of family along the integral curve that coincides with R_3, so the property that the entire segment R_3 is part of an integral curve of a single family holds only in the simplified pure gravitational problem (i.e., $\alpha = 0, \rho_1 = \rho_2$).*

Chapter 6

Hugoniot loci for vertices in the generic problem

This chapter summarizes the analysis of the Hugoniot loci of the vertices V_1, V_2 and V_3 for the general case in which the velocity parameter α has an arbitrary value. In other words, convection and buoyancy are both active. The results have an important role in the solution of the Riemann solutions with data for $x > 0$ corresponding to a vertex of the saturation triangle. Nevertheless, as in this work we only solve Riemann problems for the "pure gravitational" case ($\alpha = 0$), it is sufficient to use the results in Prop. 6.1 and Prop. 6.3, the rest of the chapter can be skipped.

We want to study the Hugoniot locus for the three vertices of the saturation triangle. Without loss of generality we can analyze the Hugoniot locus through the point V_3. We will consider the 2×2 system of conservation laws (2.23) that originates from dropping the equation corresponding to the phase 3 in the equations for Corey model with flux functions (2.20)-(2.22). If we employ the system of coordinates given by saturations of phases 1 and 2 and use the definition of the saturation triangle given in (2.24), we have $V_3 = (0,0)$. We consider an arbitrary state $U = (u_1, u_2)$; the Rankine-Hugoniot relation for a shock joining the state V_3 with U is

$$F_1(0,0) - F_1(u_1, u_2) = -\sigma(u_1 - 0) \qquad (6.1)$$

$$F_2(0,0) - F_2(u_1, u_2) = -\sigma(u_2 - 0), \qquad (6.2)$$

with σ representing the shock speed.
Using the flux expressions (2.20)-(2.21) into (6.1)-(6.2) we obtain the following Rankine-Hugoniot expression

$$\sigma u_1 = \frac{u_1^2}{\mu_1}[\alpha + (\frac{u_3^2}{\mu_3}\rho_{13} + \frac{u_2^2}{\mu_2}\rho_{12})]/\Lambda, \qquad (6.3)$$

$$\sigma u_2 = \frac{u_2^2}{\mu_2}[\alpha + (\frac{u_3^2}{\mu_3}\rho_{23} + \frac{u_1^2}{\mu_1}\rho_{21})]/\Lambda, \qquad (6.4)$$

where $\Lambda = \Lambda(u_1, u_2, u_3)$ is given in (2.19). To obtain (6.3)-(6.4) we took advantage of the fact that F_1 and F_2 given in (2.20)-(2.21) vanish at V_3.

There are essentially two types of solutions for equations (6.3)-(6.4). One type corresponds to two-phase flow. The other type corresponds to three-phase flow.

For concreteness, in order to analyze the two-phase flow solutions for (6.3)-(6.4) let us consider fluids 2 and 3 (the case of fluids 1 and 3 is analogous), so assume $u_1 = 0$. For this type of solution we are taking $U \in \partial_1$, equation (6.3) is satisfied trivially for all values of σ. The entire edge ∂_1 of the saturation triangle belongs to $\mathcal{H}(V_3)$. For a given state on this edge $U = (0, u_2), u_2 > 0$, the speed of the discontinuity is determined from (6.4) as

$$\sigma = \frac{\frac{u_2}{\mu_2}\left[\alpha + \frac{(1-u_2)^2}{\mu_3}\rho_{23}\right]}{\frac{u_2^2}{\mu_2} + \frac{(1-u_2)^2}{\mu_3}}. \tag{6.5}$$

Notice that for this case, the first equation of (2.23) is satisfied trivially, so the system reduces to the scalar Buckley-Leverett equation (second equation of (2.23)). This type of solution for Eqs. (6.3)-(6.4) is a two-phase discontinuity on the edge ∂_1 (or on the edge ∂_2, if $u_2 = 0$).

Let us consider the case of genuine three-phase flow, *i.e.*, assume $u_1 \neq 0, u_2 \neq 0$. For this type of solution, U belongs to the interior branch of $\mathcal{H}(V_3)$. We eliminate σ in (6.3)-(6.4), and obtain, for $u_3 = 1 - u_1 - u_2$

$$\frac{u_2}{\mu_2}\left(\alpha + \frac{u_3^2}{\mu_3}\rho_{23} + \frac{u_1^2}{\mu_1}\rho_{21}\right) - \frac{u_1}{\mu_1}\left(\alpha + \frac{u_3^2}{\mu_3}\rho_{13} + \frac{u_2^2}{\mu_2}\rho_{12}\right) = 0. \tag{6.6}$$

As we already saw, both edges ∂_1 and ∂_2 are trivial branches of $\mathcal{H}(V_3)$. We define the non-trivial branch of the Hugoniot locus of V_3 as

$$\hat{\mathcal{H}}(V_3) = \{U \in T, \text{ such that (6.6) holds}\}. \tag{6.7}$$

This represents a curve through the vertex V_3 given in implicit form. The speed σ can be recovered from any one of the equations (6.3) or (6.4).

Recall that Λ_1 and Λ_2 are the mobilities of the phases 1 and 2 respectively (see the definitions in (2.19)). Multiplying (6.3) by Λ_2, (6.4) by Λ_1 and subtracting the results (notice that both Λ_1 and Λ_2 are different from zero for this type of solution), we obtain after some calculations

$$\sigma\left(\Lambda_2 u_1 - \Lambda_1 u_2\right) = \Lambda_1 \Lambda_2 \rho_{12}. \tag{6.8}$$

The above equation is a necessary condition that must be satisfied by any state U of the non-trivial branch $\hat{\mathcal{H}}(V_3)$. This equation will provide interesting information. We will split our analysis in two cases. First we analyze the case in which phases 1 and 2 have equal densities.

6.1   Three-phase flow with two equal-density fluids

Here we analyze the simplest case in which the density difference ρ_{12} vanishes. Let us use the notation $\rho = \rho_{13} = \rho_{23}$.

Assume $\sigma \neq 0$, so for $U \in \hat{\mathcal{H}}(V_3)$ we obtain from (6.8) that necessarily $\Lambda_2 u_1 = \Lambda_1 u_2$ and therefore $u_1/\mu_1 = u_2/\mu_2$ (*i.e.*, $U \in R_3$ (see Eq. (2.29) and Fig. 6.1). From (6.3)-(6.4), we can see that condition $U \in R_3$ is also sufficient for U to belong to $\hat{\mathcal{H}}(V_3)$.

For the case $\sigma = 0$, as we have $u_1 \neq 0$, $u_2 \neq 0$, and $\rho_1 = \rho_2$ we obtain from the Rankine-Hugoniot conditions (6.3)-(6.4) that necessarily $\alpha + u_3^2 \rho/\mu_3 = 0$; therefore if $0 \leq -\alpha\mu_3/\rho \leq 1$, there exists a segment parallel to ∂_3, given by $u_3 = \sqrt{-\alpha\mu_3/\rho}$ that belongs to $\mathcal{H}(V_3)$ with speed σ equal to zero. We are led to define

$$C_3^\alpha = \begin{cases} \left\{ U \in T : u_3 = \sqrt{-\alpha\mu_3/\rho} \right\} & \text{if } 0 \leq -\alpha\mu_3/\rho \leq 1, \\ \emptyset & \text{otherwise.} \end{cases}$$

Notice that we have proved the following result:

Proposition 6.1. *Assume that $\rho_1 = \rho_2$, then the Hugoniot Locus of the vertex V_3 is given by $\mathcal{H}(V_3) = \partial_1 \cup \partial_2 \cup R_3 \cup C_3^\alpha$. See Fig. 6.1.*
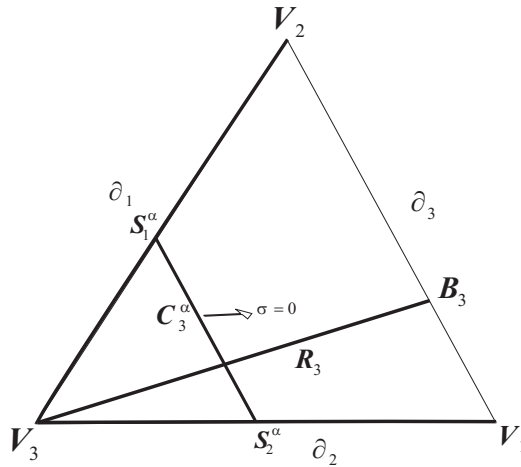
Figure 6.1: *Dark curves: Hugoniot Locus of vertex V_3 for the case $\rho_1 = \rho_2$ when $\alpha \neq 0$ with $0 < -\alpha\mu_3/\rho \leq 1$*

Remark 6.1. *Notice that $C_3^0 = \partial_3$, so for the simplified pure gravitational problem ($\alpha = 0, \rho_{12} = 0$) the edge ∂_3 not only is a diagonalization line but it also belongs to $\mathcal{H}(V_3)$ with speed $\sigma = 0$. This fact was expected because of the Triple Shock rule.*

Remark 6.2. *It is well known (see [1]) that in the absence of buoyancy (i.e., $\rho_1 = \rho_2 = \rho_3$), the straight line segment R_3 is part of the Hugoniot-Locus of the point V_3. So we see that Proposition 6.1 is a generalization of that result for the case in which the phases 1 and 2 have equal densities while phase 3 has a different density.*

6.2   Three-phase flow with three different-density fluids

Now we will analyze the general case $\rho_{21} \neq 0$ in which the curve $\hat{\mathcal{H}}(V_3)$ has a more complicated shape (it is not composed by straight line segments).

We have the following lemmas.

Lemma 6.1. *For α non-zero, $\hat{\mathcal{H}}(V_3)$ intersects the edge ∂_3 at a unique point P_3. For the case $\alpha = 0$, $\hat{\mathcal{H}}(V_3)$ intersects the edge ∂_3 at the vertices V_1 and V_2.*

Proof. Let us consider $u_3 = 0$ in equation (6.6). First notice that when $\rho_{21} = 0$ the point B_3 with coordinates given by (2.30) is the unique solution of Eq. (6.6). For $\rho_{21} \neq 0$, after some calculations, we obtain

$$u_2^2 - (1 + \alpha(\mu_1 + \mu_2)/\rho_{21})u_2 + \alpha\mu_2/\rho_{21} = 0. \tag{6.9}$$

The solutions of equation (6.9) are

$$u_2^{\pm} = \frac{1}{2}\left(\left(1 + \frac{\alpha(\mu_1 + \mu_2)}{\rho_{21}}\right) \pm \sqrt{\left(1 + \frac{\alpha(\mu_1 + \mu_2)}{\rho_{21}}\right)^2 - 4\frac{\alpha\mu_2}{\rho_{21}}} \right). \tag{6.10}$$

If $(\alpha/\rho_{21}) < 0$, the solution u_2^- is negative and has no interest, while the solution u_2^+ lies in $(0, 1)$, therefore P_3 has coordinates $(1 - u_2^+, u_2^+, 0)$. Performing a similar analysis for the case $(\alpha/\rho_{21}) > 0$ we have u_2^- as the unique valid solution of (6.9), giving rise to $P_3 = (1 - u_2^-, u_2^-, 0)$. For the case $\alpha = 0$, we obtain $u_2^- = 0$ and $u_2^+ = 1$; therefore $\hat{\mathcal{H}}(V_3)$ intersects the boundary ∂_3 at the vertices V_1 and V_2. $\qquad\square$

Lemma 6.2. *The intersection of $\hat{\mathcal{H}}(V_3)$ with the edges of the saturation triangle are described as follows.*
(i)   (1) Consider $\rho_{13} = 0$. We have:
  (a) $\alpha = 0 \Leftrightarrow \partial_2 \subset \hat{\mathcal{H}}(V_3)$.
  (b) $\alpha \neq 0 \Leftrightarrow \hat{\mathcal{H}}(V_3) \cap \partial_2 = \{V_3\}$.
  (2) If $\rho_{13} \neq 0$ then $(\alpha\mu_3/\rho_{31}) \in [0, 1) \Leftrightarrow \exists! S_2^\alpha \in \hat{\mathcal{H}}(V_3) \cap \partial_2$ such that $S_2^\alpha \neq V_3$.

(ii) (1) Consider $\rho_{23} = 0$. We have:
  (a) $\alpha = 0 \Leftrightarrow \partial_1 \subset \hat{\mathcal{H}}(V_3)$.
  (b) $\alpha \neq 0 \Leftrightarrow \hat{\mathcal{H}}(V_3) \cap \partial_1 = \{V_3\}$.
  (2) If $\rho_{23} \neq 0$ then $(\alpha\mu_3/\rho_{32}) \in [0, 1) \Leftrightarrow \exists! S_1^\alpha \in \hat{\mathcal{H}}(V_3) \cap \partial_1$ such that $S_1^\alpha \neq V_3$.

Proof. We will prove only item (ii) since the proof of item (i) is analogous. First notice that the vertex $V_3 = (0, 0, 1) \in \hat{\mathcal{H}}(V_3) \cap \partial_1 \cap \partial_2$. In item (ii) we are interested in the intersections (out of V_3) of the non-trivial locus $\hat{\mathcal{H}}(V_3)$ with the edge ∂_1 so we take the

limit when $u_1 \to 0$ with $u_2 \neq 0$ in (6.6), we have $U = (u_1, u_2, u_3) \in \hat{\mathcal{H}}(V_3) \cap \partial_1$ if and only if

$$\alpha + \frac{u_3^2}{\mu_3} \rho_{23} = 0. \tag{6.11}$$

From (6.11) we see that item $(ii.1)$ is trivial. If $(\alpha\mu_3/\rho_{32}) \in [0, 1)$ we obtain from (6.11) that $u_3 = \sqrt{\alpha\mu_3/\rho_{32}}$ is an admissible saturation value and therefore the point

$$S_1^\alpha = (0, 1 - \sqrt{\alpha\mu_3/\rho_{32}}, \sqrt{\alpha\mu_3/\rho_{32}}) \tag{6.12}$$

satisfies $S_1^\alpha \in \hat{\mathcal{H}}(V_3) \cap \partial_1$ with $S_1^\alpha \neq V_3$, concluding the proof of item $(ii.2)$.

As we said before the proof for item (i) is analogous, specifically for $(i.2)$ we will obtain the point

$$S_2^\alpha = (1 - \sqrt{\alpha\mu_3/\rho_{31}}, 0, \sqrt{\alpha\mu_3/\rho_{31}}), \tag{6.13}$$

which satisfies $S_2^\alpha \in \hat{\mathcal{H}}(V_3) \cap \partial_2$ with $S_2^\alpha \neq V_3$. $\square$

Remark 6.3. *Notice that when $|\alpha| \to 0$ we have $S_1^\alpha \to V_2$ and $S_2^\alpha \to V_1$.*

Corollary 6.1. *Assume $\rho_{13} \neq 0, \rho_{23} \neq 0$, $(\alpha\mu_3/\rho_{32}) \notin [0, 1)$ and $(\alpha\mu_3/\rho_{31}) \notin [0, 1)$, then*

$$\hat{\mathcal{H}}(V_3) \cap \partial_1 = \hat{\mathcal{H}}(V_3) \cap \partial_2 = \{V_3\}.$$

Proof. This result is a direct consequence of items $(i.2)$ and $(ii.2)$ of Lemma 6.2. $\square$

Lemma 6.3. *Assume $\rho_1 \neq \rho_2$. We have the following assertions:*

(i) $\hat{\mathcal{H}}(V_3)$ does not intersect R_3 at any interior point of the saturation triangle.

(ii) If $U \in \hat{\mathcal{H}}(V_3)$ and U is not a vertex of the saturation triangle, then $\sigma(V_3, U) \neq 0$.

Proof. Item (i) is a direct consequence of the necessary condition (6.8) for a state U to belong to $\hat{\mathcal{H}}(V_3)$. Item (ii) will be also a consequence of (6.8) for states out of the edges ∂_1 and ∂_2. If $U \in \hat{\mathcal{H}}(V_3) \cap \partial_i$ for $i = 1$ or $i = 2$, then the conclusion follows from the shape of the two-phase flux functions along the edges, see Fig. 5.1, and from the assumption that U is not a vertex of the saturation triangle. $\square$

We continue the study of $\hat{\mathcal{H}}(V_3)$ given by (6.6) for the case $\rho_1 \neq \rho_2$. It is clear that this curve contains the point V_3. Depending of the parameter α a portion of this curve may lie outside the saturation triangle.

Assume $(\alpha + \rho_{13}/\mu_3) \neq 0$, then we can apply the implicit function theorem for $\hat{\mathcal{H}}(V_3)$ (equation (6.6)) in a neighborhood $\mathcal{N}(V_3)$ of $V_3 = (0, 0)$ (here we use the coordinates u_1, u_2 in (2.24) for the saturation triangle), obtaining u_1 as function of u_2, with slope

$$T_3(\alpha) = \frac{du_1}{du_2}(0, 0) = \frac{\mu_1}{\mu_2} \frac{(\alpha + \frac{\rho_{23}}{\mu_3})}{(\alpha + \frac{\rho_{13}}{\mu_3})}. \tag{6.14}$$

The sign of $T_3(\alpha)$ yields crucial information about the behavior of the local curve (6.6), *i.e.*, in a neighborhood of V_3.

Corollary 6.2. *If $T_3(\alpha) > 0$ the local curve (6.6) crosses the vertex V_3, possessing a portion inside the saturation triangle, so in this sense we say that $\hat{\mathcal{H}}(V_3)$ starts from V_3. If $T_3(\alpha) < 0$ the local curve (6.6) crosses the vertex V_3 and lies outside the saturation triangle. In such a case we say that $\hat{\mathcal{H}}(V_3)$ does not start at V_3.*

If $T_3(\alpha) = 0$ the local curve (6.6) is tangent at V_3 to the edge ∂_1. If the inverse of $T_3(\alpha)$ vanishes, the local curve (6.6) will be tangent at V_3 to the edge ∂_2. In both tangency cases either the whole local curve lies entirely outside the saturation triangle or one half of the local curve lies inside the saturation triangle.

Remark 6.4. *We note that for sufficiently large values of $|\alpha|$, $T_3(\alpha)$ is positive, therefore the curve $\hat{\mathcal{H}}(V_3)$ starts from the vertex V_3, (i.e., it enters the saturation triangle).*

Remark 6.5. *As expected, $\lim_{\alpha \to \infty} T_3(\alpha) = \mu_1/\mu_2$. This limit corresponds to the non-gravitational case in which $\hat{\mathcal{H}}(V_3) = R_3$.*

Remark 6.6. *Notice that the formula for $T_3(\alpha)$ in (6.14) is given in a rectangular coordinates system (u_1, u_2). Nevertheless in most of the figures along the work we use baricentric coordinates in the saturation triangle.*

Since $\rho_1 \neq \rho_2$, if $(\alpha + \rho_{13}/\mu_3) = 0$ we have $(\alpha + \rho_{23}/\mu_3) \neq 0$, so we can apply the Implicit Function Theorem to obtain u_2 as a function of u_1 in a neighborhood of V_3. Defining $T_3(\alpha)$ as the inverse of the fraction in (6.14) it is possible to reach conclusions analogous to Corollary 6.2 and Remarks 6.4, 6.5.

The following Proposition gives the qualitative behavior of the non-trivial Hugoniot branch $\hat{\mathcal{H}}(V_3)$.

Proposition 6.2. *Assume $\rho_1 > \rho_2$ and $\alpha \neq 0$, then we have the following assertions (plotting the curve in (6.6) it is possible to obtain Figs. 6.2-6.6).*

(i) *When $\rho_1 > \rho_3 > \rho_2$:*

    (i.1) *If $\alpha > (\rho_{32}/\mu_3)$ or $\alpha < (\rho_{31}/\mu_3)$ we have that $\hat{\mathcal{H}}(V_3)$ is a connected curve that starts at V_3 and finishes at $P_3 \in \partial_3$, without touching the edges ∂_1 and ∂_2; see Fig. 6.2.*

    (i.2) *If $0 < \alpha < (\rho_{32}/\mu_3)$ we have that $\hat{\mathcal{H}}(V_3)$ is a connected curve that starts at a point $S_1^\alpha \in \partial_1$ $(S_1^\alpha \neq V_3)$ and finishes at $P_3 \in \partial_3$; see Fig. 6.3.*

    (i.3) *If $(\rho_{31}/\mu_3) < \alpha < 0$ we have that $\hat{\mathcal{H}}(V_3)$ is a connected curve that starts at $S_2^\alpha \in \partial_2$ $(S_2^\alpha \neq V_3)$ and finishes at $P_3 \in \partial_3$; see Fig. 6.4.*

(ii) When $\rho_3 \geq \rho_1 > \rho_2$:

(ii.1) If $\alpha < 0$ or $\alpha > (\rho_{32}/\mu_3)$ we have that $\hat{\mathcal{H}}(V_3)$ is a connected curve that starts at V_3 and finishes at $P_3 \in \partial_3$, without touching the edges ∂_1 and ∂_2; see Fig. 6.2.

(ii.2) If $(\rho_{31}/\mu_3) < \alpha < (\rho_{32}/\mu_3)$ we have that $\hat{\mathcal{H}}(V_3)$ is a connected curve that starts at $S_1^{\alpha} \in \partial_1$ $(S_1^{\alpha} \neq V_3)$ and finishes at $P_3 \in \partial_3$; see Fig. 6.3.

(ii.3) If $0 < \alpha < (\rho_{31}/\mu_3)$ then $\hat{\mathcal{H}}(V_3)$ is a disconnected curve with two branches V_3–S_2^{α} and S_1^{α}–P_3 where $S_2^{\alpha} \in \partial_2$, $S_1^{\alpha} \in \partial_1$, $P_3 \in \partial_3$; see Fig. 6.5.

(iii) When $\rho_1 > \rho_2 \geq \rho_3$:

(iii.1) If $\alpha > 0$ or $\alpha < (\rho_{31}/\mu_3)$ we have that $\hat{\mathcal{H}}(V_3)$ is a connected curve that starts at V_3 and finishes at $P_3 \in \partial_3$, without touching the edges ∂_1 and ∂_2; see Fig. 6.2.

(iii.2) If $(\rho_{31}/\mu_3) < \alpha < (\rho_{32}/\mu_3)$ then $\hat{\mathcal{H}}(V_3)$ is a connected curve that starts at $S_2^{\alpha} \in \partial_2$ $(S_2^{\alpha} \neq V_3)$ and finishes at $P_3 \in \partial_3$; see Fig. 6.4.

(iii.3) If $0 > \alpha > (\rho_{32}/\mu_3)$ then $\hat{\mathcal{H}}(V_3)$ is a disconnected curve with two branches V_3–S_1^{α} and S_2^{α}–P_3, where $S_1^{\alpha} \in \partial_1$, $S_2^{\alpha} \in \partial_2$, $P_3 \in \partial_3$; see Fig. 6.6.
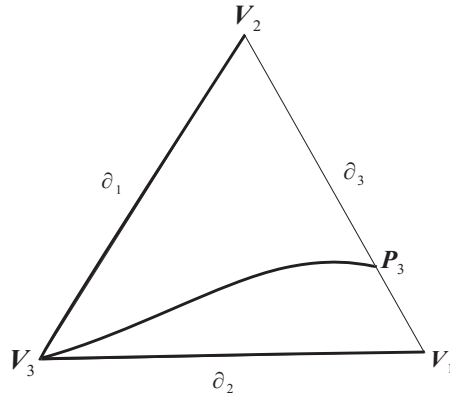
Figure 6.2: *Dark curve: Hugoniot Locus of vertex V_3 for items $(i.1), (ii.1), (iii.1)$ of Proposition 6.2*

Proof. We will prove only item (ii), the proofs for items (i) and (iii) are similar.

Assume $\rho_3 \geq \rho_1 > \rho_2$. We have $\rho_{23} < 0$ and $\rho_{13} \leq 0$, so for $\alpha < 0$ or $\alpha > (\rho_{32}/\mu_3)$ we have $T_3(\alpha) > 0$ and therefore the curve (6.6) crosses the vertex V_3 with a local portion inside the saturation triangle. Thus $\hat{\mathcal{H}}(V_3)$ starts at the vertex V_3. $\hat{\mathcal{H}}(V_3)$ finishes at $P_3 \in \partial_3$ as we proved in Lemma 6.1. The fact that $\hat{\mathcal{H}}(V_3)$ does not touch the boundaries ∂_1 and ∂_2 is a consequence of Corollary 6.1, concluding the proof of item $(ii.1)$, see Fig. 6.2.
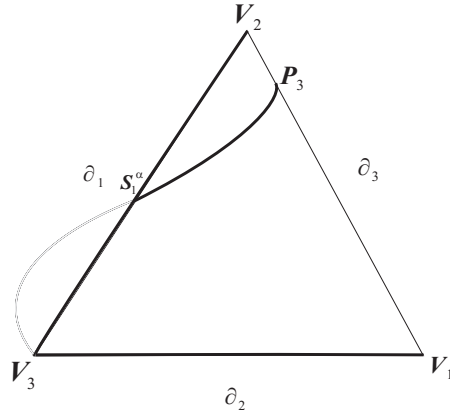
Figure 6.3: *Dark curve: Hugoniot Locus of vertex V_3 for items $(i.2)$ and $(ii.2)$ of Proposition 6.2. Light curve: points satisfying the Rankine-Hugoniot relation but lie outside the saturation triangle*
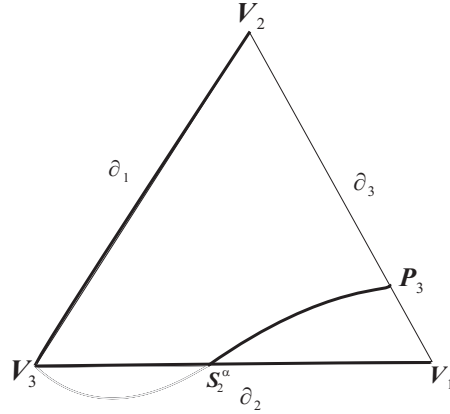
Figure 6.4: *Dark curve: Hugoniot Locus of vertex V_3 for items $(i.3)$ and $(iii.2)$ of Proposition 6.2. Light curve: points satisfying the Rankine-Hugoniot relation but lie outside the saturation triangle*

For $(ii.2)$; see Fig. 6.3, we obtain $T_3(\alpha) < 0$, so the curve (6.6) crosses the vertex V_3 lying outside the saturation triangle and $\hat{\mathcal{H}}(V_3)$ does not start at the vertex V_3. We also have

$$0 \leq (\alpha\mu_3/\rho_{32}) < 1 < (\alpha\mu_3/\rho_{31}).$$

Applying items $(i.2)$ and $(ii.2)$ of Lemma 6.2 we see that there exists a unique $S_1^\alpha \in \hat{\mathcal{H}}(V_3) \cap \partial_1$ with $S_1^\alpha \neq V_3$ while $\hat{\mathcal{H}}(V_3) \cap \partial_2 = \{V_3\}$. The branch of the Hugoniot locus joining S_1^α with vertex V_3 "lies outside" the saturation triangle and has no interest, so the curve $\hat{\mathcal{H}}(V_3)$ lying inside the saturation triangle starts at S_1^α and finishes at $P_3 \in \partial_3$ given by Lemma 6.1.

For $(ii.3)$; see Fig. 6.5, we have the condition $0 < \alpha < (\rho_{31}/\mu_3) < (\rho_{32}/\mu_3)$, here we have $T_3(\alpha) > 0$ therefore $\hat{\mathcal{H}}(V_3)$ enters the triangle in a neighborhood of the vertex V_3.
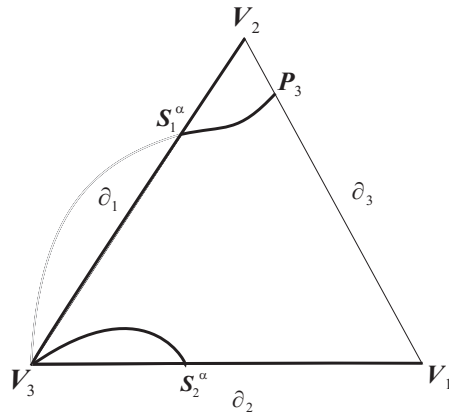
Figure 6.5: *Dark curve: Hugoniot Locus of vertex V_3 for item $(ii.3)$ of Proposition 6.2. Light curve: points satisfying the Rankine-Hugoniot relation but lie outside the saturation triangle*
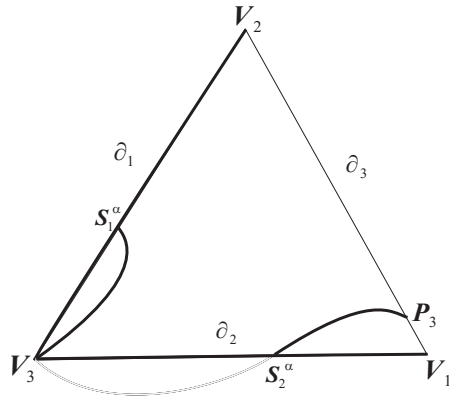
Figure 6.6: *Dark curve: Hugoniot Locus of vertex V_3 for item $(iii.3)$ of Proposition 6.2. Light curve: points satisfying the Rankine-Hugoniot relation but lie outside the saturation triangle*

We can assume $\rho_3 > \rho_1$ (notice that the case $\rho_3 = \rho_1$ is trivial) so we obtain

$$0 \leq (\alpha\mu_3/\rho_{32}) \leq (\alpha\mu_3/\rho_{31}) < 1.$$

Again applying the items $(i.2)$ and $(ii.2)$ of Lemma 6.2 there exist two points $S_1^\alpha \in \hat{\mathcal{H}}(V_3) \cap \partial_1$ with $S_1^\alpha \neq V_3$ and $S_2^\alpha \in \hat{\mathcal{H}}(V_3) \cap \partial_2$ with $S_2^\alpha \neq V_3$. The curve $\hat{\mathcal{H}}(V_3)$ has two disconnected branches. The first branch starts at the vertex V_3 and finishes at $S_2^\alpha \in \partial_2$. The second branch starts at $S_1^\alpha \in \partial_1$ and finishes at a point $P_3 \in \partial_3$ given by Lemma 6.1. $\qquad\square$

It is possible to analyze the limit cases $\alpha \to 0$, $\alpha \to (\rho_{32}/\mu_3)$ and $\alpha \to (\rho_{31}/\mu_3)$ for Prop. 6.2. As we want to solve the pure gravitational problem as a first step to understand the influence of the buoyancy in the solutions of Riemann problem, in this work we will analyze only the limit case $\alpha \to 0$.

Notice that when $\alpha = 0$ we have that all three vertices belong to $\hat{\mathcal{H}}(V_3)$ (see Lemma 6.1); the following Proposition describes the other points of the curve $\hat{\mathcal{H}}(V_3)$.

Proposition 6.3. *Assume $\rho_1 > \rho_2$ and $\alpha = 0$. The following assertions hold:*

(i) *For any of the cases $(\rho_1 > \rho_3 > \rho_2)$, $(\rho_1 = \rho_3 > \rho_2)$ or $(\rho_1 > \rho_3 = \rho_2)$ we have $\hat{\mathcal{H}}(V_3)\backslash\{V_1, V_2, V_3\} = \emptyset$, therefore $\mathcal{H}(V_3) = \partial_1 \cup \partial_2$.*

(ii) *If $\rho_3 > \rho_1 > \rho_2$, $\hat{\mathcal{H}}(V_3)\backslash\{V_1, V_2, V_3\}$ is a connected curve joining the vertices V_3 and V_1 (see Fig. 6.7(a)). This curve consists only of interior points of the saturation triangle.*

(iii) *If $\rho_3 < \rho_2 < \rho_1$, $\hat{\mathcal{H}}(V_3)\backslash\{V_1, V_2, V_3\}$ is a connected curve joining the vertices V_3 and V_2 (see Fig. 6.7(b)). This curve consists only of interior points of the saturation triangle.*

(a)   (b)
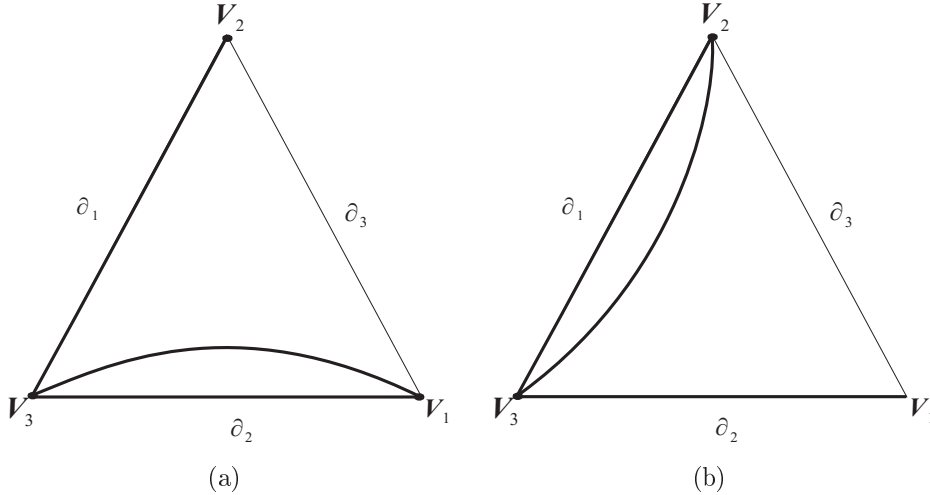
Figure 6.7: Dark curve: Hugoniot Locus of vertex V_3 for the pure gravitational problem. (a) Case of item (ii) of Prop. 6.3. (b) Case of item (iii) of Prop. 6.3.

Proof. Item (i) is a direct consequence of Eq. (6.6) since all the terms involved are negative quantities for all the cases mentioned.

In order to prove item (ii), let us assume $\alpha < 0$, then $(\alpha/\rho_{21}) > 0$. The intersection point of $\hat{\mathcal{H}}(V_3)$ with the edge ∂_3 is $P_3 = (1 - u_2^-, u_2^-, 0)$, where u_2^- is given by (6.10). Notice that in such a case we have $P_3 \to V_1$ when $\alpha \to 0^-$.

Applying item $(ii.1)$ of Proposition 6.2 for the limit case $\alpha \to 0^-$, we obtain that $\hat{\mathcal{H}}(V_3)$ starts at V_3 and finishes at V_1, without touching the edges ∂_1 and ∂_2.

In the same way we can apply item $(ii.3)$ of Proposition 6.2 for the limit case $\alpha \to 0^+$; we will obtain the same result, since $S_2^\alpha \to V_1, S_1^\alpha \to V_2$ (see Remark 6.3) and $P_3 \to V_2$.

For this limit case notice that the branch $S_1^\alpha - P_3$ yields the point V_2, while the branch $V_3 - S_2^\alpha$ yields a connected curve starting at the vertex V_3 and finishing at the vertex V_1; this curve consists of interior points except for the vertices.

The proof of item (iii) is analogous. $\qquad\qquad\qquad\qquad\qquad\qquad\qquad\qquad$ □

Lemma 6.4. *Assume* $\alpha \neq 0$. *The unique interior umbilic point* U_α^* *lies on the curve* $\hat{\mathcal{H}}(V_3)$.

Proof. Let U_α^* be the interior umbilic point, then it must satisfy the equations (4.38)-(4.40). For the quadratic mobilities (2.19) in the Corey model, Eq. (4.40) is

$$\alpha(\frac{u_1}{\mu_1} - \frac{u_2}{\mu_2}) + \left[\frac{u_1 u_3^2}{\mu_1 \mu_3}\rho_{13} + (\frac{u_1 u_2^2}{\mu_1 \mu_2} + \frac{u_1^2 u_2}{\mu_1 \mu_2})\rho_{12} - \frac{u_2 u_3^2}{\mu_2 \mu_3}\rho_{23} \right] = 0. \qquad (6.15)$$

By regrouping conveniently the terms in Eq. (6.15) we obtain (6.6), concluding that for the Corey model with quadratic mobilities, the umbilic point U_α^* is contained in $\hat{\mathcal{H}}(V_3)$. $\quad$ □

We can state the following result.

Proposition 6.4. *For* $\alpha \neq 0$, *the unique interior umbilic point* U_α^* *is the intersection point of the non-trivial Hugoniot branches for the three vertices* V_1, V_2 *and* V_3, *see for instance Fig. 6.8.*

Remark 6.7. *The fact that the umbilic point* U_α^* *is unique for the Corey model including gravity was proved by Medeiros in [33].*
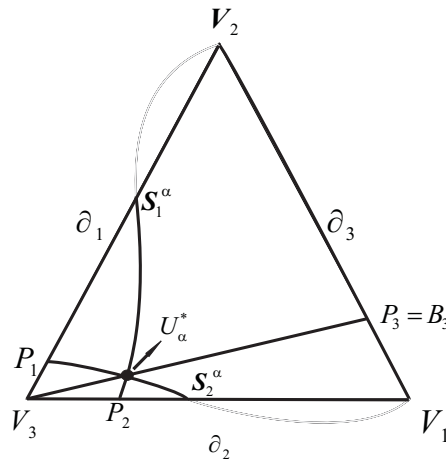
Figure 6.8: *Hugoniot loci for the three vertices in the case* $\rho_1 = \rho_2 > \rho_3$, $\mu_1 > \mu_2$ *and* $0 < \alpha < \rho_{23}/\mu_1$. *The umbilic point* U_α^* *is the intersection point of the three curves in the saturation triangle.*

Chapter 7

Hugoniot locus for edge points in the pure gravitational problem

In this chapter we analyze the Hugoniot locus for states U_L on the edges ∂_i for the pure gravitational case, in which $\alpha = 0$. Here U_L will not be a vertex of the saturation triangle, as this case was analyzed in the previous chapter. In the first section we present a new method based on a geometric construction to obtain shocks joining states on different two-phase regimes, provided that these regimes have a common state forming a wedge. This construction does not depend on the permeabilities, so it is applicable for general permeability models. In the second section we consider the case where U_L lies on an edge corresponding to equal-density phases. In third and fourth sections we describe the Hugoniot locus for the remaining cases. The results of this chapter will be very important for the construction of the Riemann solutions described in Chapters 9 and 10.

Without loss of generality we will analyze the Hugoniot locus for the edge ∂_2, which represents mixtures of phases 1 and 3. We will consider the 2×2 system of conservation law (2.23) that results after dropping the equation corresponding to phase 3. We consider a state U_L on the edge ∂_2, $U_L = (u_1^L, 0, u_3^L)$, with $u_3^L = 1 - u_1^L$. Denote by $U = (u_1, u_2, u_3)$ an arbitrary state in the saturation triangle. The Rankine-Hugoniot relation for a shock joining the left and right states U_L and U is

$$F_1(U_L) - F_1(U) = \sigma(u_1^L - u_1) \tag{7.1}$$

$$F_2(U_L) - F_2(U) = \sigma(u_2^L - u_2), \tag{7.2}$$

with σ representing the shock speed. Using the flux expressions (2.20)-(2.21) into (7.1)-(7.2) we obtain the following expressions

$$\sigma(u_1^L - u_1) = \frac{(u_1^L)^2(1-u_1^L)^2}{\mu_1 \mu_3 \Lambda_L}\rho_{13} - \frac{u_1^2}{\mu_1}(\frac{u_3^2}{\mu_3}\rho_{13} + \frac{u_2^2}{\mu_2}\rho_{12})/\Lambda(U), \tag{7.3}$$

$$\sigma u_2 = \frac{u_2^2}{\mu_2}(\frac{u_3^2}{\mu_3}\rho_{23} + \frac{u_1^2}{\mu_1}\rho_{21})/\Lambda(U), \tag{7.4}$$

52

where, from (2.19)

$$\Lambda_L = \Lambda(U_L) = (u_1^L)^2/\mu_1 + (1 - u_1^L)^2/\mu_3. \tag{7.5}$$

In Proposition 6.3 we have already found the Hugoniot locus for the vertices, so from now on we assume that $u_1^L \neq 0$ and $u_1^L \neq 1$.

From (7.4) it is obvious that the edge ∂_2 is a trivial branch of $\mathcal{H}(U_L)$. For $U \notin \partial_2$ we can divide the equation (7.4) by u_2 to obtain:

$$\sigma = \frac{u_2}{\mu_2}(\frac{u_3^2}{\mu_3}\rho_{23} + \frac{u_1^2}{\mu_1}\rho_{21})/\Lambda(U). \tag{7.6}$$

Equation (7.6) represents the speed σ of the discontinuity joining the state $U_L \in \partial_2$ with any state $U \in \mathcal{H}(U_L)$ out of the edge ∂_2.

Substituting (7.6) into equation (7.3) and performing some calculations we obtain

$$
\begin{aligned}
&\frac{(u_1^L)^3 u_2 u_3^2}{\mu_1\mu_2\mu_3}\rho_{23} + \frac{(u_1^L)^3 u_2 u_1^2}{\mu_1^2\mu_2}\rho_{21} - \frac{(u_1^L)^2 u_1 u_2 u_3^2}{\mu_1\mu_2\mu_3}\rho_{23} - \frac{(u_1^L)^2 u_1^3 u_2}{\mu_1^2\mu_2}\rho_{21} \\
&+ \frac{(u_1^L)u_2(1 - u_1^L)^2 u_3^2}{\mu_2\mu_3^2}\rho_{23} + \frac{(u_1^L)u_1^2 u_2(1 - u_1^L)^2}{\mu_1\mu_2\mu_3}\rho_{21} - \frac{u_1 u_2 u_3^2(1 - u_1^L)^2}{\mu_2\mu_3^2}\rho_{23} \\
&- \frac{u_1^3 u_2(1 - u_1^L)^2}{\mu_1\mu_2\mu_3}\rho_{21} - \frac{(u_1^L)^2 u_1^2(1 - u_1^L)^2}{\mu_1^2\mu_3}\rho_{13} - \frac{(u_1^L)^2 u_2^2(1 - u_1^L)^2}{\mu_1\mu_2\mu_3}\rho_{13} \\
&- \frac{(u_1^L)^2 u_3^2(1 - u_1^L)^2}{\mu_1\mu_3^2}\rho_{13} + \frac{(u_1^L)^2 u_1^2 u_3^2}{\mu_1^2\mu_3}\rho_{13} + \frac{u_1^2 u_3^2(1 - u_1^L)^2}{\mu_1\mu_3^2}\rho_{13} \\
&- \frac{(u_1^L)^2 u_1^2 u_2^2}{\mu_1^2\mu_3}\rho_{21} - \frac{u_1^2 u_2^2(1 - u_1^L)^2}{\mu_1\mu_2\mu_3}\rho_{21} = 0.
\end{aligned} \tag{7.7}
$$

For u_1^L fixed, (7.7) represents a local branch of the Hugoniot locus of U_L that is different from the edge ∂_2.

Definition 7.1. *We will call the portion of the curve (7.7) lying in the saturation triangle as the non-trivial branch of the Hugoniot locus of $U_L \in \partial_2$ and we will denote it by $\tilde{\mathcal{H}}(U_L)$.*

Sometimes it is simpler to work directly with Eqs. (7.3)-(7.4) rather than with Eq. (7.7). As $u_3 = 1 - u_1 - u_2$, notice that the left hand side of Eq. (7.7) is a polynomial of fourth degree in the variables u_1 and u_2. However, for some special cases, like $\rho_2 = \rho_3$, it is possible to obtain u_2 from Eq. (7.7) as an explicit function of u_1. This is a great advantage of Eq. (7.7).

In order to understand the shape of $\tilde{\mathcal{H}}(U_L)$ for U_L in ∂_2 the first step is to determine the intersections of $\tilde{\mathcal{H}}(U_L)$ with the other edges of the saturation triangle. In our particular Riemann problem it is also an essential step. We present in the next section a geometric analysis that allows to construct general edge to edge shocks for any flux functions, any density and viscosity values; however, for the sake of concreteness, we will illustrate the method only for the case $\rho_1 > \rho_3 \geq \rho_2$ and for left and right shock states in ∂_2 and ∂_3 respectively.

7.1   Edge to edge shocks: the wedge construction.

The following geometric construction determines shocks joining states on different two-phase edges of the saturation triangle. The construction is general and does not depend on the "convection/gravity ratio" α or on the form of the permeability functions, so it is applicable to general permeability models. Nevertheless in this work we only use it for the quadratic Corey model with gravity (2.23).

Two edges of the saturation triangle have a common vertex forming a wedge. Without loss of generality we assume that the common vertex is V_1. This means that phase 1 is present in both edges ∂_2 and ∂_3 of the wedge, phase 2 is present in the edge ∂_3, while phase 3 is present in the edge ∂_2.

We will illustrate the wedge construction for the case $\rho_1 > \rho_3 \geq \rho_2$. We consider the flux function (F_1, F_2) of the system (2.23) restricted to the edges ∂_2 and ∂_3 . From Remark 5.1 we see that the choice $F_1^{\partial_2}(u_1)$ or $F_3^{\partial_2}(u_3)$ does not make any difference for the solution, so we choose the pair

$$F_1^{\partial_2}(u_1) = \frac{u_1^2(1 - u_1)^2}{\mu_1 \mu_3 \left(\frac{u_1^2}{\mu_1} + \frac{(1-u_1)^2}{\mu_3} \right)} \rho_{13} \quad \text{and} \quad u_1 \tag{7.8}$$

as the two-phase flux and the conserved quantity both restricted to the edge ∂_2. As $\rho_1 > \rho_3$ the plot of this flux function is similar to the one shown in Fig. 5.1(a).

For the restriction of the flux to the two-phase edge ∂_3 we will choose for convenience

$$F_2^{\partial_3}(u_2) = \frac{u_2^2(1 - u_2)^2}{\mu_1 \mu_2 \left(\frac{u_2^2}{\mu_2} + \frac{(1-u_2)^2}{\mu_1} \right)} \rho_{21}, \tag{7.9}$$

where u_2 is the conserved quantity. The plot of this function is shown in Fig. 5.1(b).

The scalar flux functions $F_1^{\partial_2}$ and $F_2^{\partial_3}$ govern different two-phase regimes with a common state V_1. However we will create a useful construction by defining an extended flux function involving both $F_1^{\partial_2}$ and $F_2^{\partial_3}$ in the same graph in a conveniently way. We define for $-1 \leq u \leq 1$

$$F_{ext}^{\partial_2\partial_3}(u) = \begin{cases} F_1^{\partial_2}(1 + u) & \text{if } -1 \leq u \leq 0, \\ F_2^{\partial_3}(u) & \text{if } 0 \leq u \leq 1. \end{cases} \tag{7.10}$$

Notice that $F_{ext}^{\partial_2\partial_3}$ is a continuous function of the variable u defined in the interval $[-1, 1]$. For negative values of u, the function $F_{ext}^{\partial_2\partial_3}$ coincides with the flux $F_1^{\partial_2}$ restricted to the edge ∂_2 while for positive values of u this extended flux function coincides with the flux $F_2^{\partial_3}$ restricted to the edge ∂_3. For that reason in this section we will abuse the notation denoting by V_1 the origin $\left(u = 0, F_{ext}^{\partial_2\partial_3}(0) = 0 \right)$, V_2 is the point $\left(u = 1, F_{ext}^{\partial_2\partial_3}(1) = 0 \right)$ and V_3 is the point $\left(u = -1, F_{ext}^{\partial_2\partial_3}(-1) \right) = 0$, see the Fig. 7.1.
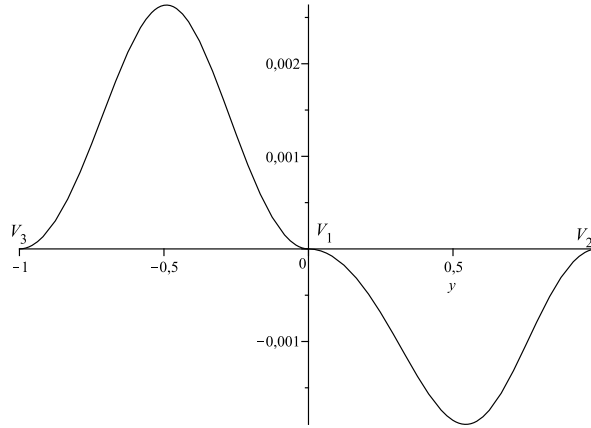
Figure 7.1: *Example of the extended flux function* $F_{ext}^{\partial_2 \partial_3}$ *for* $\mu_1 = 1$, $\mu_2 = 1.7$, $\mu_3 = 0.9$ *and* $\rho_2 = \rho_3$

Remark 7.1. *Notice that the extended flux* $F_{ext}^{\partial_2 \partial_3}$ *does not represent a genuine flux function in a neighborhood of the state* V_1, *the junction of the edges* ∂_2 *and* ∂_3 *where both flux functions* $F_1^{\partial_2}$ *and* $F_2^{\partial_3}$ *are defined.*

Remark 7.2. *Differentiability at* $u = 0$ *of the function* $F_{ext}^{\partial_2 \partial_3}$ *is a consequence of Eq.* (5.2).

The following Lemma will be crucial for the applicability of our construction.

Lemma 7.1. *Consider a state* U_L *in the edge* ∂_2. *If there exists* $U \in \partial_3$ *such that* $U \in \mathcal{H}(U_L)$ *then* $\sigma(U_L, U) = \sigma(U, V_1) = \sigma(U_L, V_1)$.

Proof. See Fig. 7.2(a). Notice that the shock speed $\sigma(U_L, U)$ given in Eq. (7.4) coincides with the slope of the straight line segment joining the vertex V_1 to the point $(u_2, F_2^{\partial_3}(u_2))$, so we have that $\sigma(U_L, U) = \sigma(U, V_1)$. As U_L, V_1, U are not aligned states in the saturation triangle, we apply the Triple Shock Rule to conclude that $\sigma(U_L, U) = \sigma(U, V_1) = \sigma(U_L, V_1)$. $\qquad\square$

Remark 7.3. *The converse also holds: if* $U \in \partial_3$ *is such that* $\sigma(U, V_1) = \sigma(U_L, V_1)$, *then* $U \in \mathcal{H}(U_L)$ *and* $\sigma(U_L, U) = \sigma(U_L, V_1)$. *It follows from the second version of the Triple-Shock Rule.*

The geometric construction: Consider a state U on one of the edges ∂_2 or ∂_3. Lemma 7.1 yields a constructive way to obtain all the intersection points of $\mathcal{H}(U)$ with the other edge. As we did in Fig. 7.2(a), we have to construct the secant joining $V_1 = (0, 0)$ (notice that this is the origin of the system of coordinates in Fig. 7.1; these coordinates do not correspond to the coordinates in the saturation triangle) to $(u, F_{ext}^{\partial_2 \partial_3}(u))$, and determine the intersection points with the extended flux on the other side relative to the origin. The abscissae of these points determine the states on the other edge that belong to $\mathcal{H}(U)$. Of course, the number of intersection points of the secant with the graph on the other side coincides with the number of states of $\mathcal{H}(U)$ that lie on the other edge.

(a)

(b)
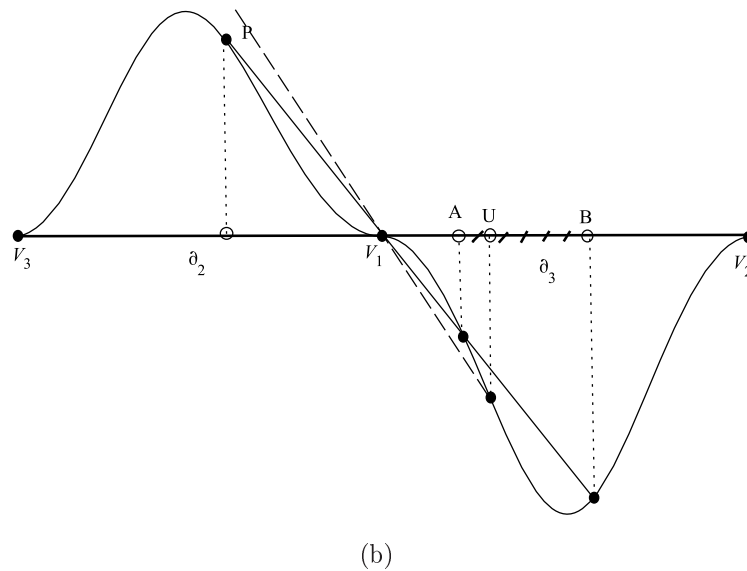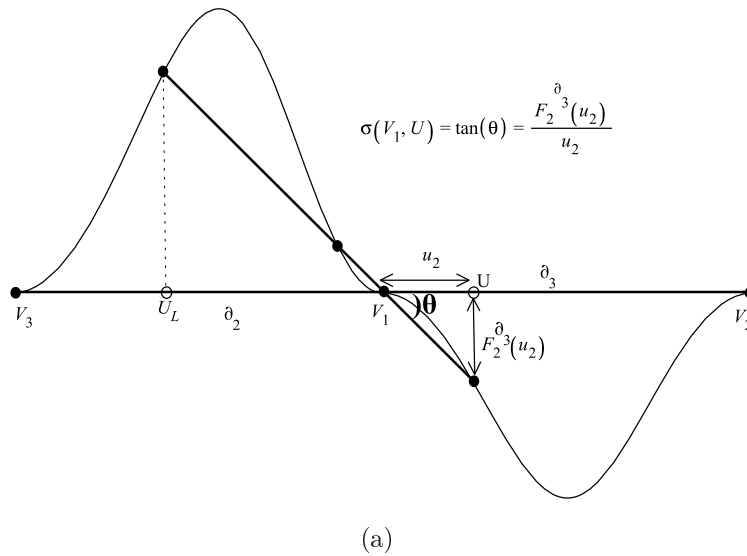
Figure 7.2: (a) Extended flux $F_{ext}^{\partial_2 \partial_3}$ for $\mu_1 = \mu_2 = 1$, $\mu_3 = 0.5$. The figure illustrate the application of Triple Shock Rule and the result of Lemma 7.1. (b) Extended flux $F_{ext}^{\partial_2 \partial_3}$ for $\mu_1 = \mu_2 = 1$, $\mu_3 = 1.5$. In this case for U in the interval (A, B), $\tilde{\mathcal{H}}(U)$ does not intersect the other edge.

Remark 7.4. *An interesting case occurs when the segment is tangent to the extended flux graph on one side while it is secant to the graph on the other side. In this case, there exists an interval of states U (the interval (A, B) in Fig. 7.2(b)) for which $\mathcal{H}(U)$ does not intersect the other edge.*

Remark 7.5. *Notice that for the results in Lemma 7.1 and for the geometric construction, the fact that the constructed secant crosses the origin V_1 is crucial in order to obtain a valid geometric description of the shocks from one edge to the other.*

Let us denote by $U^* = (1 - u_2^*, u_2^*, 0)$ the unique state on the edge ∂_3 satisfying $\sigma(V_1, U^*) = (dF_2^{\partial_3}/du_2)(u_2^*)$. The value of u_2^* can be shown to be the unique real root of the following cubic polynomial in v:

$$(\mu_1 + \mu_2)v^3 + (\mu_1 - 3\mu_2)v^2 + 3\mu_2 v - \mu_2. \tag{7.11}$$

Let us denote by P^* the point on the graph of $F_{ext}^{\partial_2\partial_3}$ corresponding to the state U^*. Let us denote by S the straight line segment that is tangent at P^* to the graph of $F_{ext}^{\partial_2\partial_3}$; this line crosses the origin of the coordinates system (which corresponds to the vertex V_1). Depending of the quantities μ_2, μ_3, ρ_{13}, ρ_{21} we will have zero, one (double) or two intersection points $(u, F_{ext}^{\partial_2\partial_3}(u))$ of the segment S with the graph of $F_{ext}^{\partial_2\partial_3}$ for negative values of u. In Fig. 7.3 we illustrate this fact for three different values of μ_3, keeping the parameters μ_2, ρ_{13}, ρ_{21} fixed. The three flux curves of Fig. 7.3 coincide above the edge ∂_3 because we only changed the parameter μ_3 to obtain the three curves.

For the case in which the extended flux is like the solid curve in Fig. 7.3, the pair of states U_0 in ∂_2 and U^* in ∂_3 corresponding to the tangency points P_0 and P^* belongs to the double contact manifold (see Def. 3.7). As we show in Fig. 7.3 small perturbations of the parameters μ_2, μ_3, ρ_{13}, ρ_{21} give rise to bifurcations of this "double-tangency" case.
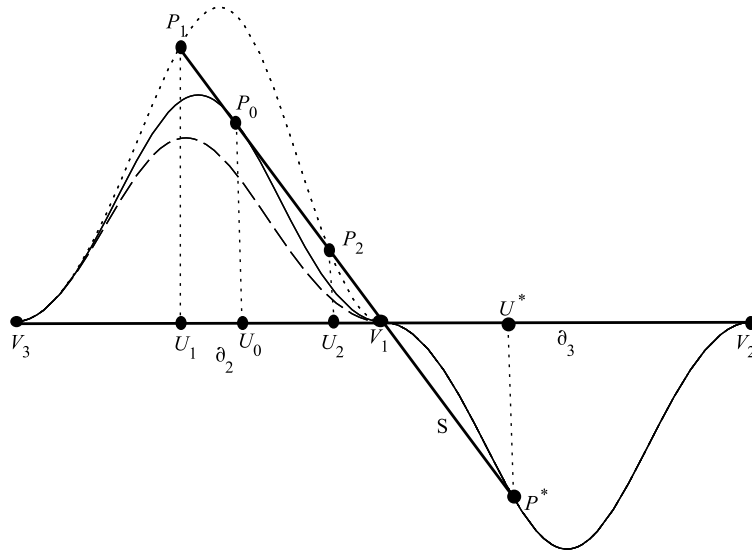
Figure 7.3: *Extended flux function $F_{ext}^{\partial_2\partial_3}$ for three different cases. Solid curve: $\mu_1 = \mu_2 = \mu_3 = 1$, dashed curve $\mu_1 = \mu_2 = 1$, $\mu_3 = 1.5$, dotted curve $\mu_1 = \mu_2 = 1$, $\mu_3 = 0.5$. The parameters ρ_{13} and ρ_{21} are the same for all the cases. Because μ_1 and μ_2 are fixed the flux is the same on ∂_3.*

Proposition 7.1. *Given the parameters μ_2, μ_3, ρ_{13}, ρ_{21}, we can describe the intersection points with the edge ∂_3 of the Hugoniot locus $\mathcal{H}(U_L)$ for a state U_L on ∂_2 as follows:*

(i) When the segment S does not intersect the graph of $F_{ext}^{\partial_2\partial_3}$ for negative values of u (this is the case for the dashed curve in Fig. 7.3), consider an arbitrary state U_L in
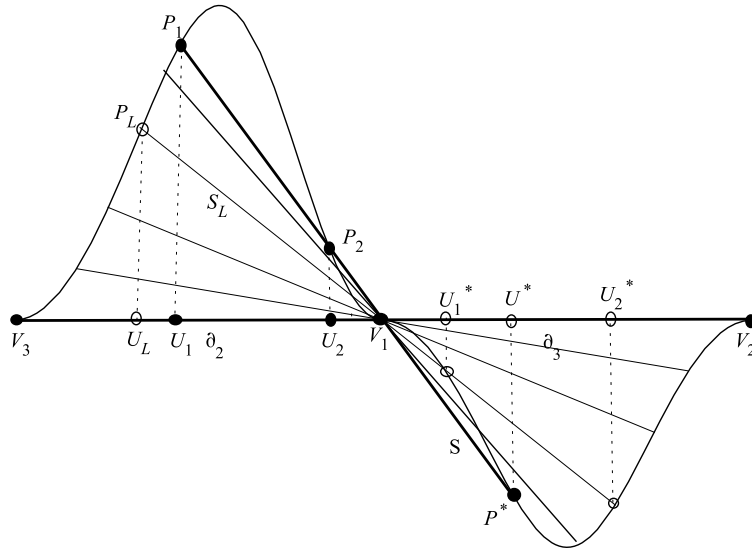
Figure 7.4: *Extended flux function $F_{ext}^{\partial_2 \partial_3}$ for the dotted flux curve of Fig. 7.3. Illustration for the proof of item (ii) in Proposition 7.1.*

∂_2, then $\tilde{\mathcal{H}}(U_L)$ intersects the edge ∂_3 at two points. When S is tangent at a point P_0 to the graph of $F_{ext}^{\partial_2 \partial_3}$ (the case of the solid curve in Fig. 7.3), for $U_L \in \partial_2$ with $U_L \neq U_0$, $\tilde{\mathcal{H}}(U_L)$ intersects the edge ∂_3 at two points while $\tilde{\mathcal{H}}(U_0)$ intersects the edge ∂_3 only at the point U^*.

(ii) *Assume that S intersects at two points P_1 and P_2 the graph of $F_{ext}^{\partial_2 \partial_3}$ for negative values of u (dotted curve in Fig. 7.3). Let us denote by U_1 and U_2 the states on ∂_2 corresponding to P_1 and P_2 respectively. For $U_L \in \big(V_3, U_1\big)$ or $U_L \in \big(U_2, V_1\big)$ we have that $\tilde{\mathcal{H}}(U_L)$ intersects the edge ∂_3 at two points different from U^*. If $U_L = U_1$ or $U_L = U_2$ we have that $\tilde{\mathcal{H}}(U_L)$ intersects the edge ∂_3 only at the point U^*. If $U_L \in \big(U_1, U_2\big)$ there are no intersection points between $\tilde{\mathcal{H}}(U_L)$ and the edge ∂_3.*

Proof. We only prove item (ii) since item (i) is trivial using the same argument. In Fig. 7.4 we draw only the dotted flux of Fig. 7.3. The proof is a consequence of the geometrical construction and the Triple Shock Rule. The fan of light segments in Fig. 7.4 represent the possible lines that cross the state V_1 intersecting the graph of $F_{ext}^{\partial_2 \partial_3}$ at two points for positive values of u. Consider a state $U_L = (u_1^L, 0, 1 - u_1^L)$ on the edge ∂_2 such that $P_L = F_1^{\partial_2}(u_1^L)$ lies inside the fan. Denote by S_L the segment of the fan that crosses the point P_L, denote by U_1^* and U_2^* the states on ∂_3 corresponding to the intersection points of the straight line S_L with $F_{ext}^{\partial_2 \partial_3}$ for positive values of u. From Lemma 7.1 (see the geometric construction) we have $U_1^*, U_2^* \in \mathcal{H}(U_L)$ and $\sigma(U_L, U_1^*) = \sigma(U_L, U_2^*) = m = \sigma(U_L, V_1) = \sigma(V_1, U_1^*) = \sigma(V_1, U_2^*)$, where m is the slope of the segment S_L and σ denotes the shock speed. If $U_L = U_1$ or $U_L = U_2$ the points U_1^* and U_2^* collapse into U^*. If $U_L \in (U_1, U_2)$ then P_L lies out of the fan and therefore there does not exist a state in ∂_3 belonging to $\mathcal{H}(U_L)$. $\square$

Proposition 7.2. *Consider U_L such that $\tilde{\mathcal{H}}(U_L)$ intersects the edge ∂_3 at two points U_1^* and U_2^* (see Fig. 7.5), then we have $\lambda^-(U_1^*) < \sigma(U_L, U_1^*) = \sigma(U_L, V_1) = \sigma(U_L, U_2^*) < \lambda^-(U_2^*)$*

Proof. First remember that for $U = (1 - u_2, u_2, 0)$ in the interval (V_1, Q_3) we have $\lambda^-(U) = (dF_2^{\partial_3}/du_2)(u_2)$, $\lambda^+(U) = 0$ while in the interval (Q_3, V_2) we have $\lambda^+(U) = (dF_2^{\partial_3}/du_2)(u_2)$, $\lambda^-(U) = 0$ (here Q_3 is the local minimizing point of the flux $F_2^{\partial_3}$ on the edge ∂_3). The proof is a consequence of Lemma 7.1 (see the wedge construction) and of the fact that the states U_1^* and U_2^* lie in opposite sides with respect to U^*, see Fig. 7.5.   □

Remark 7.6. *Given the states U_L and $U^* \in \mathcal{H}(U_L)$ in different edges of the wedge, it is possible to compare the characteristic speeds in both U_L and U^* with the shock speed and determine all the information about the Lax admissibility of the shock joining these states. This is an important advantage of the wedge construction.*
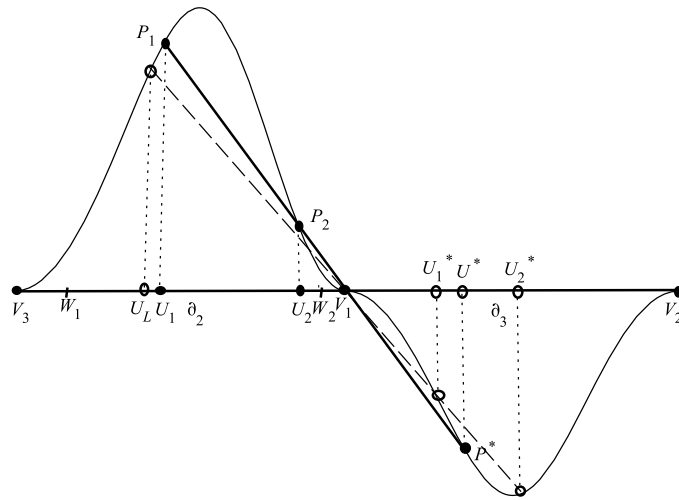
Figure 7.5: *Extended flux function $F_{ext}^{\partial_2 \partial_3}$ for the case $\mu_1 = 1, \mu_2 = 1, \mu_3 = 0.5$ and $\rho_2 = \rho_3$. The black line is tangent to the extended flux graph in P^*. Notice that the states U_1^* and U_2^* lie in opposite sides relative to U^*. The state U_2^* does not coincide necessarily with the local minimum of the flux $F_{ext}^{\partial_2 \partial_3}$.*

Remark 7.7. *An important fact about the wedge construction is that it can be extended to other two-phase regimes besides the edges of the saturation triangle, for example: in the simplified problem $\rho_1 = \rho_2$ we can construct the wedge using the vertex V_3, the two-phase regimes ∂_1 (or ∂_2) and the critical line R_3.*

Now we will describe the shape of the Hugoniot loci for points on the edges. We know that each edge ∂_i, $i = 1, 2, 3$ of the saturation triangle represents a two-phase regime where the phase i is absent and the other two fluids coexist. In this sense we say that associated to each edge of the saturation triangle there are two fluids. We will split the exposition in several cases.

7.2   The two fluids on the edge have equal densities

We will analyse the case in which the phases 1 and 3 that are coexisting in the edge ∂_2 of the saturation triangle have equal densities. So we assume that $\rho_1 = \rho_3 \neq \rho_2$, and let us use the notation $\rho = \rho_{21} = \rho_{23}$. For this case, we see that all the remaining terms in (7.7) contain u_2 as a common factor, so we can divide by $u_2 \neq 0$ and rewrite equation (7.7) in a convenient way

$$\left[(u_1 - u_1^L)(u_1^2/\mu_1 + u_3^2/\mu_3) + u_1^2 u_2/\mu_1\right]\rho\Lambda_L/\mu_2 = 0. \qquad (7.12)$$

The easiest way to obtain Eq. (7.12) is directly in (7.3)-(7.4). If we set $u_1 = 0$ into Eq. (7.12) we obtain that necessarily u_3 must be equal to zero, so the unique intersection point of $\tilde{\mathcal{H}}(U_L)$ with the edge ∂_1 is the vertex V_2. In a similar way, setting $u_3 = 0$ into Eq. (7.12) we obtain V_2 as the unique intersection point of $\tilde{\mathcal{H}}(U_L)$ with the edge ∂_3.

In order to obtain the intersection points of $\tilde{\mathcal{H}}(U_L)$ with the straight line segment R_2 (see (2.29)), we set $u_1/\mu_1 = u_3/\mu_3$ into Eq. (7.12), obtaining

$$u_3/\mu_3[(u_1 - u_1^L)(1 - u_2) + u_1 u_2] = 0. \qquad (7.13)$$

Using again the definition of R_2 and remembering that $\sum u_i = 1$, we perform some calculations starting with Eq. (7.13) to obtain

$$(1 - u_2)^2[1 - u_1^L(1 + \mu_3/\mu_1)] = 0. \qquad (7.14)$$

Equation (7.14) shows that an arbitrary state U on R_2 with $U \neq V_2$, belongs to $\tilde{\mathcal{H}}(U_L)$ if and only if $U_L = B_2$ (see definition of B_2 in (2.30)), so we have $\tilde{\mathcal{H}}(B_2) = R_2$ and $\tilde{\mathcal{H}}(U_L) \cap R_2 = V_2$ for $U_L \neq B_2$. The fact $\tilde{\mathcal{H}}(B_2) = R_2$ was expected because the flow has two-phase behavior along R_2 (see Theorem 5.1). The following proposition summarizes the results above.

Proposition 7.3. *Consider the simplified pure gravitational problem ($\alpha = 0$ and $\rho_1 = \rho_3 \neq \rho_2$). Assume $U_L \in \partial_2$ with $U_L \notin \{V_1, V_3, B_2\}$. Then (see the Fig. 7.6):*

(i) $\mathcal{H}(V_1) = \partial_2 \cup \partial_3$, $\mathcal{H}(V_3) = \partial_1 \cup \partial_2$, $\mathcal{H}(B_2) = \partial_2 \cup R_2$.

(ii) $\mathcal{H}(U_L) = \tilde{\mathcal{H}}(U_L) \cup \partial_2$ where $\tilde{\mathcal{H}}(U_L) \cap \partial_1 = \tilde{\mathcal{H}}(U_L) \cap \partial_3 = \tilde{\mathcal{H}}(U_L) \cap R_2 = V_2$.

Remark 7.8. *Notice that all the calculations of this section would be avoided if we use the geometrical wedge construction of Section 7.1. Indeed this tool makes Proposition 7.3 trivial (see Fig. 7.7) since the two-phase flux function restricted to the edge ∂_2 is identically zero and the two-phase flux functions in ∂_1, ∂_3 and R_2 are as in Fig. 5.1.*
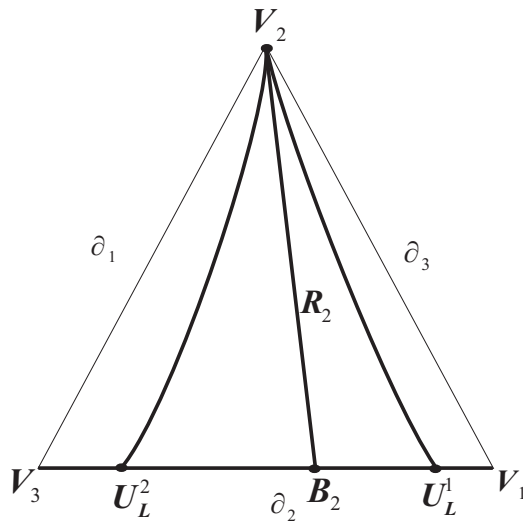
Figure 7.6: *Hugoniot locus for three different states $U_L = U_L^1$, $U_L = U_L^2$ and B_2 on the edge ∂_2 for the simplified pure gravitational problem $\alpha = 0$, $\rho_1 = \rho_3 \neq \rho_2$, see Prop. 7.3. The edge ∂_2 is a common branch for the loci of all states. We do not show the Lax admissibility of the states in the loci because it depends on the sign of $\rho = \rho_{21} = \rho_{23}$.*
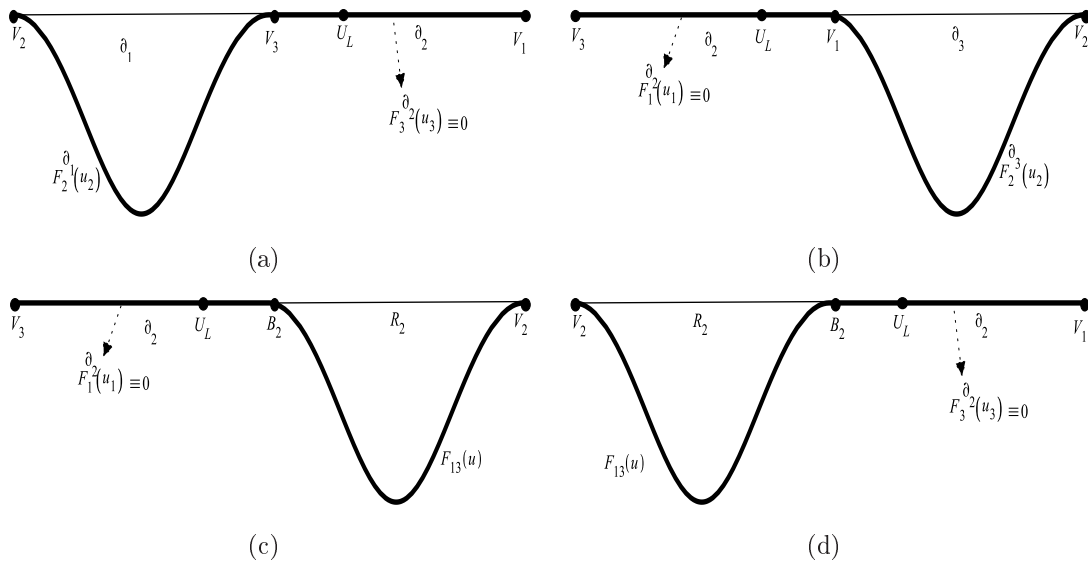
Figure 7.7: Illustration of extended flux functions for the simplified pure gravitational problem $\rho_1 = \rho_3 > \rho_2$ connecting the following two-phase regimes: (a) ∂_2 and ∂_1, (b) ∂_2 and ∂_3, (c) interval (V_3, B_2) and R_2, (d) interval (V_1, B_2) and R_2. The function F_{13} denotes the two-phase "flux" function along R_2 analogous to the one defined in Eq. (5.10). The figures show that for an arbitrary U_L in ∂_2 the intersections of $\tilde{\mathcal{H}}(U_L)$ with ∂_1, ∂_3 or R_2 is precisely the vertex V_2. See Remark 7.8.

7.3   The fluids in the edge have different densities, the third fluid is lighter

We analyze the case in which the phases 1 and 3 that coexist on the edge ∂_2 of the saturation triangle have distinct densities; without loss of generality we assume $\rho_1 > \rho_3$.

There are three cases $\rho_1 > \rho_3 \geq \rho_2$, $\rho_2 \geq \rho_1 > \rho_3$ and $\rho_1 > \rho_2 > \rho_3$. In this section we consider the case $\rho_1 > \rho_3 \geq \rho_2$; the remaining cases will be the subject of another section.

In order to understand the shape of the Hugoniot locus for an arbitrary state U_L on ∂_2 the first step is to analyze the intersections of $\tilde{\mathcal{H}}(U_L)$ with all the edges of the saturation triangle.

First we will show that for U_L on ∂_2 the curve $\tilde{\mathcal{H}}(U_L)$ given by (7.7) does not intersect the edge ∂_1 at any point. This fact is easily obtained by setting $u_1 = 0$ in (7.7) and by regrouping conveniently to obtain

$$\frac{(u_1^L)u_2 u_3^2}{\mu_2 \mu_3} \Lambda(U_L)\rho_{23} - \frac{(u_1^L)^2(1 - u_1^L)^2}{\mu_1 \mu_3} \Lambda(U)\rho_{13} = 0. \tag{7.15}$$

As $U_L \neq V_1, U_L \neq V_3$ and $\rho_1 > \rho_3 \geq \rho_2$ the first term in Eq. (7.15) is non-positive and the second one is negative, concluding that $\tilde{\mathcal{H}}(U_L)$ does not intersect ∂_1. This conclusion also can be obtained using the wedge construction described in Section 7.1.

Now we analyze the intersections of the curve $\tilde{\mathcal{H}}(U_L)$ with the edge ∂_2. Setting $u_2 = 0$ into Eq. (7.7) and performing some calculations we obtain

$$(u_1 - u_1^L)P(u_1) = 0, \tag{7.16}$$

where

$$P(u_1) = \left[-(u_1^L)^2/\mu_1 + (1 - u_1^L)^2/\mu_2 \right] u_1^3 + (2 - u_1^L)\left[(u_1^L)^2/\mu_1 - (1 - u_1^L)^2/\mu_2 \right] u_1^2 +$$
$$+ \left[(1 - 2u_1^L)(1 - u_1^L)^2/\mu_2 \right] u_1 + u_1^L(1 - u_1^L)^2/\mu_2 \tag{7.17}$$

is a cubic polynomial in u_1 for each U_L fixed. Tedious calculations show that

$$P(u_1^L) = 2(u_1^L)^3(1 - u_1^L)/\mu_1,$$

so u_1^L is not a root of the polynomial P (we are assuming that $U_L \neq V_1$ and $U_L \neq V_3$).

On the other hand, we have strong numerical evidence showing that polynomial (7.17) has one real root in the interval (0,1) so there exists $U_L' \in \tilde{\mathcal{H}}(U_L) \cap \partial_2$ such that $U_L' \neq U_L$. The state U_L' is a point of self-intersection of the Hugoniot locus of U_L, which means that each $U_L \in \partial_2$ is a secondary bifurcation point for one of the families. The fact that all states on the edges belong to the bifurcation manifold for one of the families will be proved rigorously in Theorem 8.2.

Now we analyze the intersection points of $\tilde{\mathcal{H}}(U_L)$ with the edge ∂_3. Setting $u_3 = 0$ into Eq. (7.7) we have that the intersection points of $\tilde{\mathcal{H}}(U_L)$ with the edge ∂_3 are the roots in

the interval $(0,1)$ of the cubic polynomial $P_{U_L}(u_1)$ in u_1:

$$
\begin{aligned}
P_{U_L}(u_1) = & \left[\Lambda(U_L)(1 - u_1^L) \right] u_1^3 - \left[\frac{(1 - u_1^L)}{\mu_1 \mu_2} \Lambda(U_L) + \right. \\
& + \left. \left(1/\mu_1 + 1/\mu_2 \right) \frac{(u_1^L)^2 (1 - u_1^L)^2 (\rho_{13}/\rho_{21})}{\mu_1 \mu_3} \right] u_1^2 + \\
& + 2 \left[\frac{(u_1^L)^2 (1 - u_1^L)^2 (\rho_{13}/\rho_{21})}{\mu_1 \mu_2 \mu_3} \right] u_1 - \frac{(u_1^L)^2 (1 - u_1^L)^2 (\rho_{13}/\rho_{21})}{\mu_1 \mu_2 \mu_3}.
\end{aligned}
\tag{7.18}
$$

As $\rho_{13} > 0$ and $\rho_{21} < 0$, notice that

$$
\lim_{u_1 \to -\infty} P_{U_L}(u_1) = -\infty, \quad P_{U_L}(0) > 0, \quad P_{U_L}(1) > 0.
\tag{7.19}
$$

We conclude that independently of the state U_L there exists at least one negative root for the polynomial P_{U_L}, therefore the possibilities for P_{U_L} to have real roots at interval $(0,1)$ are the following: two different roots, one double root or no real roots. We avoid the analysis of the discriminant Δ_L for the cubic polynomial P_{U_L} by using the simpler geometric analysis presented in the Section 7.1. This construction provides all the information about the intersections of $\mathcal{H}(U_L)$ with the edge ∂_3. Notice that we illustrated the method in Section 7.1 exactly for the case $\rho_1 > \rho_3 \geq \rho_2$ studied in this section, so the number of intersection points (zero, one or two) of the segment S_L in Fig. 7.4 with the extended flux function for positive values of u determines the sign of the discriminant Δ_L of the polynomial P_{U_L} in Eq. (7.18) ($\Delta_L < 0$, $\Delta_L = 0$ or $\Delta_L > 0$ respectively).

In order to study the shape of the Hugoniot locus for an arbitrary $U_L \in \partial_2$, besides the intersections with the boundary, which we already analyzed, it is necessary to know the secondary bifurcation points along ∂_2, which influence the interior of the saturation triangle. We have numerical evidence showing the existence of two states W_1 and W_2 on the edge ∂_2 for which the Hugoniot locus has a self-intersection point inside the saturation triangle. These points W_1 and W_2 belong to the secondary bifurcation manifold of the fast family.

As we mentioned in the geometrical construction in Section 7.1, there are three different possibilities for the relative position of the extended flux function with respect to the segment S (see Fig. 7.3). Proposition 7.1 explains some differences between the three cases with regard to intersections with the edge ∂_3 of the Hugoniot locus of $U_L \in \partial_2$. Nevertheless if the parameters μ_1, μ_2, μ_3 and ρ_{13}, ρ_{21} for the tree cases are not too different, when we move the state U_L along the edge ∂_2 from V_3 to V_1, the Hugoniot locus of U_L describes qualitatively a similar behavior for all the three cases, with the only difference that for one of the cases (dotted curve in Fig. 7.3) a branch of the locus eventually gets out of the saturation triangle, while for the other two cases (dashed and solid curves in Fig. 7.3) a portion or a point of the above mentioned branch stays in the saturation triangle.

As an illustration, we show in Fig. 7.8 the sequence of Hugoniot loci $\mathcal{H}(U_L)$ when we let the state U_L move along the edge ∂_2 from the vertex V_3 to the vertex V_1, for the case

(a)

(b)

(c)

(d)

(e)

(f)

(g)   (h)
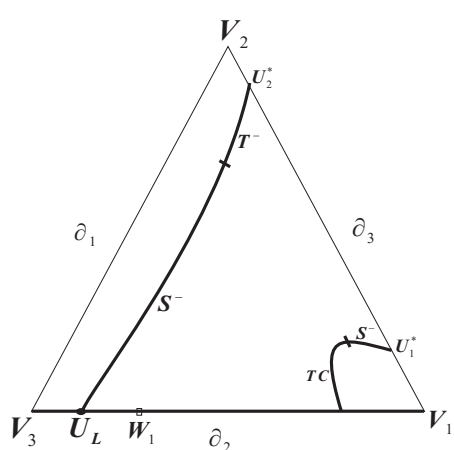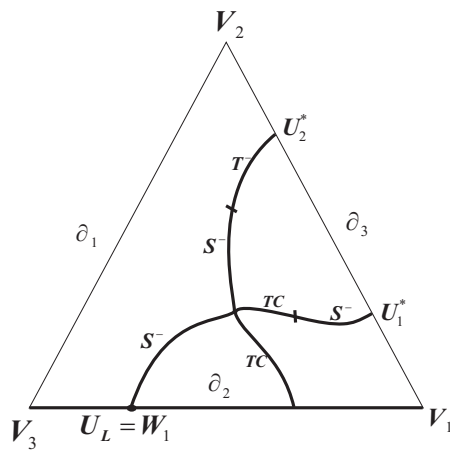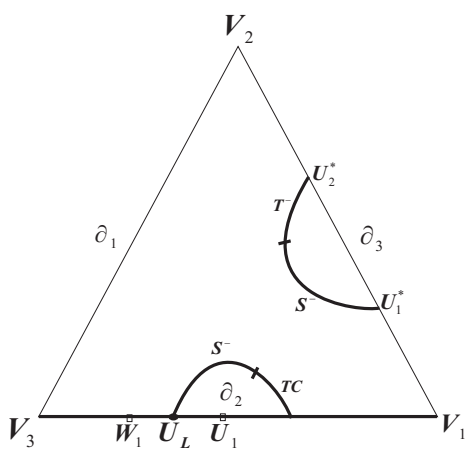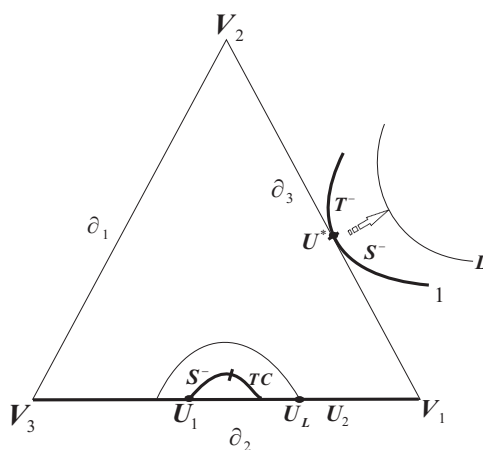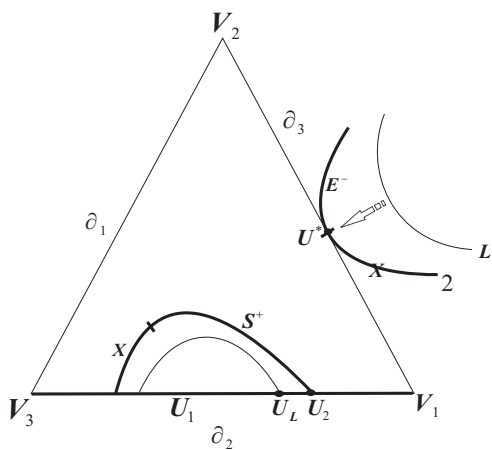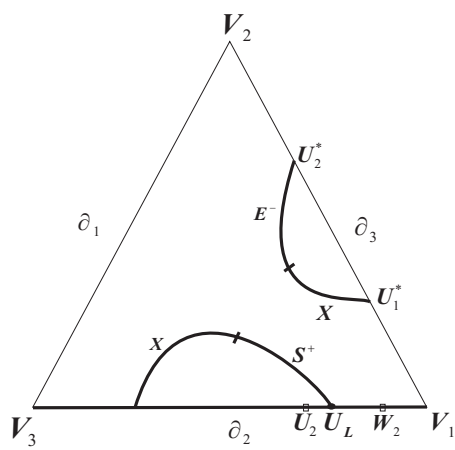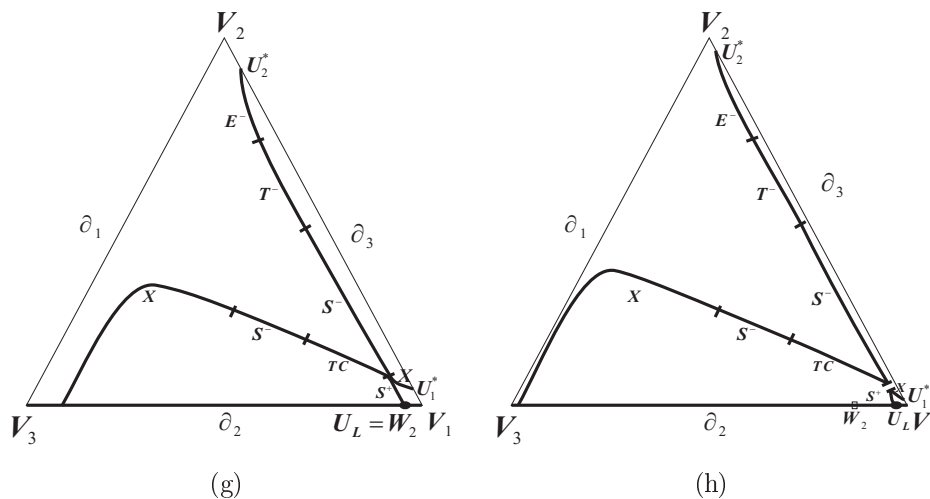
Figure 7.8: Hugoniot locus of $U_L \in \partial_2$ for the case $\rho_1 > \rho_3 = \rho_2$, with parameters μ_2, μ_3, ρ_{13}, ρ_{21} such that $F_{ext}^{\partial_2 \partial_3}$ behaves like the dotted curve of Fig. 7.3 (two intersection points with the segment S). Figures (a)-(h) show the sequence of $\mathcal{H}(U_L)$ when U_L moves from V_3 to V_1. We used the same notation for the relevant points in this figure and in Fig. 7.5. In figures (b) and (g) the state U_L coincides with the secondary bifurcation points W_1 and W_2. Figures (d) and (e) show the Hugoniot locus for the states U_1, U_2 defined in Fig. 7.5 and for an intermediate state U_L; the arrows describe the motion of the non-local branch when U_L moves from U_1 to U_2. In all the figures we show the Lax admissibility for the Hugoniot curves. Only the parts denoted by S^- and S^+ represent admissible (slow and fast) Lax shocks. The other symbols represent inadmissible shocks.

where the extended flux function is like the dotted curve of Fig. 7.3. We denote by U_1 and U_2 the states on ∂_2 corresponding to the points P_1 and P_2 respectively, see Fig. 7.5. The states W_1 and W_2 on ∂_2 belong to the secondary bifurcation manifold of the fast family; their relative positions with respect to the states U_1 and U_2 are shown in Fig. 7.5. All the figures can be obtained by plotting the curve in (7.7). Only the parts of the loci denoted by S^- and S^+ represent admissible Lax shocks. The other symbols represent inadmissible shocks. In Fig. 7.8 we did not illustrate all the intermediate steps of sequence of Hugoniot loci mentioned above; therefore, new segments of shocks sometimes appear or disappear when comparing consecutive figures.

Remark 7.9. *In Fig. 7.8 we took $\rho_2 = \rho_3$; this is irrelevant because for $\rho_1 > \rho_3 > \rho_2$ we obtain qualitatively the same sequence of Hugoniot locus shapes (with a few differences in the admissibility for the locus branches that will not affect the Riemann solution). The other difference occurs in the limit when $U_L \to V_1$, see the results of Prop. 6.1 and Prop. 6.3.*

Remark 7.10. *Consider the case in which the extended flux $F_{ext}^{\partial_2 \partial_3}$ is like the solid curve of Fig. 7.3, so that the states U_1 and U_2 collapse into the state U_0 (see Fig. 7.3). In such a case the pair of points U_0 and U^* belong to the double contact manifold of the slow family (see Def. 3.7). All the Hugoniot loci shown in the figures 7.8(d) and 7.8(e) collapse into*

a single locus.

Remark 7.11. *If the extended flux $F_{ext}^{\partial_2 \partial_3}$ is like the dashed curve of Fig. 7.3 we will have qualitatively the same behavior for $\mathcal{H}(U_L)$ except that the non-local branches always keeping a portion inside the saturation triangle. The sequence of Hugoniot loci for this case would be Figs. 7.8(a), 7.8(b), 7.8(c), 7.8(f), 7.8(g) and 7.8(h) (skipping figures 7.8(d) and 7.8(e)).*

7.4   Remaining cases

Case $\rho_2 \geq \rho_1 > \rho_3$.

This case is completely analogous to the one of the previous section where $\rho_1 > \rho_3 \geq \rho_2$. In the particular case in which $\rho_2 = \rho_1 > \rho_3$ the sequence of Hugoniot loci is the same as that shown in Fig. 7.8 provided we interchange the indices 3 and 1 everywhere. However there will be a change in the admissibility of the Hugoniot curves because of the symmetry between the simplified pure gravitational problems $\rho_2 = \rho_1 > \rho_3$ and $\rho_2 = \rho_3 < \rho_1$, (see Theorem 8.1 for details). Because of this change of admissibility, the Rieman solutions with data $U_L \in \partial_2$, $U_R = V_2$ for the two cases will be drastically different.

As in the case studied in Section 7.3, where we found W_1, W_2 (see Figs. 7.8(b) and 7.8(g)), here we have numerical evidence of the existence of two states on the edge ∂_2 (denoted by W_3 and W_4) that belong to the secondary bifurcation manifold; now they correspond to the slow family. An explanation for this change of family in the bifurcation states can be obtained from Theorem 8.1 for small density differences, considering $\rho_2 \geq \rho_1 > \rho_3$ as a perturbation of the simplified pure gravitational problem $\rho_2 = \rho_1 > \rho_3$.

Case $\rho_1 > \rho_2 > \rho_3$.

In this case when $U_L \in \partial_2$ the non-trivial branch $\tilde{\mathcal{H}}(U_L)$ (see Def. 7.1) could intersect the edge ∂_1 or ∂_3. In order to understand this phenomenon we will consider a super-extended flux function connecting the three edges ∂_i, $i = 1, 2, 3$, see Fig. 7.9. This super-extended flux coincides with $F_1^{\partial_2}$ on ∂_2, with $F_2^{\partial_3}$ on ∂_3 and with $F_3^{\partial_1}$ on the edge ∂_1. The construction procedure is analogous to the extended flux $F_{ext}^{\partial_2 \partial_3}$ in Eq. (7.10), so we will not give more details.

There exist some relevant states on ∂_2 where the number of intersection points of the Hugoniot locus with the edges ∂_1 and ∂_3 changes. These relevant states are denoted by U_1, U_2, U_3, U_4 in Fig. 7.9. These four states exist if each of the segments denoted by S_1 and S_2 intersect the super-extended flux in two points corresponding to the edge ∂_2. In order to simplify the exposition, we will assume that the relative position between these four states is preserved. For the case illustrated by the dashed curve in Fig. 7.9 the situation would be qualitatively different since the segment S_1 does not intersect the dashed graph.

In Fig. 7.10, we see that for arbitrary states $A \in (V_3, U_4)$ and $E \in (U_2, V_1)$ the

Figure 7.9: *Dark curve: super-extended flux for* $\mu_1 = \mu_2 = \mu_3 = 1$, $\rho_{13} = 1, \rho_{12} = 0.5$, *dashed curve: super-extended flux for* $\mu_1 = \mu_2 = 1$, $\mu_3 = 3$, $\rho_{13} = 1, \rho_{12} = 0.5$. *The states* U_1, U_2, U_3 *and* U_4 *correspond to the intersection points of the super-extended flux with the segments* S_1 *and* S_2.

Figure 7.10: *Super-extended flux for* $\mu_1 = \mu_2 = \mu_3 = 1$, $\rho_{13} = 1, \rho_{12} = 0.5$, *The states* U_1, U_2, U_3 *and* U_4 *correspond to the intersection points of the super-extended flux with the segments* S_1 *and* S_2.

corresponding Hugoniot loci intersect each edge ∂_1 and ∂_3 at two points. For state B in (U_4, U_1) the Hugoniot locus intersects the edge ∂_3 at two points but it does not intersect the edge ∂_1. For an arbitrary state $C \in (U_1, U_3)$ the Hugoniot locus does not intersect any of the edges ∂_1 or ∂_3. For the state $D \in (U_3, U_2)$ the Hugoniot locus intersects the edge ∂_1 at two points but it does not intersect ∂_3. So the states U_1, U_2, U_3, U_4 subdivide the edge ∂_2 into smaller intervals where the number of intersection points of $\tilde{\mathcal{H}}(U_L)$ for U_L in ∂_2 with the other two edges is fixed.

For small density differences we can regard the case $\rho_1 > \rho_2 > \rho_3$ as a perturbation of both simplified pure gravitational problems $\rho_1 = \rho_2 > \rho_3$ and $\rho_1 > \rho_2 = \rho_3$. The presence of features of both simplified problems in the case $\rho_1 > \rho_2 > \rho_3$ is natural. The numerical evidence for this case shows existence of four secondary bifurcation states on ∂_2. Two of them, denoted by W_1, W_2, are associated to the fast family while the other two, W_3, W_4, are associated to the slow family, see for example Fig. 7.11.

(a)

(b)

(c)

(d)

(e)

(f)

Figure 7.11: Hugoniot locus of $U_L \in \partial_2$ for the case $\rho_1 > \rho_2 > \rho_3$, with parameters μ_2, μ_3, ρ_{13}, ρ_{21} such that the super-extended flux function behaves like the solid curve of Fig. 7.9 (two intersection points with each of segments S_1 and S_2). Figures (a)-(j) show the sequence of $\mathcal{H}(U_L)$ when U_L moves from V_3 to V_1. We used the same notation for the relevant points as in Fig. 7.9. In figures (b), (d), (h) and (i) the state U_L coincides with secondary bifurcation states. The Hugoniot loci for the points U_i, $i = 1, 2, 3, 4$ (defined in Fig. 7.9) are shown in figures (d), (f) and (g). In the figure (g) the dark curves is the Hugoniot locus for $U_L = U_2$ and the dashed curve is the Hugoniot-locus for $U_L = U_3$. In the figures (f) and (g) the arrows describe the motion of the non-local branch when U_L moves from U_1 to U_2. In all the figures we show the Lax admissibility for the Hugoniot curves. Only the branches denoted by S^- and S^+ represent admissible (slow and fast) Lax shocks. The other symbols represent inadmissible shocks.

We illustrate the behavior of $\mathcal{H}(U_L)$ when we let the state U_L move along the edge ∂_2 from V_3 to V_1 for a case where the super-extended flux function is like the solid curve in Fig. 7.9. The sequence of the Hugoniot loci and the admissibility of the curves is shown in the Fig. 7.11; we did not illustrate all the intermediate steps of sequence of Hugoniot loci mentioned above; therefore, new segments of shocks sometimes appear or disappear when comparing consecutive figures. All the figures can be obtained by plotting the curve in (7.7).

Chapter 8

Symmetry and bifurcations in the simplified pure gravitational problem

In this chapter we prove a "reversal symmetry" theorem, which holds for the simplified pure gravitational problem (SPGP). We also prove additional theoretical results for bifurcation manifolds in SPGP. These results will be used to provide support for the Riemann solution obtained via numerical calculations that implement the wave curve method.

8.1   Symmetry in the SPGP

Our goal is to solve the Riemann problem for the "simplified pure gravitational problem" (*i.e.*, $\alpha = 0$, $\rho_1 = \rho_2 \neq \rho_3$). Denoting by $\rho = \rho_{13} = \rho_{23}$ we will analyze separately the cases $\rho > 0$ and $\rho < 0$ since their solutions are drastically different. However the two cases have similarities: *e.g.*, in both cases the vertex V_3 is an umbilic point (see Theorem (4.1)), and there exist two quasi-umbilic points $Q_1 \in \partial_1, Q_2 \in \partial_2$; also the entire edge ∂_3 is a diagonalization line. The Hugoniot locus of the vertices does not depend on the sign of ρ. From Propositions 6.1 and 6.3 we have:

$$\mathcal{H}(V_3) = \partial_1 \cup \partial_2 \cup \partial_3 \cup R_3, \tag{8.1}$$

$$\mathcal{H}(V_1) = \partial_2 \cup \partial_3, \tag{8.2}$$

$$\mathcal{H}(V_2) = \partial_1 \cup \partial_3. \tag{8.3}$$

Next we present a crucial result establishing a connection for characteristic speeds and integral curves between the cases $\rho > 0$ and $\rho < 0$.

Theorem 8.1. *(Reversal symmetry.) Assume $\alpha = 0$, $\rho_1 = \rho_2 \neq \rho_3$ and denote $\rho = \rho_{13} = \rho_{23}$. If $\rho > 0$ we define $\rho_p = \rho$ and $\rho_n = -\rho_p$. If $\rho < 0$ we define $\rho_p = -\rho$ and $\rho_n = -\rho_p$. We consider characteristic eigenvalues and eigenvectors for the two problems*

corresponding to the densities ρ_p and ρ_n. Then we have the following relations

$$\lambda_n^- = -\lambda_p^+, \quad r_n^- = r_p^+, \tag{8.4}$$

$$\lambda_n^+ = -\lambda_p^-, \quad r_n^+ = r_p^-, \tag{8.5}$$

where $\lambda_p^+, r_p^+, \lambda_p^-, r_p^-$ denote the characteristic speeds and the associated right eigenvectors corresponding to the problem with positive parameter ρ_p while $\lambda_n^+, r_n^+, \lambda_n^-, r_n^-$ denote the characteristic speeds and the associated right eigenvectors corresponding to the problem with negative parameter $\rho_n = -\rho_p$.

Proof. Let us define $\tilde{J}_{ij} = J_{ij}/\rho$; we obtain from (4.8) that

$$\lambda^{\pm} = \frac{\rho(\tilde{J}_{11} + \tilde{J}_{22}) \pm |\rho|\sqrt{\tilde{D}}}{2}, \tag{8.6}$$

where $\tilde{D} = \left(\tilde{J}_{11} + \tilde{J}_{22}\right)^2 - 4\left(\tilde{J}_{11}\tilde{J}_{22} - \tilde{J}_{12}\tilde{J}_{21}\right)$. For $\rho = \rho_n = -\rho_p$ we have

$$\lambda_n^{\pm} = \frac{\rho_n(\tilde{J}_{11} + \tilde{J}_{22}) \pm |\rho_n|\sqrt{\tilde{D}}}{2} = -\frac{\rho_p(\tilde{J}_{11} + \tilde{J}_{22}) \mp |\rho_p|\sqrt{\tilde{D}}}{2} = -\lambda_p^{\mp}, \tag{8.7}$$

concluding the proof of (8.4)-(a) and (8.5)-(a).
We will denote by J_p (respectively J_n) the Jacobian matrix for $\rho = \rho_p$ (respectively $\rho = \rho_n$).
Using the notation above and the properties (8.4)-(a), (8.5)-(a), we have that

$$\begin{aligned}
0 &= (J_n - \lambda_n^{\pm}I)r_n^{\pm} = (\rho_n\tilde{J} - \lambda_n^{\pm}I)r_n^{\pm} = (-\rho_p\tilde{J} + \lambda_p^{\mp}I)r_n^{\pm} \\
&= -(\rho_p\tilde{J} - \lambda_p^{\mp}I)r_n^{\pm} = (J_p - \lambda_p^{\mp}I)r_n^{\pm}
\end{aligned} \tag{8.8}$$

therefore we have proved that $r_n^{\pm}$ is a right eigenvector associated to the eigenvalue $\lambda_p^{\mp}$ concluding the proof of (8.4)-(b) and (8.5)-(b). $\qquad\square$

Remark 8.1. *Conclusions analogous to those in Theorem 8.1 can be stated for the Hugoniot loci as well, under reversal symetry in the SPGP: the shock speeds change sign; this change can be verified from the R-H condition (3.6) because the flux functions change sign under the symmetry. Therefore as a consequence, we have that the integral curves, shock curves and all bifurcation manifolds defined in Chapter 3 (inflection, secondary bifurcation, boundary contact, double contact, etc.) are still identical but have opposite family when we pass from the case $\rho > 0$ to the case $\rho < 0$.*

8.2   Bifurcation manifolds

Next we present some theoretical results describing interesting properties of some bifurcation manifolds.

First we state two lemmas that will be used in this section. Lemma 8.1 is a classical result and its proof can be found in Smoller [47]. The proof of Lemma 8.2 can be found in Appendix B.

Lemma 8.1. *Let A be a 2×2 square diagonalizable matrix. Assume that the eigenvalues of A are distinct $(\lambda_1 \neq \lambda_2)$. Let X_R be a matrix formed by the columns of the right eigenvectors of A and X_L be a matrix formed by the rows of the left eigenvectors of A. Then $C \equiv X_L X_R$ is a diagonal matrix.*

Lemma 8.2. *Consider the "pure gravitational problem" $(\alpha = 0)$ with $\rho_1 = \rho_2 \neq \rho_3$ and $\mu_1 = \mu_2$ and let us denote $\rho \equiv \rho_{13} = \rho_{23}$, $\mu \equiv \mu_1 = \mu_2$. Then the characteristics speeds given by (4.8) are symmetric with respect to the variables u_1 and u_2 (i.e., $\lambda^-(u_1, u_2) = \lambda^-(u_2, u_1)$ and the same for λ^+).*

Proposition 8.1. *For the " simplified pure gravitational problem" $(\alpha = 0$, $\rho_1 = \rho_2 \neq \rho_3)$ with $\mu_1 = \mu_2$, we have $R_3 \subset Inf_+ \cap Bif_+$ if $\rho > 0$, and $R_3 \subset Inf_- \cap Bif_-$ if $\rho < 0$ (R_3 was defined in (2.29)). In other words the segment R_3 belongs to the inflection and bifurcation manifolds corresponding to the fast or slow family for each case $\rho > 0$ or $\rho < 0$, respectively.*

Proof. We will present the proof for the case $\rho > 0$. Then the case $\rho < 0$ will be a direct consequence of Theorem 8.1 (see Remark 8.1). Under the hypotheses for the theorem, we have that at each point of R_3 the vector $(r_1^-, r_2^-)^T = (1, 1)^T$ is a right eigenvector associated to the slow family (see proof of Theorem 5.1).

Consider the matrices $X_R = \begin{pmatrix} 1 & r_1^+ \\ 1 & r_2^+ \end{pmatrix}$ and $X_L = \begin{pmatrix} l_1^- & l_2^- \\ l_1^+ & l_2^+ \end{pmatrix}$, where $l^- = (l_1^-, l_2^-)$ is a left eigenvector associated to the slow family and $r^+ = (r_1^+, r_2^+)^T$, $l^+ = (l_1^+, l_2^+)$ are right and left eigenvectors associated to the fast family, respectively. Applying Lemma 8.1 we obtain that

$$X_L X_R = \begin{pmatrix} l_1^- + l_2^- & l_1^- r_1^+ + l_2^- r_2^+ \\ l_1^+ + l_2^+ & l_1^+ r_1^+ + l_2^+ r_2^+ \end{pmatrix} \tag{8.9}$$

is a diagonal matrix and therefore

$$\begin{cases} l_1^+ + l_2^+ = 0 \\ l_1^- r_1^+ + l_2^- r_2^+ = 0. \end{cases} \tag{8.10}$$

From the first equation of the above system we obtain that for all U in R_3, $l_1^+(U) = -l_2^+(U)$ so that $l^+(U) \propto (1, -1)$. In other words, along the segment R_3 the left eigenvector associated to the fast family is orthogonal to the segment direction. On the other hand, for all U, U' in R_3 we have $(U' - U) = \propto (1, 1)^T$ so we have

$$l^+(U)(U' - U) = 0 \quad \forall U, U' \in R_3 \tag{8.11}$$

On the other hand, after some calculation we obtain the following expression for the fast-characteristic speed along the critical line R_3:

$$\lambda^+(U) = \frac{(1 - u_3)u_3^2}{\mu\mu_3\Lambda(U)} \quad \forall U \in R_3. \tag{8.12}$$

From (8.12) and utilizing the Rankine-Hugoniot relation for shocks joining two states on the critical line R_3, is possible to show that

$$\forall U \in R_3, \exists U' \in R_3 \text{ such that } \lambda^+(U') = \sigma(U, U'). \tag{8.13}$$

Equations (8.11) and (8.13) yield $R_3 \subset Bif_+$, see Definition 3.4.

In order to show that $R_3 \subset Inf_+$, we first note that $J_{12}(U) = J_{21}(U) \ \forall U \in R_3$ (see (4.4)-(4.7)), *i.e.*, dF restricted to segment R_3 is a symmetric matrix, therefore left and right eigenvectors "coincide", so we have $r^+(U)^T = l^+(U) \propto (1, -1) \ \forall U \in R_3$. On the other hand, applying Lemma 8.2, we obtain that the characteristic speeds $\lambda^\pm(U)$, $U = (u_1, u_2)$ are symmetric functions of the variables u_1 and u_2, so we have

$$\frac{\partial\lambda^\pm}{\partial u_1} = \frac{\partial\lambda^\pm}{\partial u_2} \Rightarrow \nabla\lambda^\pm \propto (1, 1)^T, \tag{8.14}$$

in particular we have that

$$\nabla\lambda^+(U) \cdot r^+(U) = 0, \tag{8.15}$$

concluding that $R_3 \subset Inf_+$ (see Definition 3.5). $\qquad\square$

Remark 8.2. *We can repeat the argument above for the case $\mu_1 \neq \mu_2$ to obtain again $R_3 \subset Bif_+$. However for such case $R_3 \not\subset Inf_+$.*

The following theorem describes points on the edges ∂_1 and ∂_2 as secondary bifurcation points.

Theorem 8.2. *Assume that $\alpha = 0$ and $\rho_1 = \rho_2 \neq \rho_3$. Define $\rho = \rho_{13} = \rho_{23}$. All the points on edges ∂_1 and ∂_2 belong to the secondary bifurcation manifold for one of the families, except for the quasi-umbilic points Q_1, Q_2 (in (4.19), (4.20)) and for the vertices V_1, V_2 of the saturation triangle. More specifically*

$$\left[(V_3, Q_2) \cup (V_3, Q_1)\right] \subset Bif_j, \tag{8.16}$$

$$\left[(Q_2, V_1) \cup (Q_1, V_2)\right] \subset Bif_k, \tag{8.17}$$

where j is "$-$" if $\rho < 0$, j is "$+$" if $\rho > 0$ and k is the opposite family to j.

Proof. We provide the proof for the case $\rho > 0$. Then the case $\rho < 0$ will be a direct consequence of Theorem 8.1 and Remark 8.1.

Let $U \in (V_3, Q_2)$, it is obvious that $\partial_2 \subset \mathcal{H}(U)$. Depending on the sign of ρ the scalar flux function $F_1^{\partial_2}$ restricted to the edge ∂_2 has the shape of one of the functions

represented in Figs. 5.1(a) or 5.1(b) so it is clear that there exists $U' \in (Q_2, V_1)$ such that $U' \in \mathcal{H}(U)$ with $\sigma(U, U') = 0$. Notice that $(U - U') \propto (1, 0)^T$ since both U and U' belong to the edge ∂_2. On the other hand

$$l^+(U')\big(DF(U') - \lambda^+(U')I\big) = 0, \tag{8.18}$$

where l^+ denotes a left eigenvector corresponding to the fast characteristic speed λ^+. As $U' \in (Q_2, V_1)$, from (4.4)-(4.8) we obtain after some calculations that $\lambda^+(U') = 0$ while $J_{11}(U') < 0, J_{12}(U') < 0, J_{21}(U') = 0, J_{22}(U') = 0$. So we obtain from (8.18):

$$l_1^+(U')J_{11}(U') = 0, \tag{8.19}$$
$$l_1^+(U')J_{12}(U') = 0, \tag{8.20}$$

therefore $l_1^+(U') = 0$ and we have that $l^+(U') \propto (0, 1)$. Finally we see $l^+(U')(U - U') = (0, 1) \cdot (1, 0) = 0$.

We have found $U' \in \mathcal{H}(U)$ such that $\sigma(U, U') = \lambda^+(U') = 0$ and $l^+(U')(U - U') = 0$, concluding that the interval (V_3, Q_2) is a subset of the bifurcation manifold corresponding to the fast family. The proofs for the other intervals are analogous. $\qquad\square$

Remark 8.3. *As a consequence of Theorem 8.2 and supported by numerical evidence, the Hugoniot locus of any non-coincidence point on the edges ∂_1, ∂_2 has a self-intersection lying on the respective edge, see Fig 7.8 for illustration.*

Chapter 9

Solution for SPGP with heavy equal-density fluids

In this chapter we study the Riemann solution for the case in which $\alpha = 0$, $\rho_1 = \rho_2 > \rho_3$. Denoting by $\rho = \rho_{13} = \rho_{23}$, we are in the case $\rho > 0$. Based on numerical calculations we will present the integral curves, the inflection manifolds and the boundary contact manifolds corresponding to this simplified pure gravitational problem (SPGP). The figures shown in this section are crucial for the solution of the Riemann problem. Although we show figures for the symmetrical viscosity case $\mu_1 = \mu_2 = \mu_3$, they illustrate the general case.

For the SPGP, with $\rho > 0$, the integral curves of each family are shown in Figure 9.1. Notice that the segments $(Q_1, V_2) \subset \partial_1$ and $(Q_2, V_1) \subset \partial_2$ are integral curves of the slow family while the segments $(Q_1, V_3) \subset \partial_1$ and $(Q_2, V_3) \subset \partial_2$ are integral curves of the fast family. This change of family along the edges when crossing the quasi-umbilic points was proved in Theorem 4.1.

The inflection manifolds of each family are shown in Fig. 9.2. Here we use the superscripts s and f (instead of $-$ and $+$) for slow and fast family, respectively. The points denoted by $I_1^s, I_1^f \in \partial_1$ and $I_2^s, I_2^f \in \partial_2$ represent the intersections between the inflection manifolds of each family and the edges ∂_1, ∂_2. These points coincide with the inflections of the two-phase flux function $F_1^{\partial_2}$ and $F_2^{\partial_1}$ studied in Chapter 5, so we can interpret the inflection branches I_1^s–I_2^s and I_1^f–I_2^f as continuations of two-phase inflection points that would appear as consequence of introducing a third phase into a given two-phase problem.

An interesting fact we can observe in Fig. 9.2 is the existence, for slow-family, of an extra inflection branch. This "extra" branch arises from the quasi-umbilic points Q_1, Q_2 and crosses the critical line R_3 at an inflection point of the two-phase scalar flux function F_{12} (see definition in Eq. (5.10)) restricted to the critical line R_3. On the other hand, for the case $\mu_1 = \mu_2$, the critical line R_3 is itself an inflection branch for the fast-family (see Prop. 8.1), a fact that reflects the symmetry of phases 1 and 2 with respect to densities and viscosities. For more general cases in which $\mu_1 \neq \mu_2$, the critical line R_3 is not an
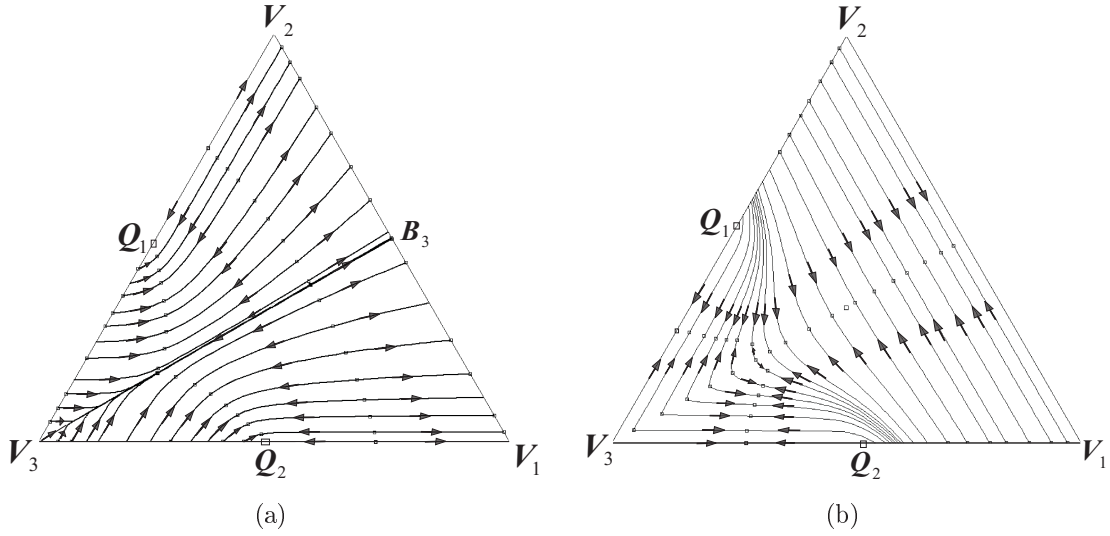
Figure 9.1: Integral curves for the simplified pure gravitational problem $\alpha = 0$, $\rho_1 = \rho_2 > \rho_3$, in the case $\mu_1 = \mu_2 = \mu_3$. (a) Slow-family integral curves. The arrows indicate the direction of increasing characteristic speed; notice the local extremal speed at the dots, which form the slow-family inflection locus. (b) Fast-family integral curves. The arrows indicate the direction of increasing characteristic speed; notice the local extremal speed at the dots, which form the fast-family inflection locus. The points Q_1 and Q_2 denote the quasi-umbilic points on the boundary.

inflection branch any more, see Fig. 9.2(b).

Remark 9.1. *In the more general case when the fluids have different densities, the "extra" inflection branch of the slow-family intersects the edges ∂_1 and ∂_2 at points that are not necessarily the quasi-umbilic points. Such points are precisely where the zero-level curves for the slow-family characteristic speed lose differentiability.*

In Fig. 9.3 we show the boundary contact curves (see Def. 3.9). We denote by $E^s_{\partial_j}, E^f_{\partial_j}$; $j = 1, 2, 3$ the branches of the boundary contact manifold corresponding to the edge ∂_j for slow and fast-family respectively. We also call these curves the extension of the edges of the saturation triangles associated to one of the families. The extension of relevant points are also plotted, recall that we denoted by P^s_A (or P^f_A), the extension of a point A on the boundary, associated to the slow-family (fast-family) (*i.e.*, the shock joining the state A with the state P^i_A is characteristic in P^i_A for the family i). This correspondence is not necessarily one to one.

Consider the simplified pure gravitational problem $\alpha = 0$, $\rho_1 = \rho_2 > \rho_3$. We want to solve the generic Riemann problem with left data U_L lying in the edge ∂_i, $i = 1, 2, 3$ of the saturation triangle, and right data U_R corresponding to the opposite vertex V_i. For this case, there exist essentially only two distinct problems: $U_L \in \partial_2$, $U_R = V_2$ and $U_L \in \partial_3$, $U_R = V_3$; the Riemann solutions for the two sets of data $U_L \in \partial_1$, $U_R = V_1$ and $U_L \in \partial_2$, $U_R = V_2$ are analogous.
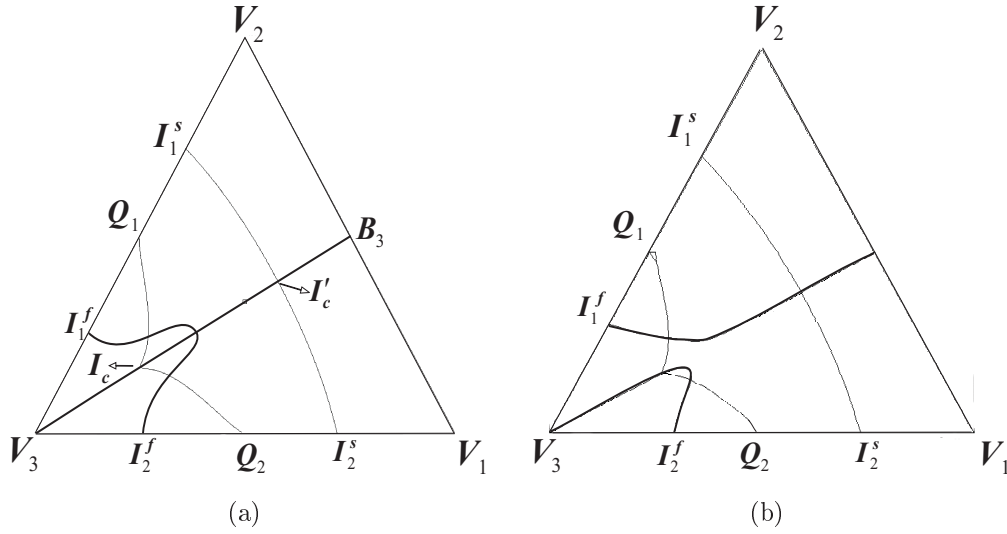
Figure 9.2: Inflection curves for the case $\alpha = 0$, $\rho_1 = \rho_2 > \rho_3$. (a) Symmetric case $\mu_1 = \mu_2 = \mu_3$. The dark curves are the inflection locus corresponding to the fast family, with branches $R_3 = V_3$–B_3 and I_1^f–I_2^f. The light curves are the inflection locus corresponding to the slow family, with branches I_1^s–I_2^s and Q_1–Q_2. (b) Non-symmetric case $\mu_1 > \mu_2$. The points Q_1 and Q_2 denote the quasi-umbilic points on the boundary. The points I_c and I_c' denote the inflection points on the critical line.

First we state the following result.

Lemma 9.1. *Assume $\rho_1 = \rho_2 > \rho_3$ and consider the states $A_i \in \partial_i$, $i = 1, 2, 3$; then:*

    (i) *We have $\sigma(U, A_i) > 0$ for all $U \in \mathcal{H}(A_i)$, $i = 1, 2$, out of the edge ∂_i.*

    (ii) *We have $\sigma(U, A_3) < 0$ for all $U \in \mathcal{H}(A_3)$ out of the edge ∂_3 and of the vertex V_3.*

Proof. The proof follows from the Rankine-Hugoniot condition (3.6) utilized for shocks joining a state $A_i \in \partial_i$ with an arbitrary state U. $\square$

9.1   RP1: Left data in ∂_2, right data V_2

For this case $\mathcal{H}(V_2) = \partial_1 \cup \partial_3$ (see item (i) of Prop. 6.3); we also notice in Fig. 9.1 that the integral curves through vertex V_2 coincide with the edges ∂_1 and ∂_3 near V_2. Thus the conceivable ways to arrive at V_2 are (see Fig. 9.1):

    (1) Arriving at V_2 by a slow rarefaction corresponding to the two-phase solution on ∂_1.

    (2) Arriving at V_2 by a zero-speed genuine contact discontinuity corresponding to the two-phase solution on ∂_3 (see Sec.5.2).
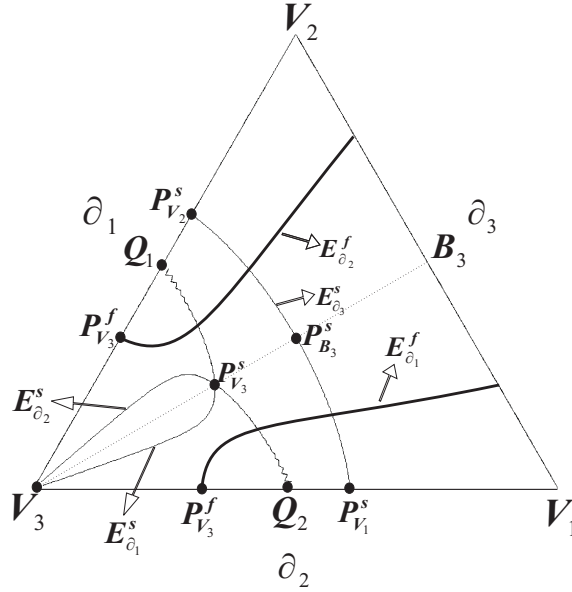
Figure 9.3: *Boundary contact manifolds (or extensions) for $\alpha = 0$, $\rho_1 = \rho_2 > \rho_3$, $\mu_1 = \mu_2 = \mu_3$. The light curves represent the slow-family boundary contact manifold, the branch $E^s_{\partial_i}$, $i = 1, 2, 3$ is the slow-family extension of the edge ∂_i. The dark curves represent the fast-family boundary contact manifold, $E^f_{\partial_1}$ is the fast-family extension of the edge ∂_1 while $E^f_{\partial_2}$ is the fast-family extension of the edge ∂_2. The edge ∂_3, representing a mixture of two equal-density fluids, has no fast-family extension. The points Q_1 and Q_2 denote the quasi-umbilic points on the boundary.*

Impossibility of alternative (1).

Consider an arbitrary state A_1 on the edge ∂_1. It is impossible to use a rarefaction to arrive at A_1, since both characteristic speeds decrease in the outward direction (see arrows in both Figs. 9.1). Thus we must use a shock to arrive at A_1 from an arbitrary state U out of the edge ∂_1. From Lemma 9.1 we have $\sigma(U, A_1) > 0$. On the other hand as $\rho_2 > \rho_3$, the sequence of waves along the edge ∂_1 joining the state A_1 with the vertex V_2 consists of one negative-speed shock followed by a rarefaction wave ending at V_2 with speed equal to zero (see Fig. 9.4). This means that the possibility of a shock joining an arbitrary state U (out of ∂_1) with A_1, followed by the two-phase solution along ∂_1, joining the states A_1 and V_2 presents speed incompatibility. For this reason we must exclude such a solution. In other words, for $U_L \in \partial_2$, $U_L \neq V_3$, $U_L \neq V_1$ we cannot construct a solution arriving first to ∂_1 and follow it by the two-phase Oleinik solution to V_2 without violating the geometric speed compatibility condition. Thus the possibility described in item (1) is excluded.

Construction of the Riemann solution.

Now we will construct the Riemann solution using the second alternative, *i.e.*, in order to arrive to V_2 we must first reach ∂_3 by a slow rarefaction curve (see arrows in Fig. 9.1(a)),
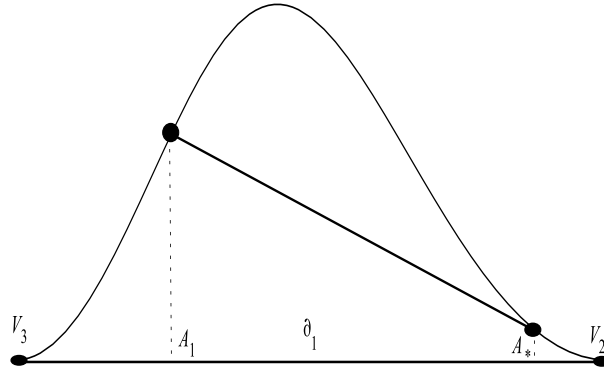
Figure 9.4: *Two-phase Oleinik solution for left state A_1 in ∂_1 and right state V_2. This solution begins with a negative-speed shock joining A_1 with A_*.*

and follow it by a zero-speed contact discontinuity on ∂_3.

Consider $U_L = (u_1^L, 0, u_3^L)$ on ∂_2. We will split our analysis in several cases:

(*i*) If $U_L = V_1$ the solution is a zero-speed genuine contact joining V_1 with V_2.

(*ii*) If $U_L = V_3$, we will have three different representations in state space of the same solution, the first one is the two-phase solution on the edge ∂_1 that is a zero-speed double contact discontinuity joining V_3 and V_2. The second representation of the solution consists in a zero-speed double contact discontinuity joining V_3 with V_1 followed by a zero-speed genuine contact joining V_1 with V_2. The third representation of the solution is obtained by the use of the two-phase flow regime along the critical line R_3, by means of a zero-speed double contact discontinuity joining V_3 with B_3 followed by a zero-speed genuine contact joining B_3 with V_2. Although these representations of the solutions are different in state space, all of them describe the same solution in physical space because all the discontinuities have zero-speed and collapse into a single discontinuity.

(*iii*) Assume $U_L \in [Q_2, V_1)$, then we have $\lambda^+(U_L) = 0$ and $\lambda^-(U_L) < 0$ (by interchanging the indices 1 and 2 everywhere in Eqs. (4.35)-(4.36)). In this case the slow-family eigenvector $r^-(U_L)$ has the direction of the edge ∂_2 since the slow integral curve trough U_L coincides with this boundary. Thus the solution of the Riemann problem begins with the two-phase Buckley-Leverett solution along this edge. For U_L to the right of the inflection point I_2^s (shown in Fig. 9.2), the slow-family wave group is a single rarefaction wave up to the vertex V_1. For $U_L \in (Q_2, I_2^s)$ the slow-family wave group consists of a negative-speed shock wave joining the states U_L and $U_* = (u_*^1, 0, 1 - u_*^1)$; where $U_* \in (I_2^s, V_1)$ satisfy $\sigma(U_L, U_*) = dF_1^{\partial_2}(u_*^1)/du_1 = \lambda^-(U_*)$, followed by a rarefaction wave joining the states U_* and V_1. Notice that the rarefaction wave arrives at V_1 with speed equal to zero. The solution continues with the "fast" wave group which consists of a zero-speed contact discontinuity joining the states V_1 and V_2.

The solution for the case $U_L \in [I_2^s, V_1)$ is shown in Fig. 9.5 (see definition of I_2^s in Fig. 9.2). The solution for the case $U_L \in (Q_2, I_2^s)$ coincides with the solution shown in

Figs. 9.6(b) and 9.6(c).

Remark 9.2. *Notice that the convention of calling a wave group as belonging to the "slow-family" or "fast-family" lacks of physical meaning for this problem, since in general, we find both negative and positive characteristic speeds. A negative-speed wave moves upwards while a positive-speed wave moves downwards. Notice that a "slow" wave could have a negative speed with larger absolute value than a "fast" wave.*

(a)   (b)
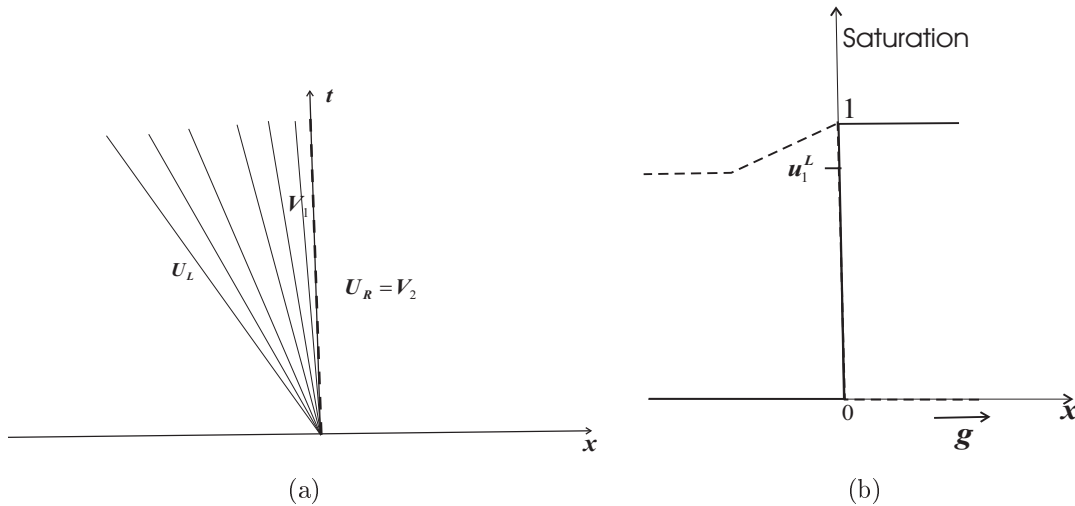
Figure 9.5: Riemann solution for $U_L \in [I_2^s, V_1)$, $U_R = V_2$ in the case $\rho_1 = \rho_2 > \rho_3$. (a) Wave groups represented in the (x, t)-space: solid lines represent the characteristic lines in a rarefaction fan, dashed lines represent shocks, light lines correspond to waves of the slow family, dark lines correspond to waves of the fast family. (b) Saturation profiles; the solid curve indicates the saturation of phase 2, the dashed curve indicates the saturation of phase 1. Notice that fluids 1 and 3 occur only for $x < 0$ and fluid 2 for $x > 0$.

(*iv*) Assume that $U_L \in (V_3, Q_2)$, then we have $\lambda^+(U_L) > 0$ and $\lambda^-(U_L) = 0$. Here the integral curve of the fast family trough U_L coincides with the boundary ∂_2, while the integral curve of the slow family trough U_L is transversal to ∂_2. Apparently we can construct two solutions of the Riemann problem satisfying the Lax conditions. The first one is analogous to the previous case (*iii*) (*i.e.*, a two-phase Buckley-Leverett solution up to the vertex V_1 followed by a zero-speed contact between the states V_1 and V_2), see Figs. 9.6(b) and 9.6(c). Notice that this solution can be constructed without using the slow wave curve through U_L. So in principle it would be possible to construct "another" solution using the slow wave curve through U_L in order to reach ∂_3, an then follow it by a zero-speed contact up to the vertex V_2. In Appendix C we show that for this particular Riemann problem, this second construction via slow-family wave curve, does not represent a new solution.

Summarizing the results above and utilizing the notations from Section 3.1., the Riemann solution for initial left and right data $U_L \in \partial_2$ and $U_R = V_2$ has the following structure
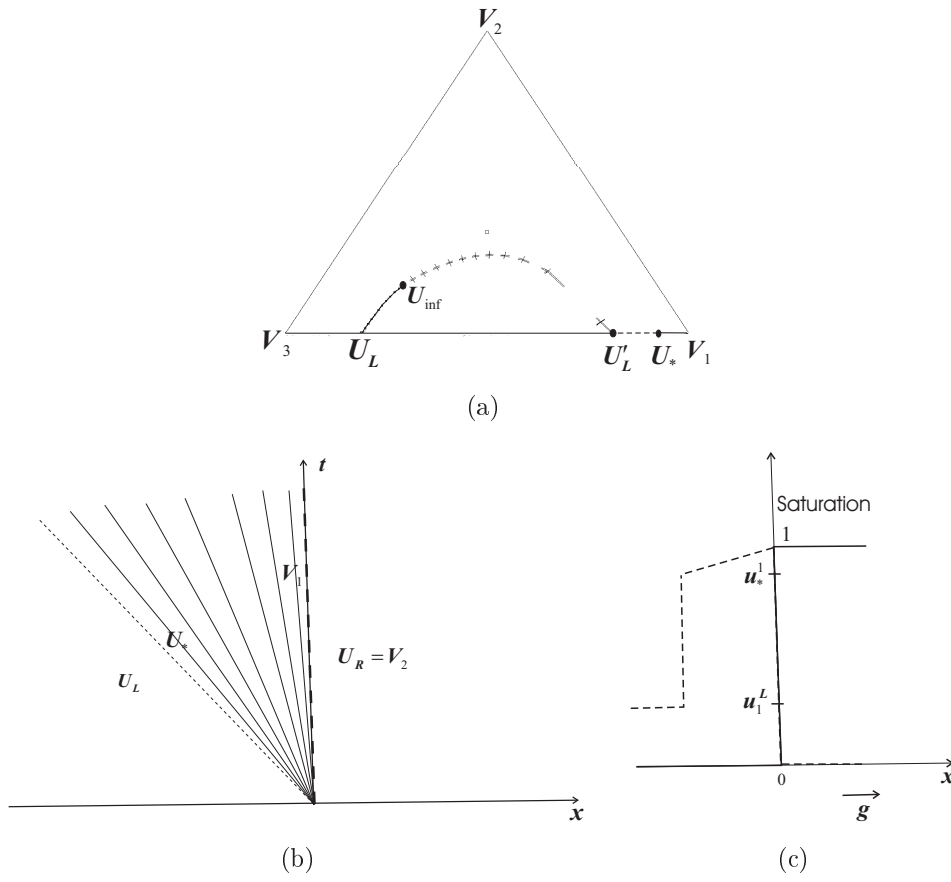
Figure 9.6: Riemann solution for $U_L \in (V_3, I_2^s)$, $U_R = V_2$ in the case $\rho_1 = \rho_2 > \rho_3$, (a) slow-family wave curve through $U_L \in (V_3, Q_2)$. The solid curve denotes a rarefaction segment, the curve marked by crosses denotes a composite segment based on states on the rarefaction curve U_L–U_{inf}. The dashed curve is a shock segment. (b) wave groups represented in the (x, t)-space: solid lines represent the characteristic lines in a rarefaction fan, dashed lines represent shocks, light lines correspond to waves of the slow family, dark lines correspond to waves of the fast family. (c) Saturation profiles, the solid curve indicates the saturation of phase 2, the dashed curve indicates the saturation of phase 1. Notice that fluids 1 and 3 occur only for $x < 0$ and fluid 2 for $x > 0$.

(i) If $U_L = V_1$: $U_L = V_1 \xrightarrow{GC} V_2 = U_R.$ (9.1)

(ii) If $U_L = V_3$: $U_L = V_3 \xrightarrow{C} V_2 = U_R.$ (9.2)

For this case we have other two representations in state space for the same physical solution:

(ii.2) $U_L = V_3 \xrightarrow{C} V_1 \xrightarrow{GC} V_2 = U_R$ and   (ii.3) $U_L = V_3 \xrightarrow{C} B_3 \xrightarrow{GC} V_2 = U_R.$

(iii) If $U_L \in [I_2^s, V_1)$: $U_L \xrightarrow{R_-} V_1 \xrightarrow{C} V_2 = U_R$. $\qquad$ (9.3)

In Figs. 9.5(a), 9.5(b) we show the corresponding Riemann solution and the saturation profiles.

(iv) If $U_L \in (V_3, I_2^s)$: $U_L \xrightarrow{SC_-} U_* \xrightarrow{R_-} V_1 \xrightarrow{C} V_2 = U_R$, $\qquad$ (9.4)

where $U_* \in \partial_2$, see Figs. 9.6(b) and 9.6(c).

Remark 9.3. *Although we do not prove rigorously that this solution is unique, the analytical and numerical arguments that we provide in the construction of the solution are compatible only with uniqueness of the solution.*

Physical interpretation of the solutions in RP1.

Items (i) and (ii) correspond to the well known two-phase flow. In both cases the solution is just as we expected because the fluid initially on top is not heavier than the fluid initially at the bottom, so it is natural to expect that the fluids do not move.

Both items (iii) and (iv) correspond to a genuine three-phase flow. In RP1 we have two equal-density fluids and a third fluid lighter. Initially, there is a pure fluid below the interface. The mixture on top involves a fluid with the same density that the bottom fluid and a third lighter fluid. We expect a priori that the bottom fluid does not move upward, because there is no heavier fluid. Thus we expect the interface to remain intact and both fluids initially on top to remain there all the time. We also expect that the density difference between the fluids on top leads to a two-phase flow involving such fluids, we expect the lightest fluid to move upwards. We verify all these facts in the solutions presented in items (iii) and (iv), depending on the initial mixture, we will have a two-phase flow above the interface with a single rarefaction wave or a rarefaction preceded by a shock.

Remark 9.4. *The Riemann problem* **RP2**, *with left data* U_L *in* ∂_1 *and right data* $U_R = V_1$, *is analogous to* **RP1**, *so we omit its description.*

9.2   RP3: Left data in ∂_3, right data V_3.

We know from Prop. 6.1 that $\mathcal{H}(V_3) = \partial_1 \cup \partial_2 \cup \partial_3 \cup R_3$. The shocks from any state on ∂_3 to V_3 have zero speed. On the other hand, the only integral curves crossing V_3 are: (I) the fast-family integral curves coinciding with the edges ∂_1, ∂_2 near the vertex V_3 and (II) the slow-family integral curve that coincides with the critical line R_3, see the Fig. 9.1. Then we have the following three possibilities to arrive at V_3.

(1) Arriving at V_3 by a fast shock along one of the edges ∂_1 or ∂_2.

(2) Arriving at V_3 by a slow shock along the critical line R_3.

(3) Arriving at V_3 by a zero-speed double contact directly from $U_L \in \partial_3$.

First we analyze the two-phase flow cases. If U_L is one of the states V_2, B_3 or V_1 we know from Chapter 5 that the behavior is like two-phase flow, so we can obtain the Riemann solution using Oleinik's construction.

As $\rho_2 > \rho_3$, if we choose $F_3^{\partial_1}$ as the flux restricted to the edge ∂_1 with conserved quantity u_3, this flux function is like the flux of Fig. 5.1(b). In Fig. 9.7(a) we show Oleinik solution for the Riemann problem $U_L = V_2$, $U_R = V_3$.

We illustrate the solution in Fig. 9.7 for $U_L = V_2$. The other cases are completely analogous. For the case $U_L = V_1$ we have the two-phase Oleinik solution along the edge ∂_2. The case $U_L = B_3$ is the two-phase Oleinik solution along the critical line R_3; this latter case presents only waves of the slow-family group as we proved in Theorem 5.1.

Now we analyze the genuine three-phase problem. We will show that when $U_L \in (V_2, B_3)$ (i.e., when initially the phase 2 is dominant with respect to the phase 1 above the interface) the solution remains in the triangle V_3–B_3–V_2, so in this case the solution consist of a slow-family wave group which reaches the edge ∂_1, a constant state, and then it continues with a two-phase fast-family wave group. For such a case we show that the other possibilities for a solution arriving to V_3 along the edge ∂_2, the critical line R_3 or by a direct zero-speed double contact must be excluded.

Let us consider $U_L \in (V_2, B_3)$, we will construct the Riemann solution for $U_R = V_3$.

Excluding a zero-speed double contact joining U_L with V_3.

As we see in Fig. 9.7(a), the two-phase solution consisting in a shock (in this case, double contact discontinuity) joining the vertices V_2 and V_3 does not satisfy Oleinik's entropy condition. The alternative solution consisting of a zero-speed double contact discontinuity joining $U_L \in (V_2, B_3)$ with V_3 coincides in the physical space with the following sequence: a genuine zero-speed contact discontinuity joining U_L with V_2 (corresponding to two-phase solution along ∂_3), followed by a zero-speed double contact joining the vertices V_2 and V_3, but as we already saw the last wave of this sequence does not satisfy Oleinik's construction, therefore it must be excluded.

Wave curve construction.

See the arrows in Fig. 9.1(a). The slow characteristic speed decreases along the slow-family integral curves inwards the saturation triangle, so the slow-family wave curve arising from U_L begins with a shock segment and finishes at a point $P_{U_L}^s$ that belongs to the

(a)

(b)

(c)
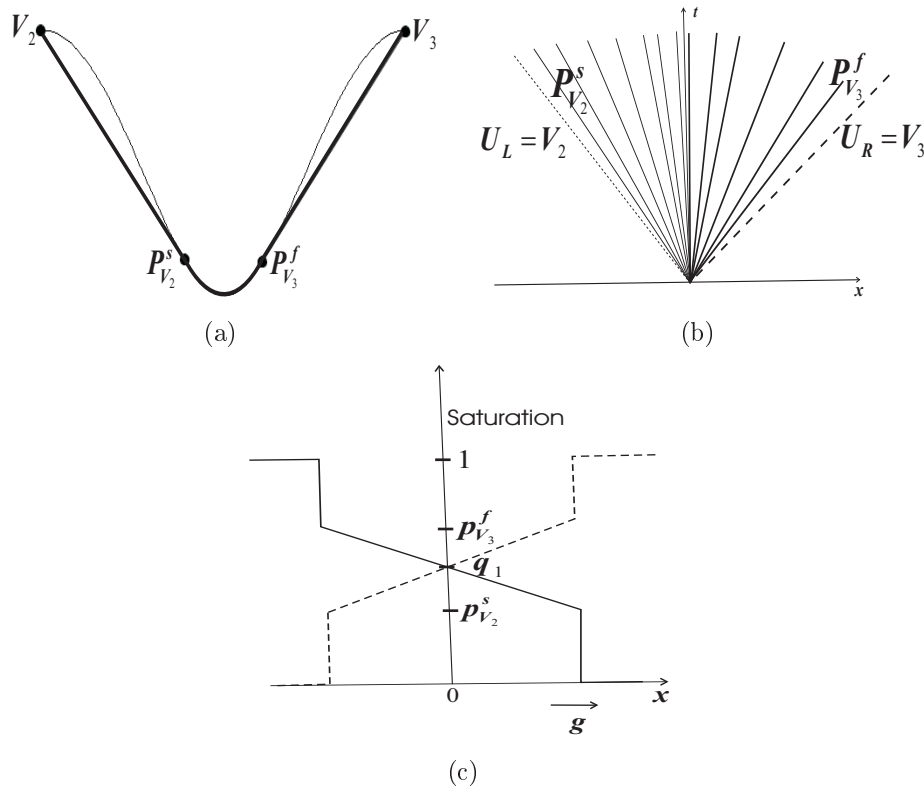
Figure 9.7: Riemann solution for $U_L = V_2$, $U_R = V_3$ in the case $\rho_1 = \rho_2 > \rho_3$, (a) Oleinik's construction. (b) Wave groups represented in the (x, t)-space: solid lines represent the characteristic lines in a rarefaction fan, dashed lines represent shock paths, light lines correspond to waves of the slow family, dark lines correspond to waves of the fast family. (c) Saturation profiles: the solid curve indicates saturation of phase 2, the dashed curve indicates saturation of phase 3. The coordinates of the following points are $P_{V_2}^s = (0, 1 - p_{V_2}^s, p_{V_2}^s)$ and $P_{V_3}^f = (0, 1 - p_{V_3}^f, p_{V_3}^f)$. The two saturation profiles intersect at the saturation value corresponding to the quasi-umbilic point Q_1 where the wave speed is zero.

slow-family extension curve $E_{\partial_3}^s$. The slow-family wave curve continues from $P_{U_L}^s$ with a rarefaction segment until it reaches the inflection manifold and then continues with a composite curve based into this rarefaction segment. As the wave curve reaches the extension curve $E_{\partial_1}^s$ of the edge ∂_1 before arriving to the inflection locus, the composite curve reaches the boundary ∂_1 at a point U_M, see Fig 9.9(a). There exist two possibilities for the structure of the fast-family wave curve arising from U_M, depending on the position of U_M relatively to the state $P_{V_3}^f$, which is the fast-family extension point on the edge ∂_1 of the vertex V_3. If $U_M \in (V_3, P_{V_3}^f)$ (as in the case shown in Fig. 9.9(a)) the fast-family wave curve consists only of a shock segment. If $U_M \in (P_{V_3}^f, Q_1)$ the fast-family wave curve consists of a rarefaction segment from U_M–I_1^f continuing with a composite curve (based on this rarefaction segment) up to V_3, see Fig. 9.10(a).

(a)

(b)
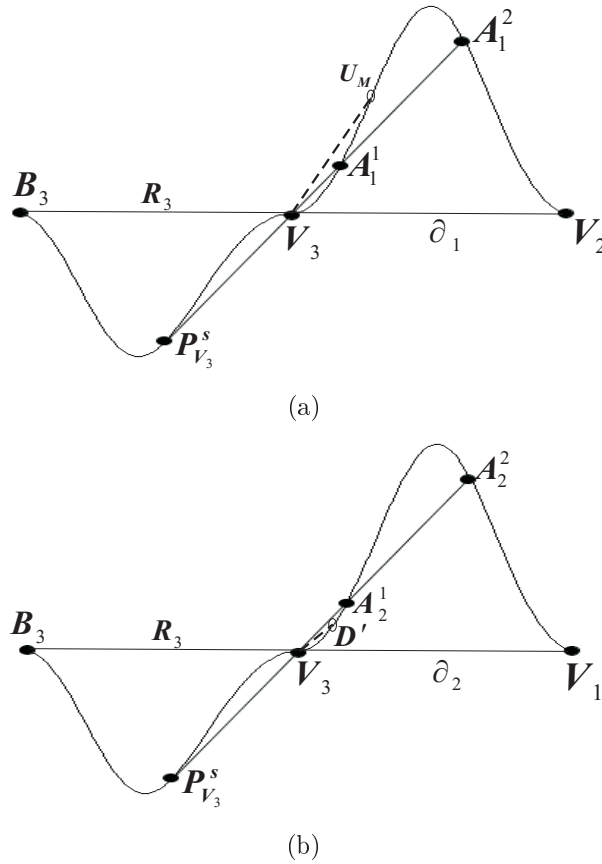
Figure 9.8: (a) Wedge construction for the two-phase regimes R_3 and ∂_1. This figure is utilized to establish the speed compatibility between wave groups in the solution. (b) Wedge construction for the two-phase regimes R_3 and ∂_2. This figure is utilized to establish the speed incompatibility between other waves that need to be excluded.

The Riemann solution consists of the following sequence of waves. There is a slow-family right-characteristic shock wave joining $U_L \in \partial_3$ to $P_{U_L}^s$, followed by a slow rarefaction wave joining $P_{U_L}^s$ to a state $P_{U_M}^s$ on the curve $E_{\partial_1}^s$, followed by a slow-family left-characteristic shock joining $P_{U_M}^s$ to state U_M in ∂_1. If $U_M \in [P_{V_3}^f, V_3)$ the last wave in the solution is a fast shock joining U_M to V_3, see Figs. 9.9(b) and 9.9(c). If $U_M \in (Q_1, P_{V_3}^f)$, the fast-family wave group consists of a rarefaction wave joining U_M to $P_{V_3}^f$ followed by a left-characteristic shock up to V_3, see Figs. 9.10(b) and 9.10(c).

Now we will show the compatibility between the speeds of the slow-family wave group joining U_L with U_M and the fast-family wave group joining U_M with V_3.

Speed compatibility of the waves.

We perform the wedge construction (described in Section 7.1) for the two-phase regimes R_3 and ∂_1 with a common vertex V_3. Along ∂_1 we choose $F_3^{\partial_1}$ and u_3 as flux function and conserved quantity; the phases coexisting in ∂_1 have viscosities μ_2 and μ_3.

On the other hand, along the critical line R_3 the flux function is given by Eq. (5.10) with conserved quantity u. The viscosities of the effective phases coexisting along R_3 are μ_3 and $\mu_1 + \mu_2$. The relative difference between the densities of the fluids involved in these two-phase regimes gives rise to a situation as in Fig. 9.8(a), where the tangent segment to the graph at $P_{V_3}^s$ intersects the extended-flux function at two points A_1^1, A_1^2 on the opposite side relative to V_3. We have $\lambda^-(P_{V_3}^s) = \sigma(P_{V_3}^s, V_3) = \sigma(V_3, A_1^1) = \sigma(V_3, A_1^2)$. In Fig. 9.11(a) all these points are drawn in the saturation triangle, and the dotted curve represents the Hugoniot locus through the relevant point $P_{V_3}^s \in R_3$.

On the other hand for $U_L \in (V_2, B_3)$ we have numerical evidence showing that $U_M \in (A_1^1, Q_1)$. Plotting the level curves for the slow-family characteristic speed we obtain $\lambda^-(P_{U_M}^s) < \lambda^-(P_{V_3}^s)$, see Fig. 9.11(c). Thus we have $\sigma(P_{U_M}^s, U_M) = \lambda^-(P_{U_M}^s) < \lambda^-(P_{V_3}^s) = \sigma(P_{V_3}^s, V_3) < \sigma(U_M, V_3)$ (see Fig. 9.8(a) for last inequality), which is evidence for the compatibility of speeds between the slow-family and fast-family wave groups.

From Fig. 9.11(a) we notice that for U_L sufficiently near B_3 the rarefaction segment of the slow-family wave curve intersects both extension curves $E_{\partial_1}^s$ and $E_{\partial_2}^s$. We have already constructed the solution using the intersection point $P_{U_M}^s$ in $E_{\partial_1}^s$, this solution always remains in the triangle V_3–B_3–V_2. We have also verified the speed compatibility between the slow-family and fast-family waves. Now we will show that the other possible solution that arises by the use of the point D on $E_{\partial_2}^s$ connecting to a point D' on the edge ∂_2 must be excluded.

<u>Excluding the solution arriving at V_3 along the edge ∂_2 for $U_L \in (V_2, B_3)$.</u>

See Fig. 9.11(b), we denote by D' a point on ∂_2 for which D is the extension, so $D' \in \mathcal{H}(D)$ and $\sigma(D, D') = \lambda^-(D)$. It is possible to show that the shock joining D and D' is a Lax slow-shock. We will show that the possibility of utilizing that shock in the solution must be excluded because of speed incompatibility with the fast-family shock joining D' with V_3.

The incompatibility can be established by performing the wedge construction for the two-phase regimes R_3 and ∂_2, see Fig. 9.8(b) and by the usage of numerical arguments: (1) plotting the level curves for the slow characteristic speed (see Fig. 9.11(c)) we note that $\lambda^-(D) > \lambda^-(P_{V_3}^s)$), (2) plotting the Hugoniot locus through D (see Fig. 9.11(b)) we determine the relative position of D' with respect to A_2^1. Because of all these reasons we conclude that $\sigma(D, D') = \lambda^-(D) > \lambda^-(P_{V_3}^s) = \sigma(P_{V_3}^s, A_2^1) > \sigma(D', V_3)$ (see Fig. 9.8(b) for last inequality). Therefore the shock sequence $D \xrightarrow{CS^-} D' \xrightarrow{S^+} V_3$ has speed incompatibility, so this solution must be excluded.

In other words, if the left state U_L of the Riemann problem belongs to the edge V_2–B_3 of the triangle V_3–B_3–V_2, then the solution remains inside this triangle. The dominant phase at the state U_L (in this case would be phase 2) remain dominant with respect to the other phase present at U_L, the Riemann solution reaches an intermediate state U_M where the non-dominant phase at U_L is missing. A similar invariance property was also observed in the three-phase problem without gravity [1].

Next we summarize the results above, we use the notations from Section 3.1, the Riemann solution for initial left and right data $U_L \in \partial_3$ and $U_R = V_3$ has the following structure:

(i) For the case $U_L = V_2$ we have the two-phase solution, see Fig. 9.7:

$$U_L \xrightarrow{SC} P_{V_2}^s \xrightarrow{R} P_{V_3}^f \xrightarrow{CS} V_3 = U_R, \tag{9.5}$$

(ii) For $U_L \in (V_2, B_3)$ such that $U_M \in (Q_1, P_{V_3}^f)$ see Fig 9.10:

$$U_L \xrightarrow{SC^-} P_{U_L}^s \xrightarrow{R^-} P_{U_M}^s \xrightarrow{CS^-} U_M \xrightarrow{R^+} P_{V_3}^f \xrightarrow{CS^+} V_3 = U_R. \tag{9.6}$$

(iii) For $U_L \in (V_2, B_3)$ such that $U_M \in (P_{V_3}^f, V_3)$, see Fig 9.9:

$$U_L \xrightarrow{SC^-} P_{U_L}^s \xrightarrow{R^-} P_{U_M}^s \xrightarrow{CS^-} U_M \xrightarrow{S^+} V_3 = U_R, \tag{9.7}$$

(iv) For $U_L \in (V_2, B_3)$ such that $U_M = P_{V_3}^f$:

$$U_L \xrightarrow{SC^-} P_{U_L}^s \xrightarrow{R^-} P_{U_M}^s \xrightarrow{CS^-} P_{V_3}^f \xrightarrow{CS^+} V_3 = U_R. \tag{9.8}$$

For the case where phase 1 is dominant at the state U_L, $i.e.$, for $U_L \in (B_3, V_1)$, the solution is completely analogous to the previous one, so we do not describe it.

Physical interpretation of the solutions in RP3.

Case (i) corresponds to the well known two-phase solution involving phases 2 and 3, which have distinct densities. The cases (ii), (iii) and (iv) correspond to genuine three-phase solutions. For these cases the mixture initially on top contains the equal-density fluids 1 and 2, with phase 2 dominant with respect to the phase 1, $i.e.$, the saturation of phase 2 is larger than the saturation of phase 1. The fluid initially at bottom is lighter. The solutions for these cases have certain similarity with the two-phase solution in case (i). We notice that phase 2 (initially dominant on top) remains dominant with respect to the phase 1 in the solution. The Riemann solution reaches an intermediate state where phase 1 is missing. However, notice that for any one of these three-phase flow cases, the sequence of waves in the solution contains an additional shock preceding a homogeneous region, see Fig 9.10 or Fig 9.9. This structure differs from the two-phase case (i) shown in Fig. 9.7.

(a)

(b)

(c)
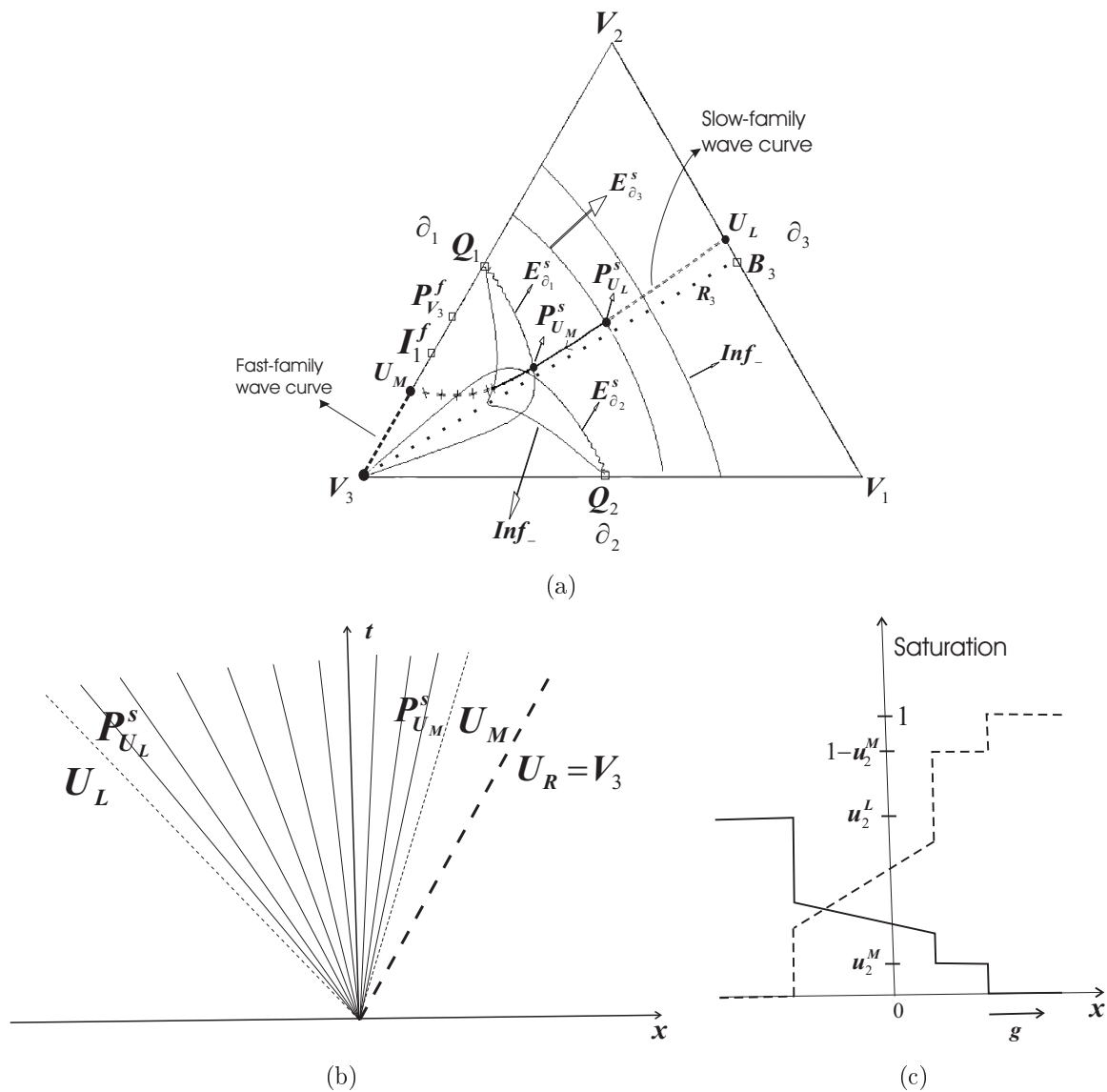
Figure 9.9: Riemann solution for $U_L \in (V_2, B_3)$, $U_R = V_3$ with $U_M \in [P_{V_3}^f, V_3)$, in the case $\rho_1 = \rho_2 > \rho_3$. (a) Riemann solution represented by wave curves in the saturation triangle. As usual, for each family, the dashed curve denotes a shock segment, the solid curve denotes a rarefaction segment and the crossed curve denotes a composite segment. We also draw the slow-family inflection branches Inf_- and the slow-family boundary contact manifolds (extensions $E_{\partial_i}^s$) corresponding to each edge ∂_i. Some relevant points are also drawn. (b) Riemann solution represented in the (x, t)-space, solid lines represent the characteristic lines for a rarefaction fan, dashed lines represent shock paths, light lines correspond to waves of the slow family, dark lines correspond to waves of the fast family. (c) Saturation profiles: the solid curve indicates saturation of phase 2, the dashed curve indicates saturation of phase 3. The constant states have coordinates $U_L = (1 - u_2^L, u_2^L, 0)$, $U_M = (0, u_2^M, 1 - u_2^M)$ and $V_3 = (0, 0, 1)$. The two saturation profiles intersect at a saturation value where the characteristic speed is negative.

(a)

(b)

(c)
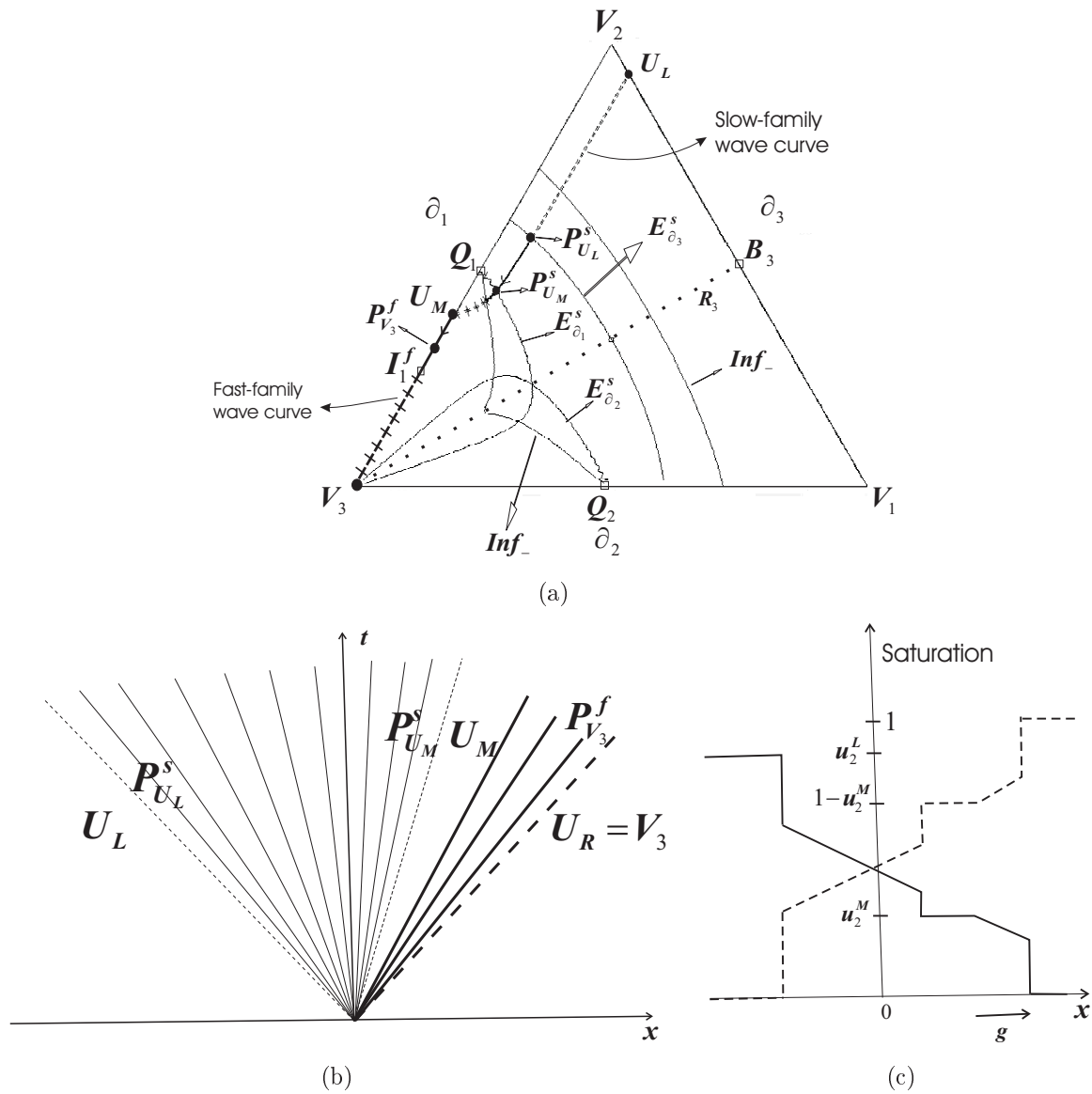
Figure 9.10: Riemann solution for $U_L \in (V_2, B_3)$, $U_R = V_3$ with $U_M \in (Q_1, P^f_{V_3})$, in the case $\rho_1 = \rho_2 > \rho_3$, (a) Riemann solution represented by wave curves in the saturation triangle. As usual, for each family, the dashed curve denotes a shock segment, the solid curve denotes a rarefaction segment and the crossed curve denotes a composite segment. We also draw the slow-family inflection branches Inf_- and the slow-family boundary contact manifolds (extensions $E^s_{\partial_i}$) corresponding to each edge ∂_i. Some relevant points are also drawn. (b) Riemann solution represented in the (x, t)-space, solid lines represent the characteristic lines for a rarefaction fan, dashed lines represent shock paths, light lines correspond to waves of the slow family, dark lines correspond to waves of the fast family. (c) Saturation profiles: the solid curve indicates saturation of phase 2, the dashed curve indicates saturation of phase 3. The constant states have coordinates $U_L = (1 - u^L_2, u^L_2, 0)$, $U_M = (0, u^M_2, 1 - u^M_2)$ and $V_3 = (0, 0, 1)$. The two saturation profiles intersect at a saturation value where the characteristic speed is negative.

Figure 9.11: (a) Slow-family wave curve for U_L near B_3. The wave curve intersect both extensions curves $E^s_{\partial_1}$ and $E^s_{\partial_2}$ at points $P^s_{U_M}$ and D respectively. The dotted curve represent the Hugoniot locus through $P^s_{V_3}$. The slow-family inflection curves was also drawn. (b) The solid dark curve is the Hugoniot locus through D. The dotted curve is the Hugoniot locus through $P^s_{V_3}$. (c) Zoomed in region drawing non-negative level curves for the slow-family characteristic speed, the dark curve represent the zero-level curve. The point denoted by I_c is the global maximizing point for $\lambda^-(U)$. This point coincides with an inflection point of the two-phase flux function F_{12} restricted to the critical line R_3. The points $D, P^s_{U_M}, P^s_{V_3}$ are the same that in figure (a).

Chapter 10

Solution for SPGP with light equal-density fluids

In this chapter we study the case in which $\alpha = 0$, $\rho_1 > \rho_2 = \rho_3$. Denoting $\rho = \rho_{31} = \rho_{21}$, we are in the case $\rho < 0$. As a consequence of the reversal symmetry in Theorem 8.1, the integral curves, the inflection manifolds and the boundary contact manifolds corresponding to this "simplified pure gravitational problem" are identical to those shown in the previous chapter, but the families are interchanged. Besides, along the integral curves of each family, the increasing direction of the characteristic speed is reversed with respect to the case analyzed in the previous chapter. For this case the integral curves of each family are shown in Figure 10.1. Notice that segments $(Q_3, V_1) \subset \partial_3$ and $(Q_2, V_1) \subset \partial_2$ are integral curves of the slow family while segments $(Q_3, V_2) \subset \partial_3$ and $(Q_2, V_3) \subset \partial_2$ are integral curves of the fast family. This change of family along the edges when crossing the quasi-umbilic points was proved in Theorem 4.1.

The inflection manifolds of each family for the symmetrical case $\mu_1 = \mu_2 = \mu_3$ is shown in Fig. 10.2.

In Fig. 10.3 we show the boundary contact curves (see Def. 3.9). As in the previous section, we denote by $E_{\partial_j}^s$, $E_{\partial_j}^f$; $j = 1, 2, 3$ the boundary contact curves of the slow and fast family respectively, corresponding to the edge ∂_j. We also call these curves the extensions of the edges of the saturation triangle. Again we recall that P_A^s (or P_A^f), is the extension of a point A on the boundary, associated to the the slow (or fast) family (*i.e.*, the shock joining the state A to the state P_A^i is characteristic at P_A^i for the family i).

Consider the simplified pure gravitational problem $\alpha = 0$, $\rho_1 > \rho_2 = \rho_3$. We want to solve the generic Riemann problem with left data U_L lying on the edge ∂_i, $i = 1, 2, 3$ of the saturation triangle, and right data U_R coinciding with the opposite vertex V_i. For this case, there exist essentially only two distinct problems: $U_L \in \partial_1$, $U_R = V_1$ and $U_L \in \partial_2$, $U_R = V_2$ (notice that the Riemann problems with data $U_L \in \partial_2$, $U_R = V_2$ and $U_L \in \partial_3$, $U_R = V_3$ are analogous).

(a)

(b)
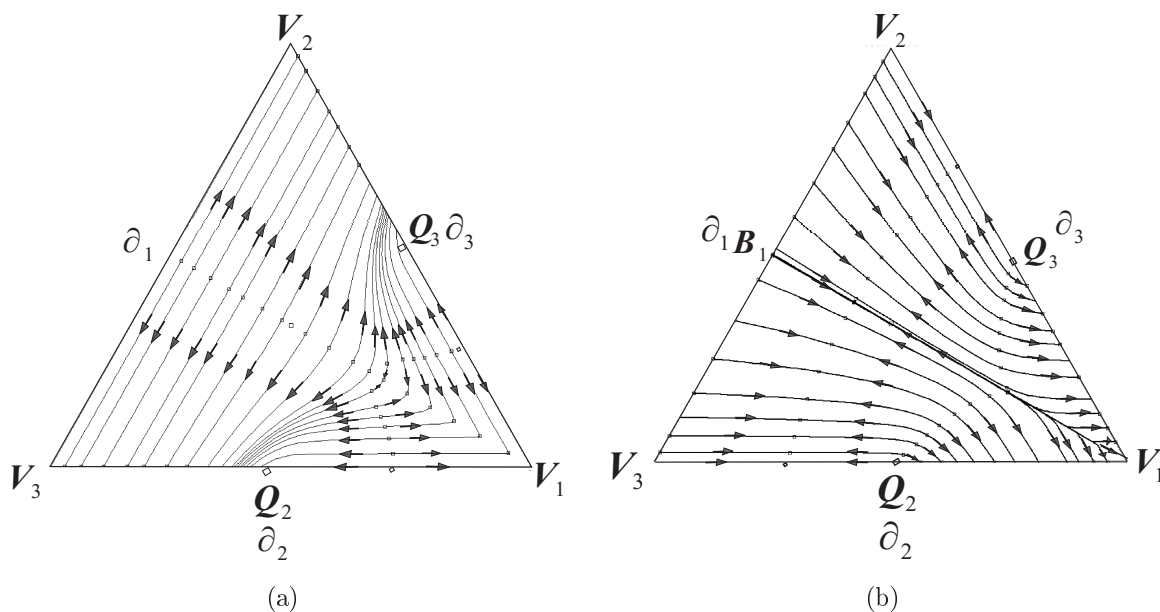
Figure 10.1: Integral curves for the simplified pure gravitational problem $\alpha = 0$, $\rho_1 > \rho_2 = \rho_3$, in the case $\mu_1 = \mu_2 = \mu_3$. (a) Slow-family integral curves. The arrows indicate the direction of increasing characteristic speed; notice the local extremal speed at the dots, which form the slow-family inflection locus. (b) Fast-family integral curves. The arrows indicate the direction of increasing characteristic speed; notice the local extremal speed at the dots, which form the fast-family inflection locus. The points Q_2 and Q_3 denote the quasi-umbilic points on the boundary.
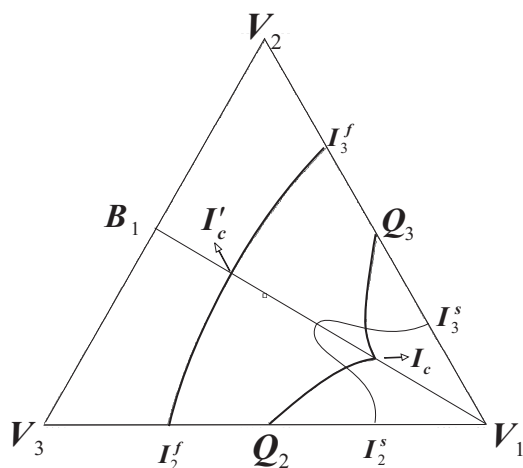
Figure 10.2: *Inflection curves for the case* $\alpha = 0$, $\rho_1 > \rho_2 = \rho_3$, $\mu_1 = \mu_2 = \mu_3$. *The light curves are the inflection locus corresponding to the slow family, with branches* $R_{31} = V_1 - B_1$ *and* $I_2^s - I_3^s$. *The dark curves are the inflection locus corresponding to the fast family, with branches* $I_2^f - I_3^f$ *and* $Q_2 - Q_3$. *The points* Q_2 *and* Q_3 *denote the quasi-umbilic points on the boundary. The points* I_c *and* I_c' *denote the inflection points on the critical line.*
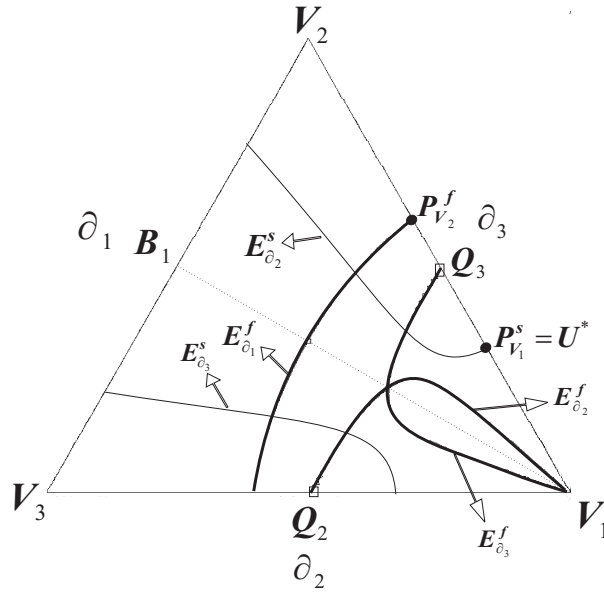
Figure 10.3: *Boundary contact manifolds for $\alpha = 0$, $\rho_1 > \rho_2 = \rho_3$, $\mu_1 = \mu_2 = \mu_3$. The light curves are the slow-family boundary contact curves, the branch $E_{\partial_2}^s$ is the slow-family extension of the edge ∂_2 and the branch $E_{\partial_3}^s$ is the slow-family extension of the edge ∂_3, the edge ∂_1 where the equal-density fluids coexist has no slow-family extension. The dark curves are the fast-family boundary contact curves, $E_{\partial_i}^f$ for $i = 1, 2, 3$ are the fast-family extension of the edges ∂_i.*

First we state the following result.

Lemma 10.1. *Assume $\rho_1 > \rho_2 = \rho_3$ and consider the states $A_i \in \partial_i$, $i = 1, 2, 3$, then:*

(i) *we have $\sigma(U, A_i) < 0$ for all $U \in \mathcal{H}(A_i)$, $i = 2, 3$ out of the edge ∂_i.*

(ii) *we have $\sigma(U, A_1) > 0$ for all $U \in \mathcal{H}(A_1)$ out of the edge ∂_1 and out of the vertex V_1.*

Proof. The proof follows from Lemma 9.1 and the symmetry result for the Hugoniot loci in Remark 8.1. The shock speed changes sign with respect to the SPGP studied in the previous chapter. $\square$

10.1   RP4: Left data in ∂_2, right data V_2

For this case $\mathcal{H}(V_2) = \partial_1 \cup \partial_3$ (see item (i) of Prop. 6.3), we also see in Fig. 10.1 that the integral curves through vertex V_2 coincide with the edges ∂_1 and ∂_3 near V_2. Thus the possible ways to arrive at V_2 are (see Fig. 10.1):

(1) Arriving by a zero-speed genuine contact discontinuity corresponding to the two-phase solution on ∂_1 (see Sec.5.2).

(2) Arriving by a fast shock corresponding to the two-phase solution on ∂_3.

<u>Excluding alternative (1).</u>

Inspecting the arrows in Fig. 10.1(b), we see that the only way to arrive at a point $A_1 \in \partial_1$ is by a fast shock with positive speed (see item (ii) of Lemma 10.1). This shock cannot precede the two-phase zero-speed genuine contact along ∂_1 up to V_2. Therefore all solutions arriving at V_2 by the edge ∂_1 must be excluded.

<u>Construction of the Riemann solution.</u>

Now we will construct the solution using the second alternative, *i.e.*, in order to arrive to V_2 we must first reach the edge ∂_3 by means of a slow-family wave group followed by a fast-family two-phase wave group up to V_2. Notice that as $\rho_1 > \rho_2$, choosing $F_2^{\partial_3}$ as the flux restricted to the edge ∂_3 with conserved quantity u_2, $F_2^{\partial_3}$ is similar to the flux in Fig. 5.1(b). We see that there exist two ways to arrive to the edge ∂_3 through a slow-family wave curve.

(2.1) Arriving to the interval (V_2, Q_3) by a slow rarefaction curve (see arrows in Fig. 10.1(a)).

(2.2) Arriving to the interval (Q_3, V_1) by a slow shock using a non-local branch of the Hugoniot locus through U_L (see for example Fig. 7.8(a)- 7.8(c)).

However the option (2.2) of reaching the edge ∂_3 at states out of the interval (V_2, Q_3) must be excluded because of Proposition 7.2; this type of shock leads to speed incompatibility between the waves in the solution. In other words, the Riemann solution must begin with a slow-family wave group, which reaches the interval (V_2, Q_3) at a point U_M, then the solution continues by means of the fast-family wave group, *i.e.*, a two-phase Oleinik solution joining U_M to V_2.

Consider $U_L = (u_1^L, 0, u_3^L)$ on ∂_2. We will split our analysis in several cases.

10.1.1   Two-phase solutions.

(i) If $U_L = V_3$ the solution is a zero-speed genuine contact joining V_3 with V_2.

(ii) If $U_L = V_1$, the solution is the same two-phase Oleinik solution described in Fig. 9.7.

10.1.2   Doubly characteristic shocks in three-phase solutions.

See Fig. 7.8, by analyzing qualitatively the motion of the non-local Hugoniot branch of $\mathcal{H}(U_L)$ when U_L moves along ∂_2 from V_3 to V_1, we notice that it reverses direction twice.

First the non-local branch leaves the saturation triangle when $U_L = U_1$ and goes away until U_L reaches a certain state D_1, where the motion of the branch reverses and starts to approach again the triangle (see the arrows in Figs. 7.8(d)- 7.8(e)). From $U_L = U_2$ the non-local branch enters the saturation triangle until U_L reaches certain state D_2 where the motion of the non-local branch reverse again to approach the edge ∂_3 (which coincides with the non-local branch in the limit case $U_L = V_1$).

We state the following conjecture, which is supported by strong numerical evidence and some analytical calculations.

Conjecture 10.1. *Consider the simplified pure gravitational problem (SPGP) in which the equal-density fluids are lighter than the other fluid (i.e., $\alpha = 0$ and $\rho_1 > \rho_2 = \rho_3$. The states D_1 and D_2 on ∂_2 where the motion of the non-local Hugoniot branch reverses, belong to the slow-family double contact manifold. In other words, there exist D_1' and D_2' such that $D_i' \in \mathcal{H}(D_i)$ and $\lambda^-(D_i) = \sigma(D_i, D_i') = \lambda^-(D_i')$ for $i = 1, 2$. The state D_2' always lies in the interior of the saturation triangle. The state D_1' may lie: (a) outside the saturation triangle, (b) on the edge ∂_3 of the saturation triangle, or (c) in the interior of the saturation triangle, depending on the shape of the extended-flux function $F_{ext}^{\partial_2\partial_3}$ as follows: case (a) occurs if the graph of $F_{ext}^{\partial_2\partial_3}$ is like the dotted curve in Fig. 7.3, case (b) occurs if the graph of $F_{ext}^{\partial_2\partial_3}$ is like the solid curve in Fig. 7.3, and case (c) occurs if the graph of $F_{ext}^{\partial_2\partial_3}$ is like the dashed curve in Fig. 7.3.*

Remark 10.1. *Notice that when the graph of $F_{ext}^{\partial_2\partial_3}$ is like the solid curve in Fig. 7.3, the double contact pair D_1, D_1' coincides with the double contact pair U_0, U^* in Fig. 7.3, this is the "double tangency" case where $U_0 \in \partial_2$, $U^* \in \partial_3$. As we can regard the other cases as bifurcations of this "double tangency" case, we see that the second part of the conjecture (about the relative position of D_1') becomes natural.*

Now we state another conjecture, which is also supported by numerical calculations.

Conjecture 10.2. *The slow characteristic speed $\lambda^-(U)$ decrease monotonically when U moves from ∂_1 to ∂_3 along the extension curve $E_{\partial_2}^s$ in Fig. 10.3.*

Proposition 10.1. *Assume that the Conjectures 10.1 and 10.2 are valid. Consider D_2^* on ∂_2 such that $\sigma(D_2^*, D_2) = \lambda^-(D_2)$. Then we have $D_2^* \in (V_3, U_1)$, where U_1 is defined in item (ii) of Prop. 7.1 and is shown in the Figs. 7.3 and 10.4.*

Proof. From Conjecture 10.2, we have that $\lambda^-(D_2) = \lambda^-(D_2') > \lambda^-(U^*)$. On the other hand we know that $\sigma(U_1, V_1) = \lambda^-(U^*)$ and we notice that $\lambda^-(D_2) = \sigma(D_2^*, D_2) < \sigma(D_2^*, V_1)$ (see Fig 10.4). Thus we obtain $\sigma(U_1, V_1) = \lambda^-(U^*) < \sigma(D_2^*, V_1)$, which implies $D_2^* \in (V_3, U_1)$. $\qquad \square$
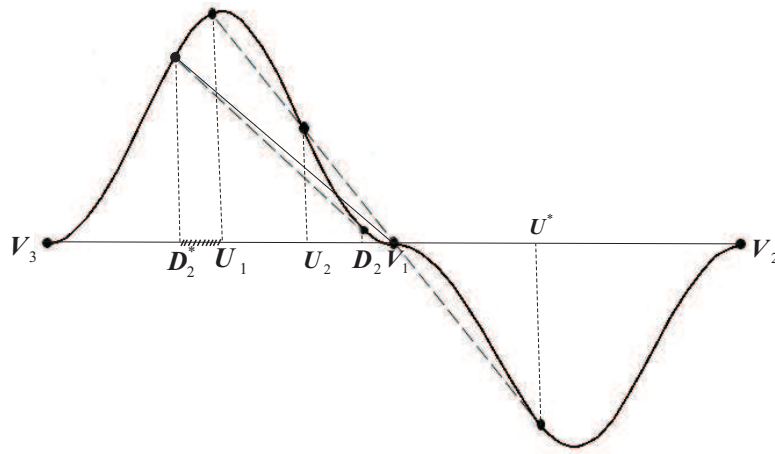
Figure 10.4: *Extended flux function. Notice that $D_2^* \in (V_3, U_1)$. In the interval (D_2^*, U_1) we have multiple solutions satisfying the generalized Lax criterion. It is necessary to use the viscous profiles criterion to choose the correct physical solution.*

Disconnected wave curves

Consider $U_L \in (V_3, V_1)$ and $U_R = V_2$, we find that the slow-family wave curve through U_L has disconnected branches. For most of the values of U_L on the edge ∂_2, we must use a non-local branch of the slow-family wave curve in order to reach the interval (V_2, Q_3) on ∂_3.

In Fig. 7.8 we illustrated the Hugoniot loci for distinct values of $U_L \in \partial_2$, for the same SPGP we are studying in the current chapter, therefore that figure can be taken as the reference for the shape of the Hugoniot loci. Recall that U_1 and U_2 were defined in item (*ii*) of Prop. 7.1, these states can be calculated easily from the wedge construction (see Fig. 7.4).

(a)   (b)
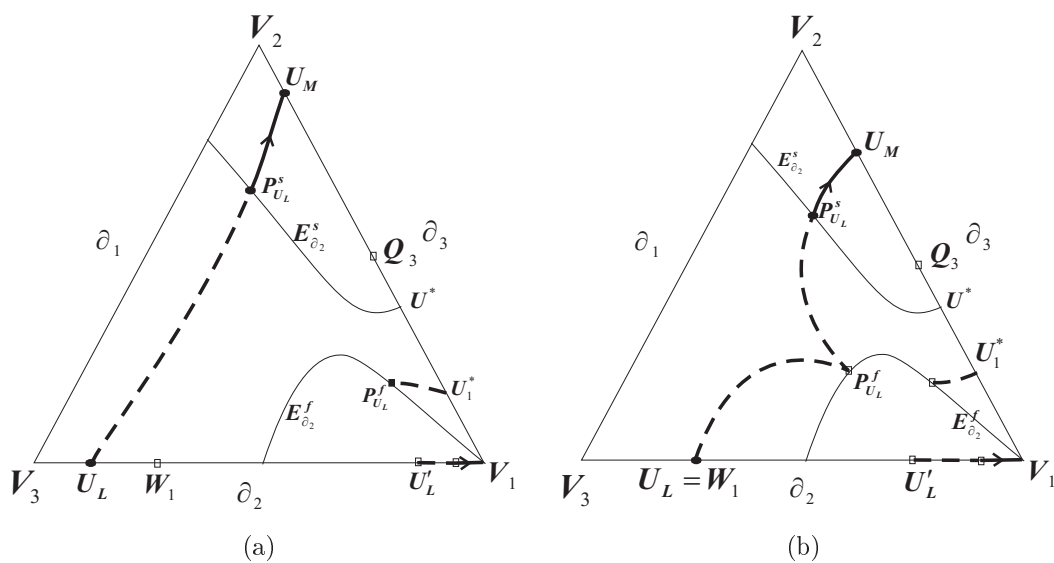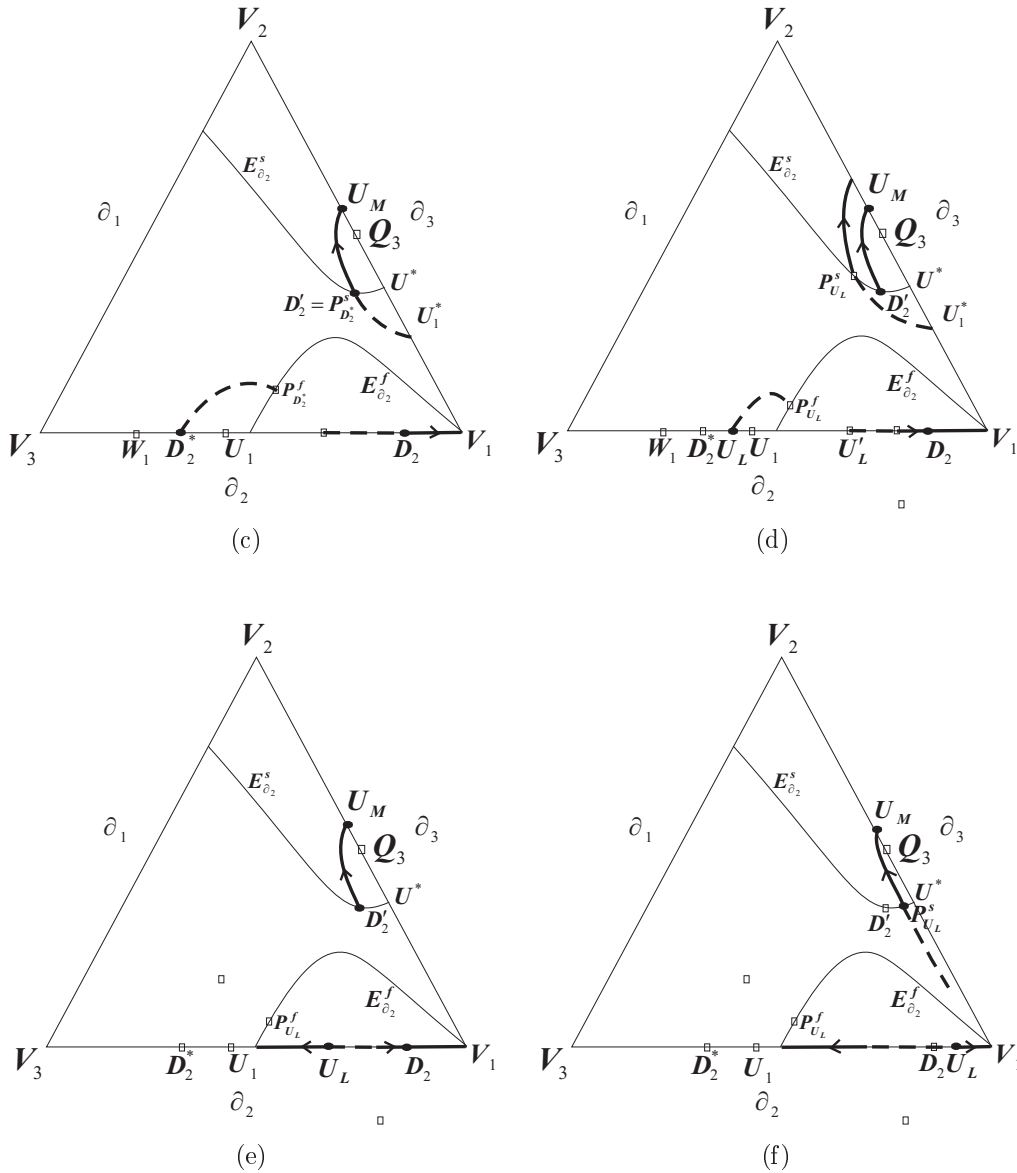
Figure 10.5: Slow-family wave curves for some states U_L on ∂_2 for the problem $\alpha = 0$, $\rho_1 > \rho_2 = \rho_3$, in the case $\mu_1 = \mu_2 = \mu_3$. The solid light curves $E^s_{\partial_2}$ and $E^f_{\partial_2}$ are the (slow and fast) extensions corresponding to the edge ∂_2. The dark curves represent the slow-family wave curve. As usual the solid part of the curves represent rarefaction curves with an arrow indicating the increasing direction of the slow characteristic speed, the dashed portions represent shock curves. (a) Wave curve for $U_L \in (V_3, W_1)$. (b) Wave curve for $U_L = W_1$. (c) Wave curve for $U_L = D_2^*$ where $D_2^* \in \partial_2$ and $\sigma(D_2, D_2^*) = \lambda^-(D_2)$. (d) Wave curve for $U_L \in (D_2^*, U_1)$. (e) Wave curve for $U_L \in (U_1, D_2)$. (f) Wave curve for U_L just to the right of the double contact state D_2. In all the figures we denoted by black dots the relevant states for the construction of the Riemann solutions, the states denoted by white squares does not belong to the solutions.

In Fig. 10.5 we show the slow-family wave curves for several values of $U_L \in \partial_2$. We note that for all values of U_L there exists at least a wave curve branch that reaches the edge ∂_3 at a point in the interval (V_2, Q_3), so the Riemann solution always exists. In this case, the speed compatibility between the fast-family waves and the slow-family waves is trivial since the last wave of the slow-family group is a rarefaction ending with zero-speed at the intermediate state U_M, while the fast-family wave group, which defines the two-phase solution joining U_M to V_2, always has positive speed. Notice that for $U_L \in (D_2^*, U_1)$ (see Fig. 10.5(d)) there exist two branches of the slow-family wave curve arriving to the interval (V_2, Q_3). The first branch arises from the use of the slow-family extension $P_{U_L}^s$ of the point U_L. However, this construction provides a sequence of waves which satisfies the generalized Lax criterion but it does not satisfy the viscous profile criterion, see Fig. 10.6(c). The other branch arises from the use of the slow-family double contact pair D_2, D_2', this type of solution satisfies both the generalized Lax criterion and the viscous profile criterion, therefore this is the physically correct solution. For $U_L \in (U_1, D_2)$ only the non local branch arising from the use of the slow-family double contact pair D_2, D_2' lies in the sauration triangle.

(a)   (b)   (c)
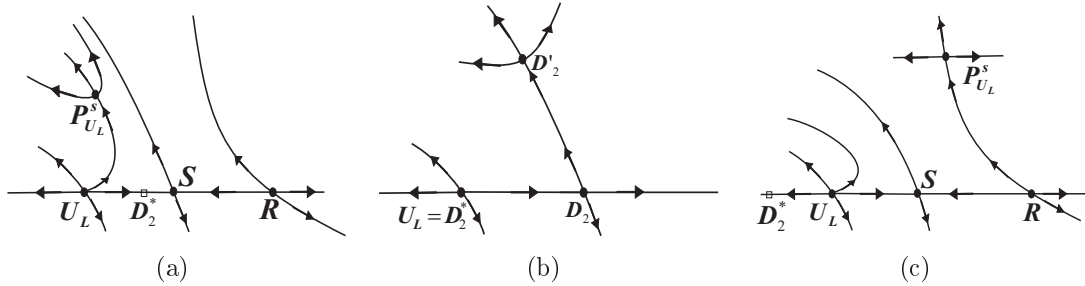
Figure 10.6: (a) Case U_L just to the left of D_2^*, there exist an orbit joining the states U_L and $P_{U_L}^s$. As expected this type of solution satisfies the viscous profile criterion. (b) Case $U_L = D_2^*$ for this case we obtain the phase portrait as a consequence of the collapse of two critical points: a repelling node and a saddle. (c) Case U_L just to the right of D_2^*, there does not exist an orbit joining U_L and $P_{U_L}^s$, there exist a saddle point which does not permit any orbit to cross to the other side. The Riemann solution for this cases must to be constructed by using the double contact pair D_2, D_2'.

In fact, for any value of U_L in (D_2^*, D_2) (see Figs. 10.5(d)- 10.5(e)) we must use the slow-family double contact pair D_2, D_2' to construct the Riemann solution, while for the cases $U_L \in (V_3, D_2^*)$ and $U_L \in (D_2, V_1)$ we use the extension $P_{U_L}^s$ of the point U_L, see Figs. 10.5(a), 10.5(b), 10.5(f).

See Fig. 10.5(c). For the case $U_L = D_2^*$, we have $P_{D_2^*}^s = D_2'$ (because of the Triple shock rule applied to D_2^*, D_2, D_2'), and we have two representations in state space of the same physical solution. The first representation consists of a slow shock joining $U_L = D_2^*$ with their extension point $P_{D_2^*}^s = D_2'$, continued by a slow-family rarefaction wave to U_M. The fast wave group is the two-phase Oleinik solution from U_M to V_2. The second representation consists of a slow shock joining $U_L = D_2^*$ with the state D_2, which is characteristic at D_2; it is followed by a double contact discontinuity joining D_2 with D_2';

from this point up to the final state V_2 we use the same sequence of waves employed in the first representation. The key fact for these different representations in state space to coincide in the physical space is that the discontinuities involved have the same speed (notice that $\sigma(D_2^*, D_2) = \lambda^-(D_2) = \lambda^-(D_2') = \sigma(D_2^*, D_2')$).

In Fig. 10.5 we denoted by black dots the states that are relevant for the construction of the Riemann solutions, the states denoted by white squares do not take part in the solutions.

Remark 10.2. *Notice a curious feature of the solution: if the mixture proportion of the state U_L lies inside the interval (D_2^*, D_2) then the faster wave in the upward direction (negative speeds) does not involve fluid 2 (i.e., the solution does not enter the saturation triangle). In other words, until the mixture proportion of the top fluids attains the critical value given by D_2, the bottom fluid (phase 2) does not move upwards.*

Now we summarize the results above, using the notations from Section 3.1.

The Riemann solution for the genuine three-phase flow of the SPGP where $\alpha = 0$, $\rho_3 = \rho_2 < \rho_1$, has the following structure

(iii) For $U_L \in (V_3, D_2^*)$ such that $U_M \in (V_2, P_{V_2}^f)$:

$$U_L \xrightarrow{SC^-} P_{U_L}^s \xrightarrow{R^-} U_M \xrightarrow{S^+} V_2 = U_R. \tag{10.1}$$

(iv) For $U_L \in (V_3, D_2^*)$ such that $U_M = P_{V_2}^f$:

$$U_L \xrightarrow{SC^-} P_{U_L}^s \xrightarrow{R^-} U_M \xrightarrow{CS^+} V_2 = U_R. \tag{10.2}$$

(v) For $U_L \in (V_3, D_2^*)$ such that $U_M \in (P_{V_2}^f, Q_3)$ or $U_L \in (D_2, V_1)$:

$$U_L \xrightarrow{SC^-} P_{U_L}^s \xrightarrow{R^-} U_M \xrightarrow{R^+} P_{V_2}^f \xrightarrow{CS^+} V_2 = U_R. \tag{10.3}$$

(vi) For $U_L \in (D_2^*, I_2^s)$, see Figs. 10.7(c) and 10.7(d), with $U_*^L \in \partial_2$:

$$U_L \xrightarrow{SC^-} U_*^L \xrightarrow{R^-} D_2 \xrightarrow{C^-} D_2' \xrightarrow{R^-} U_M \xrightarrow{R^+} P_{V_2}^f \xrightarrow{CS^+} V_2 = U_R, \tag{10.4}$$

(vii) For $U_L \in [I_2^s, D_2)$, see Figs. 10.7(a) and 10.7(b):

$$U_L \xrightarrow{R^-} D_2 \xrightarrow{C^-} D_2' \xrightarrow{R^-} U_M \xrightarrow{R^+} P_{V_2}^f \xrightarrow{CS^+} V_2 = U_R, \tag{10.5}$$

(viii) For $U_L = D_2^*$:

$$U_L = D_2^* \xrightarrow{SC^-} P_{D_2^*}^s = D_2' \xrightarrow{R^-} U_M \xrightarrow{R^+} P_{V_2}^f \xrightarrow{CS^+} V_2 = U_R. \tag{10.6}$$

For this case we have another different representation in state space for the same physical solution

$$\text{(viii.1)} \quad U_L = D_2^* \xrightarrow{SC^-} D_2 \xrightarrow{C^-} = D_2' \xrightarrow{R^-} U_M \xrightarrow{R^+} P_{V_2}^f \xrightarrow{CS^+} V_2 = U_R. \tag{10.7}$$

(ix) For $U_L = D_2$:

$$U_L = D_2 \xrightarrow{C^-} D_2' \xrightarrow{R^-} U_M \xrightarrow{R^+} P_{V_2}^f \xrightarrow{CS^+} V_2 = U_R. \tag{10.8}$$

Physical interpretation of the solutions.

We will only discuss the cases (vi) and (vii), which are more interesting, see Fig. 10.7. For this Riemann problem, one of the top fluids has the same density as the bottom fluid, while the third fluid (initially on top) is the heaviest. The solution is totally unpredictable without mathematical analysis. The solution consists of two wave groups separated by a constant state. The first wave group moves upwards. It contains a double contact shock embedded into two rarefaction waves; sometimes the upper rarefaction is preceded by an additional shock (this is the sole difference between the two cases). Within the top wave group, the waves faster than the embedded shock involve only two fluids, precisely the fluids that were on top initially; the fluid initially at the bottom is only present in the solution below the embedded shock. The second wave group moves downwards and involves two fluids only. This wave group consists of a rarefaction wave adjacent to a faster shock; in all these waves the lower-density fluid that was initially located on top is absent, *i.e.*, the lower-density fluid never moves downwards, as one could expect. There is a homogeneous region, *i.e.*, a constant state, separating the two wave groups. The span of this region grows linearly with time.

We observe a curious feature of this Riemann solution (see Remark 10.2): while the proportion in the mixture initially on top keeps within certain range away from a critical value, the mixture slows down the upward motion of the bottom fluid. This blocking property perhaps could be important in applications.

10.2   RP5: Left data in ∂_1, right data V_1

See Fig. 10.1, the edge ∂_1 coincides with the slow-family integral curves through $U_L \in \partial_1$. In this case the Riemann solution is trivial, the solution consists of a zero-speed genuine contact from U_L to the point V_2, followed by a zero-speed double contact discontinuity joining V_2 with V_1. There exist three representation of this solution in state space which coincide in the physical space:

(i) $U_L \xrightarrow{GC} V_2 \xrightarrow{C} V_1 = U_R$.

(ii) $U_L \xrightarrow{GC} V_3 \xrightarrow{C} V_1 = U_R$.
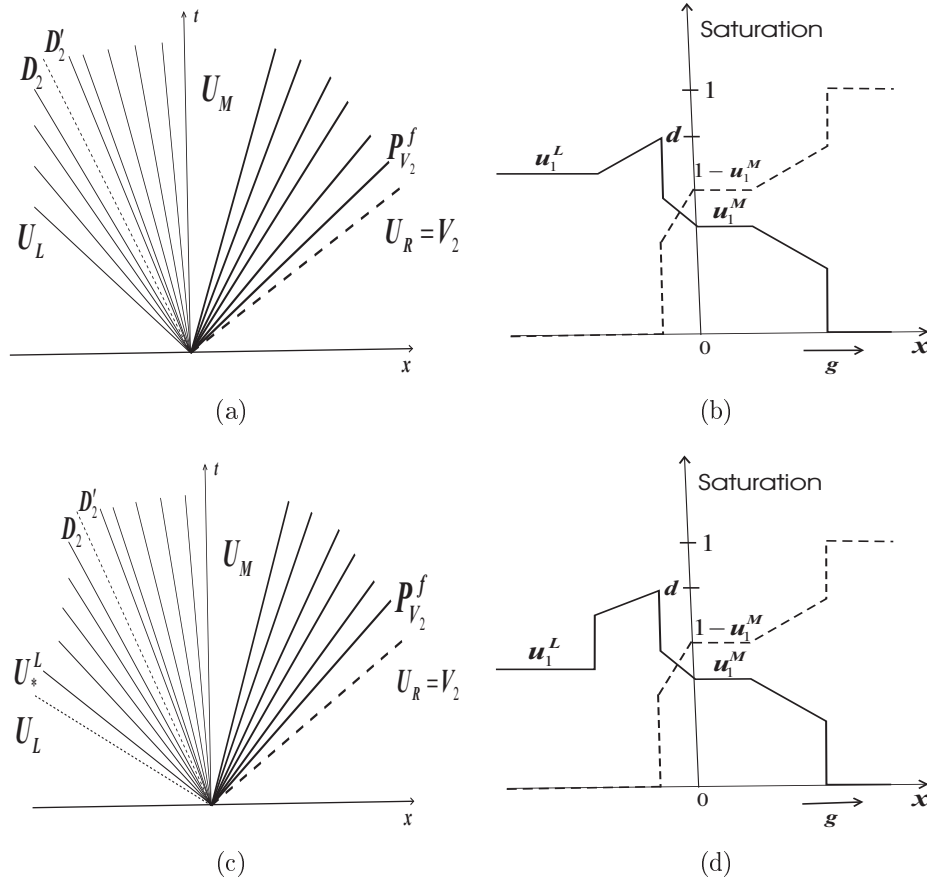
Figure 10.7: (a)-(b) Riemann solution for $U_L \in [I_2^s, D_2)$, $U_R = V_2$ (I_2^s was defined in Fig. 10.2) for the case $\rho_1 > \rho_2 = \rho_3$. (c)-(d) Riemann solution for $U_L \in (D_2^*, I_2^s)$, $U_R = V_2$. In (a) and (c): Riemann solution in (x, t)-space: solid lines represent the characteristic lines in a rarefaction fan, dashed lines represent shock paths, light lines correspond to waves of the slow family, dark lines correspond to waves of the fast family. In (b) and (d): saturation profiles; the solid curve indicates the saturation of phase 1, the dashed curve indicates the saturation of phase 2. The constant states are $U_L = (u_1^L, 0, 1 - u_1^L)$, $U_M = (u_1^M, 0, 1 - u_1^M)$ and $V_2 = (0, 1, 0)$. Other relevant states are the pair $D_2 = (d, 0, 1 - d)$, $D_2' = (d_1', d_2', 1 - d_1' - d_2')$ that belong to the double contact manifold, and states $D_2^* = (d^*, 0, 1 - d^*)$, $U_*^L = (u_*^L, 0, 1 - u_*^L)$ which satisfy $\sigma(D_2^*, D_2) = \lambda^-(D_2)$, $\sigma(U_L, U_*^L) = \lambda^-(U_*^L)$

(iii) $U_L \xrightarrow{GC} B_1 \xrightarrow{C} V_1 = U_R$.

Physical interpretation of the solutions.

The physical interpretation is trivial, since for this case the bottom fluid is the heaviest while in top we have equal-density fluids, one could expect that neither of the fluids would move.

Remark 10.3. *The Riemann problem RP6: with left data $\boldsymbol{U_L}$ in $\boldsymbol{\partial_3}$ and right data*

$U_R = V_3$, *is analogous to the case RP4, so we omit its description.*

Appendix A

Additional calculation for Theorem 5.1

The following calculations correspond to the proof of Theorem 5.1. Assume $\rho_3 < \rho_1 = \rho_2$. Let us denote $\rho = \rho_{13} = \rho_{23}$. From (4.4)-(4.7) we have

$$J_{22} - J_{11} = 2\rho\Big(\frac{u_1^2 u_2 u_3^2}{\mu_1 \mu_2 \mu_3 \Lambda^2} - \frac{u_2^4 u_3}{\mu_2^2 \mu_3 \Lambda^2} - \frac{u_1 u_2^2 u_3^2}{\mu_1 \mu_2 \mu_3 \Lambda^2} + \frac{u_1^4 u_3}{\mu_1^2 \mu_3 \Lambda^2}\Big), \tag{A.1}$$

$$J_{12} = 2\rho\Big(-\frac{u_1^2 u_2 u_3^2}{\mu_1 \mu_2 \mu_3 \Lambda^2} - \frac{u_1^2 u_2^2 u_3}{\mu_1 \mu_2 \mu_3 \Lambda^2} - \frac{u_1^4 u_3}{\mu_1^2 \mu_3 \Lambda^2}\Big), \tag{A.2}$$

$$J_{21} = 2\rho\Big(-\frac{u_1 u_2^2 u_3^2}{\mu_1 \mu_2 \mu_3 \Lambda^2} - \frac{u_1^2 u_2^2 u_3}{\mu_1 \mu_2 \mu_3 \Lambda^2} - \frac{u_2^4 u_3}{\mu_2^2 \mu_3 \Lambda^2}\Big). \tag{A.3}$$

As we are supposing that $(u_1, u_2) \in R_3$, we can substitute $\frac{u_1}{\mu_1} = \frac{u_2}{\mu_2}$ into above expression in a convenient way in order to obtain the same denominator in all terms, so we obtain

$$J_{22} - J_{11} = 2\rho\Big(\frac{u_1^3 u_3^2}{\mu_1^2 \mu_3 \Lambda^2} - \frac{u_1^2 u_2^2 u_3}{\mu_1^2 \mu_3 \Lambda^2} - \frac{u_1^2 u_2 u_3^2}{\mu_1^2 \mu_3 \Lambda^2} + \frac{u_1^4 u_3}{\mu_1^2 \mu_3 \Lambda^2}\Big)$$

$$= 2\rho\frac{u_1^2 u_3}{\mu_1^2 \mu_3 \Lambda^2}\big(u_1(1 - u_1 - u_2) - u_2^2 - u_2(1 - u_1 - u_2) + u_1^2\big) \tag{A.4}$$

$$= 2\rho\frac{u_1^2 u_3}{\mu_1^2 \mu_3 \Lambda^2}\big(u_1 - u_2\big) = 2\rho\frac{u_1^3 u_3}{\mu_1^2 \mu_3 \Lambda^2}\big(1 - \mu_2/\mu_1\big),$$

$$J_{12} = 2\rho\Big(-\frac{u_1^3 u_3^2}{\mu_1^2 \mu_3 \Lambda^2} - \frac{u_1^3 u_2 u_3}{\mu_1^2 \mu_3 \Lambda^2} - \frac{u_1^4 u_3}{\mu_1^2 \mu_3 \Lambda^2}\Big)$$

$$= -2\rho\frac{u_1^2 u_3}{\mu_1^2 \mu_3 \Lambda^2}\big(u_1(1 - u_1 - u_2) + u_1 u_2 + u_1^2\big) = -2\rho\frac{u_1^3 u_3}{\mu_1^2 \mu_3 \Lambda^2}, \tag{A.5}$$

$$J_{21} = 2\rho\Big(-\frac{u_1^2 u_2 u_3^2}{\mu_1^2 \mu_3 \Lambda^2} - \frac{u_1^3 u_2 u_3}{\mu_1^2 \mu_3 \Lambda^2} - \frac{u_1^2 u_2^2 u_3}{\mu_1^2 \mu_3 \Lambda^2}\Big)$$

$$= -2\rho\frac{u_1^2 u_3}{\mu_1^2 \mu_3 \Lambda^2}\big(u_2(1 - u_1 - u_2) + u_1 u_2 + u_2^2\big) \qquad \text{(A.6)}$$

$$= -2\rho\frac{u_1^2 u_2 u_3}{\mu_1^2 \mu_3 \Lambda^2} = -2\rho(\mu_2/\mu_1)\frac{u_1^3 u_3}{\mu_1^2 \mu_3 \Lambda^2}.$$

Let be $\Delta = (J_{22} - J_{11})^2 + 4J_{12}J_{21}$, from (A.4)-(A.6) we have

$$\Delta = 4\frac{u_1^6 u_3^2 \rho^2}{\mu_1^4 \mu_3^2 \Lambda^4}\big((1 - \mu_2/\mu_1)^2 + 4\mu_2/\mu_1\big) = 4\frac{u_1^6 u_3^2 \rho^2}{\mu_1^4 \mu_3^2 \Lambda^4}\big(1 + \mu_2/\mu_1\big)^2. \qquad \text{(A.7)}$$

Substituting (A.4) and (A.7) into (5.16) and using (A.6) we obtain

$$J_{22} - \lambda_- = 2\rho\frac{u_1^3 u_3}{\mu_1^2 \mu_3 \Lambda^2} = -\frac{\mu_1}{\mu_2}J_{21}. \qquad \text{(A.8)}$$

Appendix B

Proof of Lemma 8.2

First we see that the functions J_{11} and J_{22} are symmetric functions with respect to the variables u_1 and u_2, so the function $f_0 = J_{11} + J_{22}$ is also symmetric.

Let denote $\Theta = J_{11}J_{22} - J_{12}J_{21}$ Taking in to account the relations (4.4)-(4.7), we obtain after some calculations

$$\Theta = f_1 + f_2 + f_3 + f_4 + f_5 + f_6 + f_7, \tag{B.1}$$

where

$$f_1(u_1, u_2) = -8\rho^2 \Big(\frac{u_1^3 u_2^4 (1 - u_1 - u_2)^3}{\mu^4 \mu_3^2 \Lambda^4} + \frac{u_1^4 u_2^3 (1 - u_1 - u_2)^3}{\mu^4 \mu_3^2 \Lambda^4} \Big), \tag{B.2}$$

$$f_2(u_1, u_2) = -4\rho^2 \Big(\frac{u_1 u_2^6 (1 - u_1 - u_2)^3}{\mu^4 \mu_3^2 \Lambda^4} + \frac{u_1^6 u_2 (1 - u_1 - u_2)^3}{\mu^4 \mu_3^2 \Lambda^4} \Big), \tag{B.3}$$

$$f_3(u_1, u_2) = 4\rho^2 \Big(\frac{u_1 u_2^3 (1 - u_1 - u_2)^6}{\mu^3 \mu_3^3 \Lambda^4} + \frac{u_1^3 u_2 (1 - u_1 - u_2)^6}{\mu^3 \mu_3^3 \Lambda^4} \Big), \tag{B.4}$$

$$f_4(u_1, u_2) = 4\rho^2 \Big(\frac{u_1 u_2 (1 - u_1 - u_2)^8}{\mu^2 \mu_3^4 \Lambda^4} \Big), \tag{B.5}$$

$$f_5(u_1, u_2) = -4\rho^2 \Big(\frac{u_1 u_2^4 (1 - u_1 - u_2)^5}{\mu^3 \mu_3^3 \Lambda^4} + \frac{u_1^4 u_2 (1 - u_1 - u_2)^5}{\mu^3 \mu_3^3 \Lambda^4} \Big), \tag{B.6}$$

$$f_6(u_1, u_2) = -4\rho^2 \Big(\frac{u_1^3 u_2^2 (1 - u_1 - u_2)^5}{\mu^3 \mu_3^3 \Lambda^4} + \frac{u_1^2 u_2^3 (1 - u_1 - u_2)^5}{\mu^3 \mu_3^3 \Lambda^4} \Big), \tag{B.7}$$

$$f_7(u_1, u_2) = 4\rho^2 \Big(\frac{u_1^2 u_2^5 (1 - u_1 - u_2)^3}{\mu^4 \mu_3^2 \Lambda^4} + \frac{u_1^5 u_2^2 (1 - u_1 - u_2)^3}{\mu^4 \mu_3^2 \Lambda^4} \Big). \tag{B.8}$$

All the functions ((B.2)-(B.8)) are symmetric in the variables u_1 and u_2 (Notice that $\Lambda = \frac{u_1^2 + u_2^2}{\mu} + \frac{(1 - u_1 - u_2)^2}{\mu_3}$ is symmetric), so the function $\Theta(u_1, u_2)$ is also symmetric with respect to the variables u_1 and u_2. Then we have that characteristic speeds $\lambda_\pm = \frac{1}{2}(f_0 \pm \sqrt{f_0^2 - 4\Theta})$ are symmetric functions.

Appendix C

Uniqueness of solution for RP1

The following analysis mixes analytical and numerical arguments.

Consider the simplified pure gravitational problem $\alpha = 0, \rho_1 = \rho_2 > \rho_3$. For the Riemann problem of type RP1, consider a left data $U_L \in (V_3, Q_2)$ and the right data $U_R = V_2$.

We want to show that the solution obtained by using the slow-family wave curve coincides with the solution described in chapter 9.

Let us analyze the slow-family wave curve through U_L. The first portion of the slow-family wave curve arising from U_L consists of a rarefaction segment U_L-U_{inf} where U_{inf} belongs to the inflection manifold; the wave curve continues with a composite curve parameterizing states on the right of shocks that are characteristic at the left states on the rarefaction segment U_L-U_{inf}.

There exist several possibilities for a slow-family composite curve to finish:

- The slow-family composite curve reaches the boundary of the saturation triangle.

- The slow-family composite curve reaches a state where the shock speed is equal to one of the characteristic speeds; in such a case the wave curve either continues with a new slow-family rarefaction segment or with a fast-family rarefaction segment. The state where the composite curve finishes together with the corresponding state in the base rarefaction segment is a pair of states in the double contact manifold (maybe involving both families).

- The slow-family composite curve finishes after utilizing all the states of the base rarefaction segment; in this case the slow-family wave curve continues with a shock segment.

We perform the analysis for the slow-family composite based in the rarefaction curve U_L-U_{inf}. First notice that the slow-family composite curve cannot arrive or end at a

point A_3 on the edge ∂_3 since $\lambda_-(U) \geq 0$ for all U in the rarefaction curve U_L–$U_{\inf}$ (see Fig. 9.11(c)) while $\sigma(U, A_3) < 0$ (see item (ii) of Lemma 9.1).

We use a numerically obtained figure to show that the slow-family composite curve cannot reach a point A_2 on the edge ∂_2, before consuming the whole rarefaction curve, see Fig. C.1. The slow-family boundary contact manifold $E_{\partial_2}^s$ that extends the edge ∂_2 intersects the inflection manifold at a point P out of the triangle V_3–V_1–B_3; however the integral curve through U_L remains always inside this triangle (because the segment R_3 itself is a slow-family integral curve as we have shown in Theorem 5.1), so none of the states in the rarefaction branch U_L–$U_{\inf}$ can be right extensions of $A_2 \in \partial_2$. Thus the composite curve cannot reach ∂_2 before consuming all the states in the rarefaction curve.
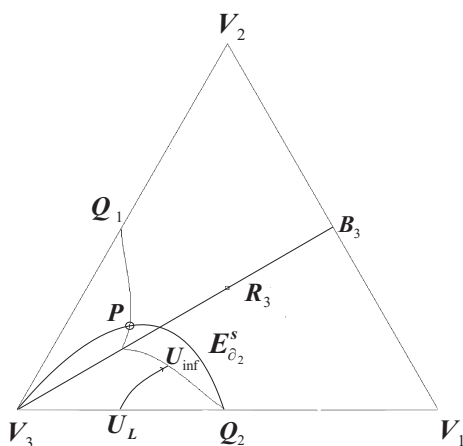
Figure C.1: $E_{\partial_2}^s$ is the portion of the slow boundary contact manifold which extends the edge ∂_2; this curve intersects the slow inflection curve at P. The rarefaction branch starting at U_L reaches the inflection curve without intersecting the curve $E_{\partial_2}^s$.

As we already eliminated the solutions arriving to V_2 along the edge ∂_1 we do not worry about the possibility of the slow-family composite curve reaching ∂_1 or reaching a point in the interior of the triangle where the shock speed coincides with the fast characteristic speed (as the fast-family wave curves lead to the edge ∂_1 too).

On the other hand, we have numerical evidence showing that there does not exist any state on the rarefaction curve U_L–$U_{\inf}$ that belongs to the slow-family double contact manifold, therefore the only remaining possibility is that the composite based on this rarefaction curve will continue until it consumes all the states of the rarefaction curve. However this cannot occur out of the edge ∂_2 because of item (i) of Lemma 9.1 and of the equality $\lambda^-(U_L) = 0$. So the composite curve will end at a point $U_L' = (u_L', 0, 1 - u_L')$ in ∂_2 such that $\sigma(U_L, U_L') = 0 = \lambda^-(U_L)$, the slow-family wave curve continues along the edge ∂_2 with the shock segment U_L'–U_* followed by a final rarefaction segment U_*–V_1, see Fig. 9.6(a). Here U_L' is the same point described in Theorem 8.2 corresponding to U_L. The state $U_* \in \partial_2$ satisfy $\sigma(U_L, U_*) = \frac{d}{du_1} F_1^{\partial_2}(u_*^1)$. As $u_L' < u_*^1$, this construction leads to the same Riemann solution in Figs. 9.6(b) and 9.6(c).

Appendix D

Extended bibliographic review

Riemann problem theory dates from 1860 when the shock tube problem was solved employing the method of characteristics, see [39]. That problem reduces to solving a piecewise constant initial value problem for a system of non-linear conservation laws that describes gas motion, Euler's equations. Riemann obtained the scale-invariant solution and explained why rarefaction waves and shock waves are generated when the membrane separating regions with gases at different pressures is broken.

Non-linear conservation laws govern flows in porous media. The simplest nonlinear problem in porous media, the two-phase flow injection problem, was solved by Buckley and Leverett [5] in 1942. Their resolution method can be interpreted geometrically by means of the graph of the standard S-shaped flux function, giving rise to the fractional flow method, of common usage in petroleum enginering. This method is a powerful and simple tool to solve flow problems involving no more than two phases, but many chemical components, see [13], [14], [49].

The Riemann problem for immiscible three-phase flow is more difficult than for two-phase flow. The fractional flow method cannot be extended to three-phase flow problems such as those arising for the rock permeability models of Corey et al. [6] and Stone [48]. The resolution of such problems requires a more general solution method, the *wave curve method*, developed by Liu [29], which generalizes the Lax's theorem [28]. This method constructs the solution by means of a sequence of rarefaction waves, shock waves, and constant states, by following a sequence of curves in state space.

The wave curve method developed by Liu assumes that the system of conservation laws is strictly hyperbolic. Nevertheless, systems of conservation laws modelling immiscible three-phase flow in porous media fail to be hyperbolic.

Marchesin, Paes Leme (unpublished, 1980) and Shearer [43] established that violation of strict hyperbolicity occurs inside the saturation triangle for immiscible three-phase flow without gravity. Bell, Trangenstein and Shubin [4] showed by means of numerical experiments that Stone's model for permeabilities possesses an elliptic region in the satu-

ration triangle which in some sense is a repeller for waves. Other important works about elliptic-hyperbolic mixed problems modelling immiscible three-phase flow in porous media are Keyfitz [26], Keyfitz [27], Holden [15], Holden [17], Holden H. and Holden L. [16].

Isaacson, Marchesin, Plohr and Temple [20] showed that for Corey model of permeabilities, there exist a sole isolated point where strict hyperbolicity fails, which was called umbilic point.

Isaacson and Temple [23] introduced the idea of studying the solutions in a neighborhood of umbilic points by using homogeneous quadratic polynomial flux functions. Schaeffer and Shearer [40] classified the umbilic points for quadratic homogeneous systems in four types, two of them, types I and II, are relevant for three-phase flow models. Some works were dedicated to the study of Riemann solutions for systems of two conservation laws with homogeneous quadratic flux functions, dealling with the different four umbilic point types. For instance see Shearer, Schaeffer, Marchesin and Paes-Leme [42], Isaacson, Marchesin, Plohr and Temple [22], Schaeffer and Shearer [41].

Holden [15], Holden H. and Holden L. [16] studied examples of quadratic systems presenting umbilic points of type I and II of the Schaeffer-Schearer classification [40] and proved nonuniqueness of Riemann solutions using Lax [28] and Oleinik [34] entropy criteria, as extended by Liu [29] rather than using the traveling wave criterion.

Azevedo and Marchesin [2] studied the Holden's model in [15], by using the condition that shock waves should be zero-diffusion limits of traveling waves for the parabolic system. They found that a moderate number of multiple solution occur for this prototype of Stone's model. Azevedo, Marchesin, Plohr and Zumbrun [3] showed that, in the presence of nontrivial diffusion terms, such as those for capillary pressure, it is not the elliptic region (resp. umbilic point) that plays the role of an instability region; rather, it is the region defined by Majda-Pego [31], which depends on the diffusion terms too and contains the elliptic region (resp. umbilic point)

Isaacson, Marchesin, Plohr and Temple [20], solved by the wave curve method the Riemann problem for Corey's model for immiscible three-phase flow in porous media neglecting gravitational effects. Their method is more general than Liu's, because it allows for loss of hyperbolicity and for other difficulties that typically occur in three-phase flow. In [20] the solution was obtained under the simplifying assumption that the three fluids have equal viscosities. De Souza [8] extended the study to the case in which one of the viscosity parameters is slightly different from the other two. Some mathematical difficulties arising in this study were resolved by Marchesin, Plohr and Schecter [32].

In their doctoral theses Xu [53] and Rezende [36] studied topological aspects of the elementary waves in the Corey's Model analyzed in [20].

Hurley and Plohr [19] studied how changing the diffusion terms affect the solutions of Riemann problems.

Schecter, Marchesin and Plohr [45], [46] initiated a systematic program to classify all

Riemann solutions for (non-strictly) hyperbolic systems of two conservation laws with the identity viscous profile criterion. In particular wave curves were studied. This work extended the doctoral work of Furtado [9] which used the Lax [28] and Oleinik [34] entropy criteria.

Recently Azevedo, De Souza, Furtado, Marchesin and Plohr [1] showed applications of the wave curve method to solve the injection problem for immiscible three-phase flow in which a mixture of water and gas is injected into a horizontal one-dimensional porous medium containing oil.

On the other hand, buoyancy effects in the flow of two immiscible fluids in porous media are quite well understood, as they are modelled by a scalar conservation law, while is easily solved through Oleinik's construction [34]. For instance Proskurowski in [35] solved the Buckley-Leverett equation for two-phase flow in the presence of gravity. There are others works on two-phase flow with gravity and their applications, see *e.g.* [37], [38], [51], [24], [12].

The state of the art for three-phase flow with gravity is quite different. Up to now, there are a few works on three-phase flow with gravity taken in to account. Medeiros [33] performed an analysis of hyperbolic singularities for certain models including gravity. Trangenstein [50] showed that Stone model with gravity present elliptic regions. Medeiros and Trangenstein's results indicate that the only three-phase permeability models that have umbilic points, rather than elliptic regions, in the presence of gravity are Corey models, in which each permeability depends solely on its own fluid saturation.

Bibliography

[1]   Azevedo, A. V., De Souza, A. J., Furtado, F., Marchesin, D. and Plohr, B., The solution by the wave curve method of three-phase flow in virgin reservoirs. *Transport in porous media*, Vol **83**, (2010) no. 1, pp. 99-125.

[2]   Azevedo, A. and Marchesin, D., Multiple viscous solutions for systems of conservation laws, *Trans. Amer. Math. Soc.* (1995) **347**, pp. 3061-3078.

[3]   Azevedo, A., Marchesin, D., Plohr, B., Zumbrun, K., Capillary instability in models for three-plase flow. *Zeitschrit Fur Angewandte Mathematik Und Physik* (2002) **v. 53**, no. 5, pp. 713-746.

[4]   Bell, J., Trangenstein, J., and Shubin,G., Conservation laws of mixed type describing three-phase flow in porous media, *SIAM J. Appl. Math.* (1986) **46**, pp. 1000-1017.

[5]   Buckley, S., Leverett, M., Mechanisms of fluid displacement in sands. *Trans. AIME* (1942) **146**, pp. 187-196.

[6]   Corey, A., Rathjens, C., Henderson, J., Wyllie, M., Three-phase relative permeability. *Trans. AIME* (1956) **207**, pp. 349-351.

[7]   Courant, R. and Friedrichs, K., Supersonic flow and shock waves, (1948) John Wiley, New York.

[8]   De Souza, A. J., Stability of singular fundamental solutions under perturbations for flow in porous media. *Mat. Aplic. Comp.* (1992) **11**, no. 2, pp. 73-115.

[9]   Furtado, F., Structural stability of nonlinear waves for conservation laws. PhD Thesis. New York University, (1989).

[10]   Gelfand, I., Some problems in the theory of quasi-linear equations. *Usp. Math. Nauk.* **14** (1959) pp. 87-158. English transl., Amer. Math. Soc. Transl., Ser. 2, **29**, pp. 295-381, (1963).

[11]   Glimm, J., Solutions in the large for nonlinear hyperbolic systems of equations. *Comm. Pure Appl. Math.* (1965) **XVIII**, pp. 697-715.

[12]   Hayek, M., Mouche, E., Mugler, C., Modeling Vertical stratification of CO_2 injected into deep layered aquifer, *Advances in Water Resours* (2009) **v. 32**, no. 3, pp. 450-462.

[13]   Helfferich, F. G., General theory of multicomponent, multiphase displacement in porous media. *Soc. Pet. Engrg. J.* (1981) **21**, pp. 51-62.

[14]   Hirasaki, G. J., Application of the theory of multicomponent, multiphase displacement to three-component, two-phase surfactant flooding. *Soc. Pet. Engrg. J.* (1981) **21**, pp. 191-204.

[15]   Holden, L., On the Riemann problem for a prototype of a mixed type conservation law, *Comm. Pure Appl. Math.* (1987) **40**, pp. 229-264.

[16]   Holden, H. and Holden, L., On the Riemann problem for a prototype of a mixed type conservation law, II, Current Progress in Hyperbolic Systems: Riemann Problems and Computations (Bowdoin, 1988), Lindquist, B. (ed.), *Contemporary Mathematics* (1989) **100**, pp. 331-367, American Mathematics Society, Providence.

[17]   Holden, L., On the strict hyperbolicity of the Buckley-Leverett equations for the three-phase flow in porous medium, *SIAM J. Appl. Math.* (1990) **50**, pp. 667-683.

[18]   Hopf, E., The partial differential equation $u_t + uu_x = \mu u_{xx}$. *Comm. Pure Appl. Math.* (1950) **III**, pp. 201-230.

[19]   Hurley, J. and Plohr, B. Some effects of viscous terms on Riemann problem solutions. *Mat. Contemp.* (1995) **8**, pp. 203-224.

[20]   Isaacson, E. L., Marchesin, D., Plohr, B. J. and Temple, J. B., Multiphase flow models with singular Riemann problems. *Mat. Aplic. Comp.* (1992) **v. 11**, no. 2, pp. 147-166.

[21]   Isaacson, E. L., Marchesin, D. and Plohr, B. J., Transitional waves for conservation laws. *SIAM Journal on Mathematical Analysis* (1990) **v. 21**, pp. 837-866.

[22]   Isaacson, E. L., Marchesin, D., Plohr, B. J. and Temple, J. B., The Riemann problem near a hyperbolic singularity: The classification of solutions of quadratic Riemann problems, *SIAM J. Appl. Math.* (1988) **48**, no. 5, pp. 1009-1032.

[23]   Isaacson, E. L. and Temple, J. B., Examples and classification of non-strictly hyperbolic systems of conservation laws, Proceedings of the Amer. Math. Soc. Meeting, Anaheim, CA, (1985).

[24]   Kaasschieter, E. F., Solving the Buckley-Leverett equation with gravity in a heterogeneous porous medium, *Comput. Geosci.* (1999) **3**, no. 1, pp. 23-48.

[25]   Johnson, J. L. and Smoller, J. A., Global solutions for an extended class of
         hyperbolic systems of conservation laws, *Arch. Rational Mech. Anal.* (1969)
         32, pp. 169-189.

[26]   Keyfitz, B. L., An analytic model for change of type in three-phase flow,
         Numerical Simulation in Oil Recovery (Minneapolis, 1986), Wheeler, M. (ed),
         IMA Volumes in Mathematics and Its Applications (1988) **11**, pp. 149-160,
         Springer, New York.

[27]   Keyfitz, B. L., Change of type in three-phase flow: a simple analogue, *J.
         Differential Equations* (1989) **80**, pp. 280-305.

[28]   Lax, P., Hyperbolic systems of conservation laws II. *Comm. Pure Appl. Math.*
         (1957) **X**, pp. 537-566.

[29]   Liu, T.-P., The Riemann problem for general 2×2 conservation laws. *Trans.
         Amer. Math. Soc.* (1974) **199**, pp. 89-112.

[30]   Liu, T.-P., The Riemann problem for general systems of conservation laws,
         J. Differential Equations, (1975) **18**, pp. 218-234.

[31]   Majda, A., Pego, R., Stable viscosity matrices for system of conservation
         laws, *J. Differential Equations* (1985) **56**, pp. 229-262.

[32]   Marchesin, D., Plohr, B., Schecter, S. An organizing center for wave curve
         bifurcation in multiphase flow models, *SIAM J.Appl. Math.* (1997) **57**,
         pp. 1189-1215.

[33]   Medeiros, H. B., Stable hyperbolic singularities for three-phase flow models in
         oil reservoir simulation. *Acta Applicandae Mathematicae* (1992) **28**, pp. 135-
         159.

[34]   Oleinik, O. A., On the uniqueness of generalized solution of Cauchy problem
         for non linear system of equations occurring in mechanics, *Uspekhi Mat. Nauk*
         (1957) **12**, pp. 169-176.

[35]   Proskurowski, W., A note on solving the Buckley-Leverett equation in the
         presence of gravity. *J. Comput. Phys.* (1981) **41**, pp. 136-141.

[36]   Rezende, F. S., Elementary waves in the three-phase flow model, Doctoral
         Thesis (in Portuguese), Pontifícia Universidade Católica do Rio de Janeiro,
         (1998).

[37]   Riaz, A. and Tchelepi, H.A., Stability of two-phase vertical flow in ho-
         mogeneous porous media, *Phys. Fluids* (2007) **Vol. 19**, no. 7, July, DOI:
         10.1063/1.2742975, 17 pags.

[38]   Riaz, A. and Tchelepi, H. A., Dynamics of vertical displacement in porous
         media associated with CO_2 sequestration. *SPE Journal* (2008), pp. 305-313.

[39]   Riemann, G. F. B., Uber die fortpflanzung ebener luftwellen von endlicher schwingungsweite. *Abhandlungen der Gesellschaft der Wissenschaften Zu Gottingen* **8**, 43, (1860).

[40]   Schaeffer, D. G., Shearer, M., The classification of 2×2 systems of non-strictly hyperbolic conservation laws, with application to oil recovery. *Comunications on Pure and Applied Mathematics* (1987) **Vol XL**, pp. 141-178.

[41]   Schaeffer, D. G., Shearer, M., Riemann problems for nonstrictly hyperbolic 2×2 systems of conservation laws, *Trans. Amer. Math. Soc.* (1987) **304**, pp. 267-306.

[42]   Shearer, M., Schaeffer, D. G., Marchesin, D., Paes-Leme, P. J., Solution of the Riemann problem for a prototype 2×2 system of non-strictly hyperbolic conservation laws, *Arch. Rat. Mech. Anal.* (1987) **97**, pp. 299-320.

[43]   Shearer, M., Loss of strict hyperbolicity of the Buckley-Leverett equations for three-phase flow in a porous medium, Numerical Simulation in Oil Recovery (Minneapolis, 1986). Wheeler, M (ed), *IMA Volumes in Mathematics and Its Applications* (1988) **11**, pp. 263-283, Springer-Verlag, New York.

[44]   Shearer, M., Trangenstein, J. Loss of real characteristics for models of three-phase flow in porous media, *Transport in Porous Media* (1989) **4**, pp. 499-525.

[45]   Schecter, S., Marchesin, D., Plohr, B., Structurally stable Riemann solutions, *J. Differential Equations* (1996) **126**, pp. 303-354.

[46]   Schecter, S., Plohr, B., Marchesin, D., Classification of codimension-one Riemann solutions. *Journal of Dynamics and Differential Equations* (2001) **v. 13**, no. 3, pp. 523-588.

[47]   Smoller, J., Shock waves and reaction-diffusion equations, 2nd edn. Springer-Verlag, New York (1994).

[48]   Stone, H. Probability model for estimating three-phase relative permeability. *J. Petr. Tech.* (1970) **22**, pp. 214-218.

[49]   Temple, J. B., Systems of conservation laws with coinciding shock and rarefaction waves. *Contemp. Math.* (1983) **17**, pp. 143-151.

[50]   Trangenstein, J., Three-phase flow with gravity, Current Progress in Hyperbolic Systems: Riemann Problems and Computations (Bowdoin 1988), Lindquist, B. (ed), *Contemporary Mathematics* (1989) **100**, pp. 147-159, American Mathematic Society, Providence.

[51]   Wangen, M., Vertical migration of hydrocarbons modelled with fractional flow theory, *Geophysical Journal International* (1993) **115**, pp. 109-131.

[52]   Wendroff, B., The Riemann problem for materials with non-convex equations of state: I isentropic flow; II general flow, *J. Math. Anal. Appl.*, **38** (1972), pp. 454-466; pp. 640-658.

[53]   Xu, Q.-P., The global structure of scale invariant solutions of the Riemann problem for a model of three-phase flow in a porous medium, Ph.D. Thesis, Dept. of Applied Mathematics and Statistics. State Univ. of New York at Stony Brook, (1992).